4 Technical description

4.1 A proton accelerator, which proton beam is converted, when the accelerator is in operation, on target material (lead, tungsten) into primary neutrons, assumes the role of an outside neutron source for subcritical core. When the proton accelerator is not in operation, the source of outside (primary) neutrons is missing.

4.2 Technical data of subcritical breeding blanket with target (SBB+T) is given in Table 4.1.

Table 4.1 – Technical description of SBB+T

Description	**Value**
Proton beam data	
Proton energy, MeV	659
Proton energy spread, MeV	6
Maximum beam power, kW	1,0
Horizontal beam emittance, cm·mrad	$\sum x = \pi(5{,}1 \pm 2{,}3)$
Vertical beam emittance, cm·mrad	$\sum y = \pi(3{,}4 \pm 1{,}4)$
Maximum current of extracted proton beam, μA	1,52
Pulse frequency, Hz	250
FWHM pulse width, μs	20
Quantity of protons in pulse	$4{,}0 \cdot 10^{10}$
Pulse microstructure: - FWHM bunch width, ns - interval between bunches, ns - number of bunches in pulse	 10 70 385
Initial data of core	
Fuel material	UO_2-PuO_2
Density, g/cm^3	10,2
Mass content of PuO_2 in mixture, %	29,7
Height of fuel column of fuel element, cm	58,0

Table 4.1, continued

Description	Value
Duration of power operation, hours	10000
Fuel element diameter (at cladding), mm	6,9
Pitch of triangle grid for fuel elements location, mm	7,6
Number of fuel elements in fuel assembly (FA)	18
Pitch of triangle grid for fuel assembly location, mm	36
Maximum number of FA, located in the core	141
Maximum flashout of fuel, % т.а.	0,1
Neutron-physical data of the core with lead target	
Number of FA for the core with lead target	134
Neutron generation intensity in target, 1/s	$1{,}21 \cdot 10^{14}$
Neutrons released to the core, 1/s	$1{,}14 \cdot 10^{14}$
Total energy release in target, kW	0,94
Loaded fuel UO_2-PuO_2, kg	396,8
K_{eff}	0,951
Lifetime of prompt neutrons, s	$2{,}4 \cdot 10^{-5}$
Effective fraction of delayed neutrons, %	0,373
Energy release in fuel, kW	26,1
Total energy release in the installation, kW	28,5
Neutron multiplication coefficient	22,6
Neutron generation intensity in the core, 1/s	$2{,}57 \cdot 10^{15}$
Maximum neutron flux density in the core at power 28,5 kW, $1/(cm^2 \cdot s)$:	
With energy from 20 to 1,0 MeV	$5{,}83 \cdot 10^{11}$
With energy from 1,0 MeV to 0,1 MeV	$1{,}62 \cdot 10^{12}$
With energy from 1,0 KeV to 100 KeV	$7{,}13 \cdot 10^{11}$
With energy from 0 to 20 MeV	$2{,}92 \cdot 10^{12}$

Table 4.1, continued

Description	Value
Average neutron flux density at the power 28,5 kW, 1/(cm^2·s): With energy from 0 to 20 MeV	$1,7 \cdot 10^{12}$
Neutron-physical data of the core with tungsten target	
Number of FA	132
Neutron generation intensity in target, 1/s	$1,14 \cdot 10^{14}$
Neutrons released to the core, 1/s	$1,04 \cdot 10^{14}$
Total energy release in target, kW	1,01
Loaded fuel UO_2-PuO_2, kg	390,9
K_{eff}	0,9526
Energy release in fuel, kW	23,8
Total energy release in the installation, kW	26,1
Neutron multiplication coefficient	23,1
Neutron generation intensity in the core, 1/s	$2,4 \cdot 10^{15}$
Lifetime of prompt neutrons, s	$2,24 \cdot 10^{-5}$
Thermohydraulic data of core and targets	
Coolant	Dried air
Direction of coolant flow through core	Top-down
Target material: - Lead target - Tungsten target	 Lead of C1 type alloy VNZh-95
Reflector material	Lead of C1 type
Pressure at core inlet, MPa	0,135
Temperature at core inlet, °C	Up to 50

Table 4.1, continued

Description	Value

Total discharge: - with lead target, kg/s - with tungsten target, kg/s	 0,60662 0,65
Average air temperature at core outlet: - with lead target, °C - with tungsten target, °C	 93 88
Pressure difference in the core: - with lead target, kPa - with tungsten target, kPa	 9,72 12,66
Discharge through lead target, kg/s	0,00662
Pressure difference on lead target, kPa	13,65
Maximum design temperature of fuel element in the core: - with lead target, °C - with tungsten target, °C	 131 159
Maximum design temperature of fuel element in the core, taking into account deviations: - with lead target. ^{0}C - with tungsten target, ^{0}C	 185 232
Maximum lead temperature in target: - without taking into account deviations. ^{0}C - taking into account deviations, ^{0}C	 176 214
Maximum tungsten temperature in target: - without taking into account deviations. ^{0}C - taking into account deviations, ^{0}C	 242 286

5 Design description

5.1 List of systems and equipment

5.1.1 Equipment composition of installation SAD is given in Table 5.1.

Table 5.1 - Equipment composition of installation SAD

DescriptionDesignation to SAD.00.000ТПQuantity1. Fuel assembly 2.Blanket housing 3. Lead target 4. Tungsten target 5.Hexahedral lead block 6. VEC case 7.Bottom reflector 8.Side reflector 9. Lead insert 10. Lead insert 11. Lead block 12. Lead block 13. Side reflector 14. Uper reflector 15. Protective plug 16. Protective plug 17. Protective plug 18. Protective plug 19. Upper ceiling 20. Turning plate 21. Reloading trolley 22. Thermoelectric converter 23. Three-zone thermoelectric converter SAD.01.000BO SAD.02.000BO SAD.03.000BO SAD.04.000BO SAD.05.000BO SAD.06.000BO SAD.07.000BO SAD.08.000BO SAD.09.000BO SAD.10.000BO SAD.11.000BO SAD.12.000BO SAD.13.000BO SAD.14.000BO SAD.15.000BO SAD.16.000BO SAD.17.000BO SAD.18.000BO SAD.19.000BO SAD.19.010BO SAD.20.000BO Пр. 75.000BO Т.107.000BO До 141 1 1 1 20 9 1 1 1 1 1 1 1 1 1 1 1 1 1 1 6 1

5.1.2 SAD.00.000 as gas-cooled subcritical system does not come under the action of the Rules PNAE G-7-008-89. Systems and equipment important for safety are classified by NP-033-01 and Design norms of seismic resistant nuclear power plants in accordance with NP-031-01 and are represented in Table 5.2.

Classified are systems and equipment, which come under responsibility zone of FSUE NIKIET in accordance with «Protocol on distribution of responsibility zones and designing limits of organisations participating in the project SAD» of December 2003. (Appendix B). An exclusion to this are fuel elements by VNIINM and intrahall temporary depositories, which design and procedure of usage are within responsibility zone of GSPI.

Table 5.2 - Classification of systems and equipment important for safety of SAD 00.000

Systems and elements Classification by NP-033-01Seismic resistivity category to NP-031-011 Fuel elements1HI2 Fuel assemblies1HI3 Blanket housing 2HI4 Target coarse (of lead target)2HI5 Equipment of average power level measurement channels3HI6 Case VEC2HI7 Pipelines of loop 1 2HI8 Remote tool for reloading FA and targets2HI9 Equipment and apparatus of KGO system2HIIб10 sensors and measurement devices of heat removal system parameters from the core3HI11 Lead reflector cases, hexahedral target blocks3HI12 Biological shielding elements3H3I13 Temporary depository in hall3H3I**5.2 Systems and equipment description**

5.2.1 General composition of SAD

The SAD is located in building, situated between Phasotron building (building No.1), YASNAPP lab building and outhouse No.4 of medical complex (KFK) at JINR site. The SAD is located in installation building in such a manner that the core center is situated 8 meters away from Phasotron building wall, along the axis of proton beam transportation channel at elevation level «+9,8 m». Proton beam is brought from below from bending magnets room. The developer of proton beam transportation channel is JINR.

The SAD is located within biological shielding, made of heavy iron-serpentinite concrete (γ=4,45 t/m3), steel and regular concrete. In the down direction, the shielding consists of regular concrete with an addition of approximately 1 % of boron carbide (B4C). Concrete thickness is 500 mm. In upper direction, the shielding

has a total thickness of 4400 mm, it consists, immediately under blanket housing, of protective plugs, made of heavy concrete (γ = 3,6 t/m3) and protective turning steel plate 200 mm thick.

The central hall floor is situated in installation building, at the elevation level +15,0 m. The central hall is a room of dimensions 14,3x 11,2 x 11 m (length x width x height), restricted by walls, made of regular concrete of maximum thickness up to 600 mm (from the direction of control room).

Central hall is a room, where personnel is addmitted to at non-operating installation only, when proton beam is not fed to target and gate valve of beam transportation channel is in position «closed».

A cran with hoisting capacity 30/5 t is installed in upper part of central hall, on constructional console supports, executed along the whole length of two opposite walls. The cran rails elevation level is «+23,0 m», elevation level of hooks in raised position 5t is - «+23,3 m», 30 t - «+22,6 m».

A vertical opening for proton beam passing E110 mm ("light size") is foreseen in the bottom part of biological shielding of installation, over the turning magnets room of proton beam transportation channel, behind gate valve in concrete ceiling (500 mm thick).

Openings E110 mm with aluminum pipe shells E108x4 for three horizontal experimental channels HEC1, HEC2 and HEC3 are situated in biological shielding at elevation levels «+9,2 m», «+9,8 m» and «+10,58 m» correspondingly.

Openings for coolant removal pipe ∅140x4 mm from the core and pipe ∅30x3 mm for coolant supply to lead target are executed at elevation level «+9,41 m» ; - opening for pipe ∅140x4 mm for coolant supply to the core as well as two slanting, at the angle 10 degrees to vertical installation axis, openings, organized for power control, which equipment is located in graphite moderator 100 mm thick, are located at elevation level «+10,22 m».

Protective plugs of biological shielding contain nine stepped openings for vertical experimental channels (VEC), six ∅60 mm times ∅43 mm for VECs above the core and three ∅90 mm times ∅70 mm above lead reflector. All openings for VEC are deadened with 3-meter steel plugs.

All three openings for HECs are output to horizontal experimantal channels room, which is not serviced during installation operation. Each opening is shut, at outlet from biological shielding, by steel gate of size 300x300 mm and 270 mm thick. Opposite to each opening, in the opposite end wall of HEC room, neutron beam stoppers, consisting of discs with diameter 450mm of various composition and thickness of materials (20 mm boron carbide, 100 mm polyethilene and 200 mm steel) are built-in.

Experimental devices, in which detectors can travel on the rope 2,5 mm in diameter by means of individual drives, can be installed in the VEC housings. The drives are mounted in the central hall, beyond the turning plate.

Openings with VECs are equipped with guiding aluminum pipes and bottom movable aluminum plugs 1400 mm long, suspended on the rope, which passes through the hole ∅5 mm in upper immobile stainless plug, installed on protective concrete plug SAD.16.000.

Central hall should provide for:

sockets for FA checking for tightness;

temporary depository for targets, cases with defect FA and VEC cases;

temporary depository for housing lids and other activated equipment;

dry assemblies for VEC with nozzles;

places for mounting «clean» protective plugs at carrying out transportation-technological operations.

Development and allocation of above equipment positions is executed by GSPI.

5.2.2 General layout of equipment, included in development responsibility zone of FSUE NIKIET, is shown in drawing SAD.00.000BO.

Steel bearing plate 120 mm thick, connected with biological shielding by 12 M20 anchor bolts is installed within cylinder coating on a frame, pored in concrete. The bearing plate has: one opening ∅90 mm for proton beam, four thread openings M30 for block fixture buckles of lead reflector, six thread openings M20 for fixture rods and two openings ∅20 mm for locating pins of blanket housing.

5.2.3 Blanket housing (drawing SAD.02.000BO) is installed in the hollow of bearing plate ∅740 mm and 66 mm deep on two locating pins and is fixed to it with six fixture rods.

Blanket housing is designed for location of replacable targets, bottom end reflector, FA, lead hexahedral blocks, other intra-housing elements, and to organise a cooling duct for air coolant. Blanket housing is made of steel of 12X18H10T type and consists of three main elements - upper tightening lid with press flange, central course and bottom end reflector, interconnected with fixture elements.

Bottom end reflector is a hermetic cavity, restricted with cylinder coarse ∅540 mm and two welded bottoms. Internal cavity volume is flooded with lead. Lead has two openings: the vertical one ∅80 mm for proton beam and horizontal one ∅110 mm for horizontal experimental channel. Lower bottom has two obtrusive segment flanges of external ∅730 mm. Flages have two holes ∅30 mm drilled for spacer rods and six holes ∅22 mm for blanket housing rods to fix to bearing plate.

Central coarse ends, in its upper part, with upper collector, made of forged element with dimensions 645x628x140mm, to which supply collector with dimensions 140x180x175 mm is welded. Supply collector is an octahedral pipe with "wrench" size of 140 mm and internal diameter of 132 mm, deadened from one end and reduced to round pipe ∅140x4 mm on the other end. Supply and upper collectors are interconnected with a rectangular-section box with "light" dimensions 440x60 mm. Upper collector flange has 16 holes M20 for press flange fixture, 4 holes M20

for cargo ring-bolts and two holes ∅5 mm installation of locating pins. Besides that, the side wall of collector has six holes ∅9 mm for cable output of thermoelectric converters (drawing Пр.75.000ВО).

The central coarse ends, in bottom part, with bottom and exit collectors, executed analogously to upper supply collector.

A hermetic chamber with internal cavity E75 mm, restricted in its lower part by welded membrane 1 mm thick, is cut in bottom collector of central part. The chamber serves as extension of proton duct and fulfils the function of pressure collector of lead target cooling loop. Coolant is supplied to chamber cavity through pipe ∅30Ч3 mm, tightly inserted in the side chamber branch pipe from one side and welded through connecting pipe into the side wall of bottom collector from the other side. At installation operation, coolant temperature at bottom collector runs up to 100°C, that is why the lead target cooling pipe inside collector is surrounded with thermoinsulation case - a pipe ∅40Ч1 mm.

Internal chamber diameter (∅75 mm) is executed to fit the mounting needs of replacable targets, besides that a pin E8mm is screwed in in the side wall of the chamber to orient targets in the core.

Bearing plate of blanket is installed and welded in holes ∅530 mm and ∅80 mm in the upper part of bottom collector. Bearing plate is a supporting structure for core elements and it is a round disc with a diameter 530 mm and 30 mm thick, perforated with holes for FA, VEC cases, lead blocks, FA simulators, peripheral

segment inserts, replaceble targets and coolant pass holes. Besides that, grooves for laying thermoelectric converters cables to control coolant output temperatures from the core and lead target are cut in it.

Upper collector of central coarse ends with a flange, in which a cut ∅545 mm and 18 mm deep is available, inside which a lid and sealing element - aluminumm alloy sealing of the type AD0 are installed. The sealing is pressed from the top by press flange by means of 16 non-falling screws of diameter M20, thus providing tightness of the blanket housing.

The lid has three connecting pipes with diameter 45 mm to install VEC cases and one connecting pipe with internal diameter 11,5 mm to install thermoelectric converter to measure thermoelectrically lead temperature in target. The given elements are tightened in blanket housing by means of sleeve nuts and sealings made from aluminum alloy AD0. The lid has a cut ∅48 mm for draw-in hold. The lid isto be replaced together with press flange and sealing element.

Dimensions of blanket housing - length 1345 mm, width 1020 mm, height 1340 mm. The mass of construction is 1250 kg.

5.2.4 The SAD core is assembled from FA (within 141 FA). The number of FA at initial loading is 134 for lead target and 132 for tungsten target. The number of FA is defined more exactly at physical start-up stage, based on designed subcriticality level of installation, equal to approximately 5%. FA are mounted in openings ∅5 mm of bearing plate on relular triangular net with a pitch 36±0,05 mm, whereas pitch

tolerance must be observed at sizing between any three holes. Total number of openings in plate is 156, three VEC cases and lead hexahedral blocks are inserted in openings not occupied byFA. External core loop is executed, to provide spacing of peripheral FA, of segments, which repeat side sizes and pitch of FA.

FA is an assembly of 18 fuel elements. Used is a rod-type fuel element, structurally it is a cylinder cladding of stainless steel, where fuel column,composed of mixed uranium dioxide and plutonium pellets, is placed. Fuel pellets are continuous, without internal opening. Cladding ends are tightened by welding of upper and bottom steel end pieces (plugs), bottom end piece is a supporting element, if fuel elements are situated in FA vertically. Fuel pellets column is pressed by a spring holder. Internal fuel element volume is filled with high purity helium. Ellipce-shaped spacing wire is spiraled on outer cladding surface.

Fuel element data are given in Table 5.3.

Table 5.3 - Technical data of fuel element

No. Designation Value Meaning1Fuel composition, % mass.70%UO2 + 30%PuO22Mass fraction of 239Pu versus plutonium isotopes sum, not less than % mass.953Mass fraction of 235U to uranium isotopes sum, not more than % mass.0,74Cladding materialSteel ЧС - 68 х.д.5Plug materialSteel ЭИ-8476Spacer wire materialSteel ЧС - 68 х.д.7Spring holder materialSteel 12Х18Н10Т8Fuel pellet size: 1) diameter, mm 2) height, mm 5,95-0,15 9,0 ± 19Cladding size: 1) external

diameter,mm 2) internal diameter,mm 6,9 ± 0,03 6,1 ± 0,0310Helium content in gas medium of intra-fuel-element volume, % vol., not less9511Spacer wire size, mm0,6 Ч 1,312Wire spiraling pitch, mm100 ±513Pellet density, g/cm10,4 ±0,214Fuel column weight in fuel element, g160 ±315Active part height of fuel element, mm580 ±10

Fuel assembly (drawing SAD.01.000BO) consists structurally of:

18 fuel elements;

supporting rod;

bottom spacer grid;

upper flange with case;

head to hold reloading tool.

Main supporting element of FA construction is bearing rod, to which bottom spacer grid, upper flange with case and FA head are welded. Bottom hexahedral grid, which is a spacer grid, i.e. a grid forming fuel elements bundle with a regular triangular net and a pitch of 7,6 mm, and , at the same time, fixing, i.e. a construction, where bottom tail ends of fuel elements are welded-fixed. The present grid has six openings of 3,5 mm diameter for passing coolant, which are superimposed with analogous in bearing plate while the fuel assembly is installed.

In upper part of supporting rod, hexahedral flange is welded, which has openings for coolant flow, and to which hexahedral steel case is welded, which is intended for forming and fixing the upper part of fuel element bundle. Each of six facets has lugs, providing FA spacing between each other in their upper part.

Lower rod part ends with a leg of 5 mm in diameter for FA landing in bearing plate of blanket housing.

Size and design of FA head is analogous to FA head of IBR-2 fast pulsed reactor and is designed to hold the FA by draw-in tool at FA loading and removing.

Steel of type 05Х12Н2М-ВИ to TU14-1-2761-79 or steel of type 05Х12Н2М to TU14-1-2836-79 is used as material of all FA constructs (with exception of fuel elements).

At SAD power operation, fuel assemblies are cooled by air flow, traveling top-down and pressing the FA to bearing plate, providing their stable position in the core.

Cases of vertical experimental channels are installed in three cells of the core (drawing SAD.06.000BO). The case is made of steel of type 12Х18Н10Т and consists of two main elements: head with sleeve nut and hexahedral pipe with "wrench" size 35 mm and internal diameter 33 mm with tail end ∅ 5 mm for mounting case in bearing plate of blanket housing. Case head has a cut ∅48 mm for draw-in hold, and pressure bronze ring, sealing from aluminum alloy AD0 and sleeve nut with "wrench"size 85 mm and thread М72Ч2 are used for sealing the case . VEC case dimensions: length 1001 mm, width 85 mm, height 98 mm. Its mass is 3,4 kg.

5.2.5 Replaceable targets.

5.2.5.1 Lead target (drawing SAD.03.000) consists of two-millimeter stainless steel housing, which is a construction resembling, by outer profile, an assembly of seven hexahedral prisms with "wrench" size 34 mm, installed with a pitch 36 mm, and

bottom and lid hermetically welded with it, also made of stainless steel. Six U-shaped stainless pipes ∅6Ч0,5 mm are installed in the internal target cavity, then the cavity is pored with lead. U-shaped pipes provide for lead target cooling at installation operation.The target has a cut ∅7 mm and 600mm deep for installation of three-zone thermoelectric converter to change lead temperature in the core center, upper and lower levels of the core.

A cylinder cavity of diameter 58 mm and 179 mm deep is made in lower target part to create optimal conditions for neutron generation.

To land the target in bearing plate of blanket housing, two landing rings ∅75f7 mm are installed through bushes at tail end of bearing plate, and groove is made for passing the rod ∅8 mm to orient target to installation angle.

A head is screwed in in the central part of target lid to effect transportation-technological operation. Head sizes are executed for draw-in hold of FA.

The lid has spacers for spacing with 12 adjacent hexahedral blocks, which are peripheral part of lead target. Overall target dimensions are: length 109 mm, width 101 mm, height 829 mm. Target mass is 52 kg.

Hexahedral lead block (drawing SAD.05.000BO) consists of hexahedral stainless pipe with "wrench"size 35 mm with internal diameter 33 mm and hermetically welded tail end and lid, made of stainless steel. Internal block cavity is pored with lead. The lid has spacers for spacing with adjacent core elements. A head with sizes for draw-in hold for FA is screwed-in in the lid. The tail end has end piece

∅6 mm to install the block in bearing plate of blanket housing. Overall block sizes: length 43 mm, width 37 mm, height 802 mm. Mass of block is 7,7 kg.

5.2.5.2 Tungsten target (drawing SAD.04.000BO) is assembled of two types of plates of alloy VNZh-95, 28 mm thick (with central opening of 58 mm in diameter or without it). Plate is a hexahedral, by external profile, assembly of 33 mm "wrench" size prisms, located with a pitch of 36 mm. Plate ends have: upper end - a recess with diameter68H7, bottom end - a boss with diameter 68f7 with three cuts. There is lead layer $0{,}2 \pm 0{,}1$ mm between plates, which assumes a role of heat conductor. While being assembled, the plates are centered to diameter 68H7/f7. Plates are drawn together by screws M6 (3 screws for each 5 plates, with a turn of thread connection place for 120° for each 5 following plates etc.). Bottom target part has a cylindrical cavity 58 mm in diameter, 179 mm deep (within 5 plates VNZh-95 and tail end of target). Tail end and lid of the target are made of steel 12X18H10T. Tail end is analogous to lead target tail end (SAD.03.000BO) as concerns orientation place by target installation angle (a cut for rod passing 8 mm) in bearing plate of blanket housing and two landing rings 75f7 in diameter and bushes. End split bush is fixed by welding (interrupted welding joint). The lid has spacer bosses for spacing with a neighbouring row of FA, providing for a 2 mm slit between fuel element surface of first row and target surface. To carry out transportation-technological operations, a head sized for draw-in hold for FA is screwed in in the central part of target lid.

Overall dimensions of tungsten target: length 109 mm, width 101 mm, height 829 mm. The mass of target is 85 kg, incl. alloy VNZh-95 - 78 kg.

5.2.6 The installation core is surrounded by lead reflector, it is about 600 mm thick in side direction and 300 mm thick in directions up and down from the core ends. The reflector is assembled of lead blocks and inserts, cased into 5 mm steel sheets. Each block is fixed, during assembly, with two bushes 78 mm in diameter, placed on buckles, which connect all blocks to a unified monolithic construction. Lead blocks forming side perimeter of reflector have two outer concentrical coarses, organising a 30-mm cavity filled with boron carbide (B4C). the same blocks have, in VEC openings, aluminum pipe sleeves ∅64Ч2 mm.

Bottom reflector (drawing SAD.07.000BO) is mounted on bearing plate on two fixing bushes. The block has openings for blanket housing, coolant supply pipe to target and coolant output pipe from the core, bottom collector lodgement, two segment niches for lead inserts (drawing SAD.09.000BO, drawing SAD.10.000BO), horizonlal opening ∅110 mm for HEC, two vertical openings ∅65 mm for VEC and four vertical openings ∅46 mm for buckling the block fixtures. The block has four openings for ring-bolts M36. Overall dimensions of block - external coarse diameter 1830 mm, height 366 mm. The mass is 8211 kg.

Side reflector (drawing SAD.08.000BO) is placed on bottom reflector on two fixing bushes. The block has openings for blanket housing, coolant supply pipe to core, upper collector lodgement, horizonlal opening ∅110 mm for HEC, two vertical

openings ∅65 mm for VEC and two vertical openings ∅46 mm for buckling the block fixtures. The block has four openings for ring-bolts M36. Overall dimensions of block - length 1830 mm, width 1257mm, height 810 mm. The mass is 10214 kg.

After lead blocks SAD.07.000 and SAD.08.000 are assembled and blanket housing SAD.02.000 is mounted, two lead inserts (drawing SAD.09.000BO, drawing SAD.10.000BO) are installed in the gap formed between the housing and bottom block. At bottom, the inserts are fixed by two pins, screwed in in blanket housing segment flanges, and at the top - by two plates inserted in corresponding pockets of upper ends of inserts and bottom block. After installation, the plates are fixed by welding.

Insert SAD.09.000 has an opening for lead target cooling pipe. Each insert has two openings for ring-bolts M10. Overall dimensions of inserts: length 365 mm, width 127 m, height 410 mm. The mass of insert SAD.09.000 - 120 kg, SAD.10.000 - 130 kg.

Space between blanket housing up to upper flange and side lead reflector is filled with two lead blocks (drawings SAD.11.000BO, SAD.12.000BO), which are fixed in reflector with plates, inserted in corresponding block pockets.After installation, the plates are fixed by welding. The block SAD.11.000BO has an opening for laying cables from thermoelectric converters Пр.75.000BO. Each block has two openings for ring-bolts M10. Overall dimensions of blocks: length 542 mm,

width 175 mm, height 774 mm. The mass of block SAD.11.000BO - 189 kg, SAD.11.000BO - 195 kg.

Side reflector (drawing SAD.13.000BO) is placed on bottom reflector on two fixing bushes. The block has opening for blanket housing upper flange, one vertical opening ∅65 mm for VEC and two vertical openings ∅46 mm for buckling the block fixtures. The block has four openings for ring-bolts M36. Overall dimensions of block - length 1694 mm, width 1098mm, height 810 mm. The mass is 8787 kg.

Upper reflector (drawing SAD.14.000BO) is placed on side reflectors on two fixing bushes. The block has opening E900 mm for protective plug (drawing SAD.15000BO), foreseen are one horizontal opening E110mm for HEC, two vertical openings ∅65 mm for VEC and four vertical openings ∅46 mm for buckling the block fixtures. The block has four openings for ring-bolts M36. Overall dimensions of block - external coarse 1830 mm, height 394 mm. The mass of block is 7857 kg.

5.2.7 Biological shielding consisting of removable and fixed protective plugs is located above blanket housing and upper reflector. Plugs layout in the pit housing is executed in such a way, that their weight load is supported by biological shielding. Structurally, all plugs consist of 10mm coarses with pipe and rip rigidity elements and bottoms and lids welded to them. To locate plugs between each other and relative to pit housing, bosses and corresponding grooves are foreseen.

Protective plug (drawing SAD.15.000BO) is filled, in its bottom part, with lead 300 mm thick, all further internal cavity is filled with heavy concrete with boron

carbide (γ=3,6 t/m3). The plug has six openings ∅43 mm for core VECs, deadened with steel plugs, one opening ∅70 mm for reflector VEC, one opening ∅110 mm for HEC and bottom cavity sized 520x310x80 mm for connecting pipes, which lug above blanket housing lid. The plug lid has 4 openings for ring-bolts M30. Overall dimensions of the plug are: lid diameter 1000 mm, coarse diameter 880 mm, height 1110 mm. Mass of the product is 4500 kg. The plug is removed when transportation-technological operations are being carried out. All internal cavity in protective plug (drawing SAD.16.000BO) is filled with heavy concrete (γ=3,6 t/m3). The plug has 6 openings ∅60 mm for the core VECs and 3 openings ∅90 mm for reflector's VECs. the plug lid has 4 holes for ring-bolts M64. Overall dimensions of the plug are: lid diameter 1860 mm, upper coarse diameter 1500 mm, bottom coarse diameter 1000 mm, height 3090 mm. The product mass is 19000 . The plug is removed when transportation-technological operations are being carried out.

Fixed protective plug (drawing SAD.17.000BO) is filled in its bottom part with heavy concrete with boron carbide for 150 mm and further all internal cavity is filled with heavy concrete. The plug has two openings of 70 mm in diameter for VECs of reflector and a cylindrical cavity 1020 mm in diameter with a step 60 mm wide for mounting removable protective plugs SAD.15.000 and SAD.16.000. Upper lid of plug at diameter 1330 mm has two housing sockets ∅160 mm for installation boxes with target, 6 sockets ∅80 mm for installation boxes with FA and 3 sockets ∅43 mm for

deadening plugs of protective plug SAD.15.000. The plug lid has 4 openings for ring-bolts M64. Overall plug dimensions are: coarse diameter 2350 mm, height 1775 mm. Mass of the product is 22000 kg.

Fixed protective plug (drawing SAD.18.000BO) is executed in the form of a ring, which internal cavity is filled with heavy concrete. A removable protective plug SAD.16.000 is installed in the internal coarse of plug E1520 mm. The plug has one opening ∅90 mm for VEC of the reflector. The plug lid has 4 openings for ring-bolts M64. Overall plug dimensions are: outer diameter 2750 mm, height 1775 mm. Mass of the product is 28550 kg.

5.2.8 Upper protectice ceiling (drawing SAD.19.000BO), designed to protect personnel during transportation-technological operations, is installed above protective concrete plugs at central hall floor level at elevation +15 m. Upper ceiling consists of main units: framework and turning plate.

5.2.8.1 Framework is a welded steel construction, consisting of two concentrical coarses, bottom and lid. To exactly locate the plate in biological shielding, six small plates are welded to bottom. Internal coarse has a boring ∅2365 mm for exact positioning of the turning plate. The cavity between two coarses is filled with concrete. Three gags are welded in the lid to install ring-bolts M36, the plate has recess 184 mm deep to mount the turning mechanism column. Overall dimensions of the plate are: outer diameter 3560 mm, height 290 mm. The mass is 8600 kg.

5.2.8.2 Turning plate (drawing SAD.19.010BO) consists of fixed steel bearing plate , which has a track filled with steel balls, on which the turning circle moves around. The rotation is effected by the column through reducer by means of bobbin transmission.The turning circle is fixed at prescribed coordinates by two set bolts. The turning circle has two openings ∅110 mm to maintain peripheral VECs of reflector, rectangular opening 350Ч1090 mm to maintain the core VECs and one VEC of the reflector, and to install, through it, a rod with TV-camera, two openings ∅195 mm to install lamps, one opening ∅383 mm to install reloading container.

All openings are closed, at installation operation, with protective plugs, besides it, a viewing port made of lead glass is installed at turning circle.

The plug, covering rectangular aperture, foresees availability of an additional aperture sized 66Ч805 mm to install reloading trolley. At installation operation, the aperture is closed with protective plug, which has an opening ∅50 mm, closed with a plug, for not-falling-out screws of blanket housing lid fixture. Overall sizes of the product are: length 2678 mm, wodth 2485 mm, height 200 mm. Its mass is 8000 kg.

5.2.9 Reloading trolley (drawing SAD.20.000BO) consists of a frame and carriage, which moves along it. The frame is welded of steel sheets and has two runners, on which the carriage with a steel protective plate attached to it travels along carriage on four wheels. A guide is inserted in plate, where the guide has an opening and landing place for tools to hold the FA, hexahedral lead blocks, VEC and target cases. Carriage guide travels in the groove, executed in frame base, the maximum

shuttle distance is 665 mm. At carrying out reloading works, the trolley is placed and fixed on turning plate, at that the carriage guide is placed in plate aperture and travels forward within shuttle distance of the carriage. Thus, disposing of circle movement of turning plate and forward movement of carriage, a possibility is provided to work with any core element and to move elements to technological sockets (housings) in protective plug SAD.000. Overall dimensions of carriage are: length 1850 mm, width 366 mm, height 530 mm. Mass of the product is 430 kg.

5.3 SAD operation mode

Subcritical multiplying blanket with target is created for experimental check of theoretical predictions and evaluation of technological possibilities to create major subcritical assemblies with proton accelerators designed for utilization (burning out) of long-lived plutonium isotopes, minor actinides of americium, neptunium, curium and some long-lived fission products.

Requirements to ressourse restrictions and operation modes of installation are defined in technical assignment (Appendix A): installation should work in the course of not less than 10 official years with average run time 1000 hours/year. Periodicidy of installation usage during each year is defined by research program and is from 24 hours to 300 hours per cycle (start-up, power increase to full power, operation at full power, shut-down).

The project assumes that first experimental program for the core with lead target is carried out, and, upon its completion, the core is recomposed for tungsten target and, in this composition, the SAD works untill the end of its design ressource.

Regular SAD operation mode is operation mode at average heat power of installation not higher than 30kW, at power of target-incident proton beam not higher than 1kW, at regular operation of all heat removal, control and protection systems with nominal parameters defined for them, controlled by control means within measurement precision limits of these parameters.

Neutron-physical parameters of subcritical core, thermohydraulic parameters of heat removal systems are defined and calculation estimates of temperature fields in fuel and constructs are represented in sections 6 and 7.

Assumed operation limits related to subcriticality level are not less than 2 %, fuel element cladding temperature - 250°C, lead target converting material temperature not higher than 250°C, tungsten - not higher than 300°C, coolant pressure-bearing element temperature not higher than 400°C, are not reached, according to calculation investigations under regular (see section 6 and 7) and emergency (12.6) operation conditions.

5.4 Transportation-technological operations

Main transportation-technological operations at installation are carried out at assembling of initial load of the core with lead target, at lead target replacement for tungsten target and at an accident, connected with FA depressurization.

The works are carried out on permission of dosimetry control service by personnel, duely admitted to carry out such works in accordance with technological instruction of carrying out reloading works at SAD installation. The core subcriticality level should be controlled during the whole cycle of above works. The works should be carried out under control of duty physicist.

5.4.1 Initially, the core is loaded with manual tool from turning plate by replacing FA imitators for FA, and by installation lead target with lead hexahedral blocks and is described in section 6 in detail.

5.4.2 Transportation-technological operations related both to target replacement and defect FA search are carried out at switched off accelerator after six-month time lag and are to be executed after a number of preliminary operations, such as:

5.4.2.1 To check readiness of all services and systems, availability and intactness of tools, accessories and rigging required for works.

5.4.2.2 If VEC with hanging elements are available in the core, remove rectangular protective plug from turning plate by crane, disconnect the rope from drive, having fixed it in cutoff point, connect crane ropes to ring-bolts on VEC flange, remove VEC by crane through aperture in turning plate and place it in dry assembly in central hall, then close the aperture with protective plug.

5.4.2.3 Install ring-bolts in turning plate SAD.19.010, connect to them crane ropes. By crane, remove turning plate from its regular place, move it to preliminary storage place in central hall (Figure 5.1).

5.4.2.4 Repeat analogous operations for «clean» protective plug SAD.16.000 (Figure 5.2).

5.4.2.5 Remove protective plug SAD.15.000 from its regular place and move it to specially alotted cell in central hall. At carrying out this operation, the personnel in the hall should hide themselves behind shadow shielding from direct visibility of bottom active part of the plug (Figure 5.3).

5.4.2.6 Return, by crane, the turning plate SAD.19.010 from its pleliminary storage place in central hall to its regular place and fix it with two set bolts. Remove by crane, in turn, protective plugs from plate and install, in corresponding openings, two lamps and TV camera rod, after that install protective plugs at their regular places. Apply power to lamps and TV camera (Figures 5.4 - 5.6). The lamps must be in the area of elevation «+13,0 m», and TV camera - in elevation area «+11,5 m».

5.4.2.7 Remove, by crane, from rectangular plug of turning plate, and install on the floor of central hall the round protective plug, located on one vertical axis with VEC case, drop, by crane through opening, nut-turning device onto sleeve nut of VEC case head (drawing SAD.06.000 BO). With nut-turning device, unscrew the sleeve nut, thus disconnecting VEC case from connecting pipe of blanket housing lid.

Return nut-turning device by crane to its regular place on the wall of central hall, install round protective plug to its regular place in turning plate (Figure 5.7).

5.4.2.8 Produce analogous operations to item 5.4.2.7 with sleeve nuts on the heads of two remaining VEC cases.

5.4.2.9 Through horizontzl aperture for HEC3, disconnect, by special tool, the plug connector at the head of three-zone thermoelectric converter. (drawing T.107.000BO).

5.4.2.10 Remove, by crane, from rectangular plug of turning plate, and install on the floor of central hall the round protective plug, closing aperture above the head of three-zone thermoelectric converter. Sink, by crane through opening, nut-turning device onto sleeve nut and unscrew the sleeve nut, thus disconnecting the product from connecting pipe of blanket housing lid. Return nut-turning device by crane to its regular place on the wall of central hall.

5.4.2.11 Sink the tool by crane through the same aperture on the head of thermoelectric converter, capture it, lift it to central hall and install it in corresponding dry storage cell. After that put the tool by crane to central hall wall. During product transportation through central hall, personnel must hide themselves behind shadow shielding (Figure 5.8).

5.4.2.12 In turning plate, replace by crane the rectangular plug with four round plugs for rectangular plug with rectangular aperture, designed for installation of reloading trolley.

5.4.2.13 Install by crane the reloading trolley in aperture (drawing SAD.20.000BO). Fix it with bolts on turning plate.

5.4.2.14 By crane, install the manual tool with VEC case head hold in landing opening of trolley carriage. Unfix the moving plate.

5.4.2.15 By combined rotation of turning plate and linear movement of reloading trolley carriage, place the synchronously moving , by crane, tool rod over VEC case head, fix the turning plate in this position by two set bolts, capture and lift the product from the core cell.

5.4.2.16 Move the TV camera upwards to area with elevation level «+13,5 m». By crane, lift the tool with suspended VEC case to elevation level «+12,485 m» (landing socket level in protective plug SAD.17.000) unfix the turning plate, and rotating turning plate and moving reloading trolley carriage synchronously with crane, install the tool above reloading case , having fixed turning plate, and drop VEC case in corresponding reloading case. Uncouple the product from tool, move the TV camera to previous level, unfix the turning plate (Figure 5.9).

5.4.2.17 Carry out, in analogous way, operations under items 5.4.2.15 and 5.4.2.16 to move remaining VEC cases.

5.4.2.18 By crane, install guiding pipe and protective container on turning plate instead corresponding protective plug.

5.4.2.19 Rotate turning plate till vertical container axis coincides with reloading case axis with VEC case inside it, fix turning plate in this position by two set bolts.

5.4.2.20 Capture VEC case head with container tool, carry the product, by means of winch installed on container, inside container and fix it in the container.

5.4.2.21 By crane, move the container to specially alotted temporary storage cell in central hall, move VEC case from container to depository cell. Return the container to guiding pipe, installed on turning plate. Unfix the turning plate (Figure 5.10).

5.4.2.22 In analogous way, carry out operations under items 5.4.2.19 - 5.4.2.21 to reload two remaining VEC cases.

5.4.2.23 After the last VEC case is unloaded in temporary storage cell, place, by crane, the protective container with guiding pipe, tool and reloading trolley in their regular places in central hall, having closed apertures in turning plate with corresponding protective plugs. Return the TV camera to lower level.

5.4.2.24 Remove round protective plug from rectangular protective plug of turning plate, sink, by crane, the nut turning device in opening, rotating the turning plate with column handle, combining the "mouth" of nut turning device with the head of screw fixing the lid to blanket housing flange, unscrew them. Fix turning plate at each operation (Figure 5.11).

5.4.2.25 After uncoupling operation, return nut turning device, by crane, to its regular place on the wall of central hall, having closed the opening in turning plate with a plug.

5.4.2.26 Remove, by crane and in series, protective plugs with corresponding lamps and TV camera from turning plate, having disconnected them beforehand from power supply, locate lamps and TV rod to their regular places in central hall, return protective plugs, by crane, to their regular places in turning plate.

5.4.2.27 By crane, remove turning plate from its regular place and move it to temporary storage place on the floor of central hall.

5.4.2.28 By crane, move protective plate 200 mm thick with screw hold from its regular place in central hall to elevation level +11,42 m in SAD pit, and install it there, having combined vertical axis of screw hold and thread opening in blanket housing lid. The personnel of installation must go downstairs on protective plate in the pit. Being on protective plate, screw in the screw hold into thread opening of blanket housing lid. The personnel has to quit the pit and to move, by crane, the protective plate with suspended lid into corresponding special pit in the central hall, uncouple the plate from "dirty" lid, move protective plate to its regular place in central hall, close the special pit with "dirty" lid with protective plug. During lid transportation in central hall, the personnel must hide themselves behind shadow shielding (Figure 5.12).

5.4.2.29 By crane, move turning plate from temporary storage place in central hall to its regular place in upper ceiling.

5.4.2.30 Remove, by crane and in turn, protective plugs from plate and install two lamps and the rod with TV camera in corresponding openings, then install

protective plugs in their regular places. Supply power to lamps and TV camera (Figure 5.7).

5.4.3 Transportation-technological operations at replacement of lead target for tungsten target.

5.4.3.1 By crane, remove rectangular protective plug covering aperture for reloading trolley installation from turning plate and install it on the floor of central hall.

5.4.3.2 Move reloading trolley from its regular place in central hall and install it the aperture. Fix it on turning plate with bolts.

5.4.3.3 Place manual tool with hold for FA, target and hexahedral lead block heads in landing opening of the trolley carriage.

5.4.3.4 By, at the same time, rotating turning plate and linear move of reloading trolley carriage, place the tool rod above lead taget head moved synchronously by crane, fix turning plate in this position with two set bolts, capture and lift the product from the core cell.

5.4.3.5 By crane, lift the tool with suspended lead target to elevation level not higher than"+11,0 м", take it to the side of central axis to blanket housing flange level, then lift it to elevation level «+12,485 m» (level of landing sockets in protective plug SAD.17.000) , unfix turning plate and, rotating turning plate and moving reloading trolley carriage synchronously with crane, place the tool above free reloading case, having fixed turning plate and drop lead target into the case (the second case is

occupied with tungsten target, which was installed there during initial loading of the core). Uncouple the product from the tool, unfix turning plate (Figure 5.13).

5.4.3.6 Direct the turning plate with tool suspended on crane towards the case with tungsten target, fix the turning plate.

5.4.3.7 Capture the product head and lift it from reloading case, unfix the turning plate.

5.4.3.8 By combined rotation of turning plate and linear movement of reloading trolley carriage synchronously with crane, install the tool with suspended tungsten target over corresponding core cell, fix the turning plate , by crane, sink the tool in landing opening of reloading trolley carriage, at that, the target will take its place in the core.

Uncouple tool hold from tungsten target head, unfix turning plate.

5.4.3.9 By combined rotation of turning plate and linear movement of reloading trolley carriage, install the tool rod synchronously to moved by crane over head of one of twelve hexahedral lead block (succession of blocks moves is defined by reloading cartogram). Fix the turning plate in this position with two set bolts, capture the product and lift it from core cell.

5.4.3.10 By crane, lift the tool with suspended lead block to elevation level "+12,485 м", unfix turning plate and, rotating turning plate and moving reloading trolley carriage synchronously with crane, place the tool above reloading case,

intended for FA of lead block. Fix turning plate and sink the product in reloading case.

Uncouple lead block head from tool hold, unfix turning plate.

5.4.3.11 Move turning plate with tool suspended at crane to a FA in utmost peripheral row of the core (succession of rearrangement of FA with lead blocks is defined by reloading cartogram). Fix the turning plate , by crane, sink the tool in landing opening of reloading trolley carriage. Capture the FA head with tool and lift it from core cell, unfix turning plate.

5.4.3.12 By combined rotation of turning plate and linear movement of reloading trolley carriage simultaneeously with crane, install the tool with suspended FA above cell freed after removal from there of lead block. Fix the turning plate, and sink it in FA cell. Uncouple tool hold from FA head, unfix turning plate.

5.4.3.13 By combined rotation of turning plate and linear movement of reloading trolley carriage, place the tool rod synchronously to that at crane above the head of next lead block according to lead block rearrangement. Fix turning plate in this position, capture the product with tool and lift it from core cell.

5.4.3.14 Unfix turning plate and, turning it with synchronously moving reloading trolley carriage and crane, install the tool with lead block above a cell of peripheral core row that was freed from FA. Fix turning plate and sink it in lead block cell. Uncouple tool hold from lead block head, unfix turning plate.

5.4.3.15 Carry outanalogous operations under items 5.4.3.11 -5.4.3.14, thus replacing 12 hexahedral lead blocks for 12 FA from peripheral row of the core. Two FA from peripheral row replace with two lead blocks, placed in corresponding reloading cases in protective plug sockets SAD.17.000 during initial loading of the core. Carry out replacement operations in the same succession as replacing lead target for tungsten target (see items 5.4.3.5 - 5.4.3.8).

5.4.3.16 By crane, place guiding pipe and protective container, instead of corresponding protective plug, on turning plate.

5.4.3.17 Rotate turning plate till vertical container axis coincides with reloading case axis with lead target inside, fix turning plate in this position by two set bolts (Figure 5.14).

5.4.3.18 Capture lead target head with container tool, bring the product, by means of winch, installed on container, inside container and fix it there.

5.4.3.19 By crane, move the container to specially alotted temporary storage cell in central hall, move lead target from container to storage cell, return container to guiding pipe installed on turning plate. Unfix turning plate.

5.4.3.20 In analogous way, carry out operations under items 5.4.3.17 - 5.4.3.19 to reload two FA from reloading cases to alotted temporary storage cells in central hall.

5.4.3.21 All works to replace lead target for tungsten target must be controlled by TV camera, which position height in SAD pit is defined by a particular reloading operation.

5.4.4 Transportation-technological operations related to search of a defect FA.

5.4.4.1 Defect FA search operations consist in serial removal of FA from the core and their subsequent delivery to sockets in container, where they are checked for hermeticity. Checked hermetic FA are placed back in the core instead of those being removed for check.

5.4.4.2 By crane, remove, from turning plate, and install on central hall floor the rectangular protective plug that overlaps aperture for installation of reloading trolley and plug closing aperture for installation of guiding pipe with container.

5.4.4.3 By crane, move from regular place in central hall and install on turning plate, in corresponding apertures, reloading trolley and guiding pipe with container.

5.4.4.4 By crane, install manual tool with hold for FA heads in landing opening of reloading trolley carriage.

5.4.4.5 By combined rotation of turning plate and linear movement of reloading trolley carriage placel the tool rod synchronously to that at crane above the head of FA, fix turning plate in this position with two set bolts, capture the product with tool and lift it from core cell.

5.4.4.6 By crane, lift the tool with suspended FA to elevation level "+12,485 m" (landing sockets level in protective plug SAD.17.000), unfix turning plate and,

rotating turning plate and moving reloading trolley carriage synchronously with crane, place the tool above free reloading case, and sink the FA in case (the second case is occupied by FA imitator, installed during initial loading of the core). Uncouple product from container tool, unfix turning plate.

5.4.4.7 Direct the turning plate with tool suspended on crane towards the case with FA imitator, fix turning plate.

5.4.4.8 Capture product head and lift it from reloading case, unfix the turning plate.

5.4.4.9 By rotating the turning plate and moving reloading trolley carriage synchronously with crane, place the tool with suspended FA imitator above corresponding core cell, fix turning plate, by crane, sink the tool in landing opening of reloading trolley carriage, at that the FA imitator takes its place in the core. Uncouple tool hold from FA imitator head, unfix the turning plate.

5.4.4.10 Turn the turning plate untill container vertical axis is combined with the axis of reloading case with FA, fix the turning plate in this position with two set bolts.

5.4.4.11 Capture FA head with container instrument, move the product, by means of winch installed on container, inside container and fix it there.

5.4.4.12 By crane, move the container to specially alotted socket to check FA hermeticity in central hall, move the FA from container to socket. Move container to neighbouring socket, where checked hermetic FA is installed, carry out item 5.4.4.11.

Return container to guiding pipe, installed on turning plate. Above free reloading case, sink the FA in case. Uncouple the product from container tool, unfix turning plate.

5.4.4.13 Reloading operations under items 5.4.4.5 - 5.4.4.12 are to be carried out untill a defect FA is found, then load the core additionally according to regular loading cartogram.

5.4.4.14 All works, related to defect FA search, must be monitored with TV camera, which height location in SAD pit is defined by a particular reloading operation.

5.4.5 After operations under item 5.4.3 or 5.4.4, the following operations should be carried out:

5.4.5.1 By crane, place protective container with guiding pipe and reloading trolley in their regular places in central hall, close apertures in turning plate with corresponding protective plugs.

5.4.5.2 By crane and in series, remove protective pluds with corresponding lamps and TV camera, after prior having deenergized them, from turning plate, place lamps and TV camera rod in their regular place s in central hall, by crane, return protective plugs in their regular places in turning plate.

5.4.5.3 Apply «clean» blanket housing lid to protective plate by screw hold (after prior having deadened the connecting pipe for thermoelectric converte with a plug with aluminum sealing).

5.4.5.4 By crane, remove turning plate from its regular place, move it to temporary storage place on central hall floor.

5.4.5.5 By crane, move protective plate with "clean" lid from central hall to elevetion level «+ 11,42 m» in SAD and install the lid on blanket housing flange, fix it on two guiding pins. Uncouple protective plate from lid.

5.4.5.6 Place, with manual tool, three "clean" VEC cases in corresponding reloading channels in protective plug SAD.17.000.

5.4.5.7 By crane, move the plate to its regular place in central hall.

5.4.5.8 By crane, move turning plate from temporary storage place to its regular place in upper ceiling.

5.4.5.9 By crane and in turn, remove protective plugs from the plate and placel two lamps and TV camera rod in corresponding openings, than place protective plugs in their regular places. Apply power to lamps and TV camera.

5.4.5.10 By crane, remove the round protective plug from rectangular plug, then by crane through opening, sink the nut turning device rotating the turning plate with column handle, coinciding, in turn, "the mouth" of nut turning device with head of lid fixture screw to blanket housing flange. Fix turning plate at each operation. Return round protective plug to its regular place .

5.4.5.11 By crane, remove rectangular plug from turning plate, thus freeing aperture for reloading trolley.

5.4.5.12 By crane, place reloading trolley in aperture, fix it on turning plate with bolts.

5.4.5.13 By crane, install manual tool with hold for VEC case head in landing opening of reloading trolley carriage.

5.4.5.14 By combined rotation of turning plate and linear move of reloading trolley carriage, place the tool rod, synchronously moved at crane, above VEC case head, located in reloading case at elevation level «+ 12,485 m». Fix turning plate, capture and lift the product from case.

5.4.5.15 Unfix turning plate and by combined rotation of turning plate and linear move of reloading trolley carriage synchronously with crane, place the tool with VEC case above opening in connecting pipe of blanket housing lid, which is on the same axis as the free core cell.

5.4.5.16 Fix the turning plate, by crane, sink the tool in landing opening of reloading trolley carriage, at that the VEC case will take its place in the core. Uncouple the hold of the tool from VEC case head, unfix the turning plate.

5.4.5.17 In analogous way, carry out in series operations under items 5.4.5.14 - 5.4.5.16 to move other VEC cases.

5.4.5.18 By crane, remove from turning plate and install tool and reloading trolley in their regular places in central hall. Close the aperture in turning plate with protective plug.

5.4.5.19 By crane, replace, in turning plate, rectangular plug of reloading trolley for rectangulat plug with four round plugs.

5.4.5.20 By crane, remove from rectangular plug of turning plate and install on central hall floor the round protective plug, located on one vertical axis with VEC case; then by crane through opening, sink the nut turning device on sleeve nut of VEC case head. Tighten the sleeve nut with nut turning device. By crane, return nut turning device to its regular place on central hall wall, return round protective plug to its regular place in turning plate.

5.4.5.21 Carry out analogous operations under item 5.4.5.20 with sleeve nuts on heads of two other VEC cases.

5.4.5.22 By crane, in series, remove from turning plate protective plugs with corresponding lamps and TV camera, previously having disconnected them from power, locate lamps and the rod with TV camera in their regular places in central hall, by crane, return protective plugs in their regular places in turning plate.

5.4.5.23 By crane, remove turning plate from its regular place and move it to temporary storage place on central hall floor.

5.4.5.24 By crane, move protective plug SAD.15.000 from the cell in central hall to its regular place in SAD pit. During this operation, personnel must hide behind shadow shielding out of direct visibility of bottom active part of the plug.

5.4.5.25 Move protective plug SAD.16.000 from central hall floor to its regular place in the SAD pit.

5.4.5.26 By crane, return turning plate from temporary storage place in central hall to its regular place in upper ceiling.

6. Results of neutron-physical calculations

6.1 Calculation model and method of calculations

Subcritical multiplying blanket with target (SAD) of the SAD installation is a core, collected from fuel assemblies, where a lead or tungsten target converting the proton beam into neutrons is located along the central axis of the core. The core is surrounded by side and butt-end reflectors and other constructs. Proton beam is conducted to target from bottom through a hollow channel.

The calculation model of installation describes in detail fuel elements, fuel assemblies, target, displacers in the core (lead and steel), fuel assemblies simulators, reflectors, boron carbide absorbent layer on external surface of side reflector. The calculation model includes also concrete constructions described by homogenized layers, which surround the external surface of reflectors and that of absorbent layer.

Neutron-physical data of the subcritical assembly were calculated at two stages. At the first stage, proton beam interaction with target was calculated and space-energy distribution of neutrons generated in the target was formed. At the second stage, space-energy distribution of neutron flux densities of reactor energies (below 20 MeV) and neutron and gamma-ray field functionals were calculated for a subcritical task with external source (results of the first stage were used). At the second stage, K_{eff} is also calculated in conditionally critical approximation to determine the subcriticality level and reactivity effects.

The program LAHET [1] was used to calculate neutron generation and energy release field in target (first stage). This program realizes the Monte-Carlo-method to describe the transfer, in the target, charged high-energy particles and secondary particles, generated in nuclear reactions. The program LAHET is the most world-known and world-used program for such calculations. It can be used both independently and in combination with MCNP in a united complex MCNPX.

For neutron-physical calculations of the core (second stage), the program MCNP-4B [2], realizing the Monte-Carlo method, was used. It allows to adequately describe three-dimensional structure and materials of an assembly, it uses point-to-point representation of sections, it models, in the framework of a single calculation, the transfer of neutrons, photons and electrons, it allows to yield all data needed for the project with a very high precision. The authors of the present section supplemented the program MCNP with some additions, which allowed to calculate the delayed neutron transfer. The possibility of use of this program and nuclear data library ML-45 [3] was substantiated on calculation modeling of experiments, carried out at putting into operation the acting reactor IBR-2, as well as on experiments on small critical assemblies with similar features. [4].

6.2 Choice of core composition and main neutron-physical data of SAD.

The FA, target and displacers located within the core housing are constructs, allocated according to a regular triangular netting with a pitch of 3,6 cm. Lead

target consists of 13 elements. An element, joining 7 hexagonal prisms, is situated in the center of target, it is surrounded by 12 hexagonal prisms along its periphery, the “wrench size” is 3,45 cm, the mounting pitch is 3,6 cm. The tungsten target is executed as a construction of a united element, which includes 7 hexagonal prisms.

The base variant of core composition choice was a variant with lead target. Based on results of preliminary neutron-physical calculations, a core cartogram was chosen, which included 141 cells for allocation of fuel assemblies with a pitch of 3,6 cm, and three experimental vertical channels, located in cells, which are not occupied by fuel assemblies. One channel is located near target, another – in the middle of radial thickness of the core, and one channel – in external row of FA with a displacement of 120 degrees. Outer side surface of the core is surrounded by steel displacers, which complete it to cylinder shape. Further, blanket housing, side lead reflector, absorbent boron carbide layer, concrete and air gaps of various thickness are situated. In connection with customer’s wish to reduce, as far as possible, the loading of fuel in the core, the thickness of side reflector was developed up to 60 cm. Further increase of thickness practically does not influence the multiplication factor K_{eff}. Absorbent layer is also introduced into the design according to customer’s request, it allows to reduce the lifetime of prompt neutrons from $5{,}5 \cdot 10^{-5}$ s to $2{,}4 \cdot 10^{-5}$ s.

The choice of base composition of the core was based on the following presuppositions. The quantity of core cells for allocation of fuel assemblies is

restricted and, as preliminary calculations have shown, it is close to FA quantity, required to form the core with K_{eff}≈0,95. This quantity of cells should be sufficient to achieve the required K_{eff} at the maximum unfavorable change of fuel properties within tolerances as well as at a negative contribution of calculation method error, because it will be not possible to increase the K_{eff}, if need be, at the expense of loading additional FA. The base composition was chosen under the following assumed fuel data: the mass of UO_2-PuO_2 in fuel column is 163,0 g/cm^3, mass content of PuO_2 in the mixture UO_2-PuO_2 is 30.0%, Plutonium has isotope composition of 95% ^{239}Pu and 5% ^{240}Pu. These are values, which corresponds to technical assignment for a fuel element [5], taking into account tolerances for Plutonium content in the fuel and Plutonium composition [6]. Such assumptions yielded that K_{eff}=0,951 is achieved at loading in the core 134 FA and 7 lead displacers in the outer row of FA (displacer: hexagonal lead prism, which is identical to outer row prisms of the lead target). Horizontal section of the core and its surroundings is given in Figure 6.1, integral data of the core are given in Table 6.1.

At the second stage of work of the installation SAD, the lead target will be replaced for tungsten target, i.e. central part of lead target will be replaced for tungsten target, 12 prisms of lead target will be moved to the periphery of the core, and their places will be occupied by FA. In this case, there are 153 cells in the core for location of FA and lead displacers. The assumed fuel data yielded that

$K_{эфф}$=0,9526 is achieved at loading into the core of 132 FA and 21 lead displacers in the outer row of FA. Horizontal section of the core and its surroundings is given in Figure 6.2, integral data of the core are given in Table 6.1.

Table 6.1 – Main neutron-physical data of installation

Description	Value
Initial data of the core	
Fuel material	UO_2-PuO_2
Density, g/cm^3	10,2
Mass content of PuO_2 in the mixture, %	29,7
Length of fuel column of fuel element, cm	58,0
Duration of power operation, hours	10000
Proton beam data	
Proton energy, MeV	659
Maximum beam power, kW	1,0
Calculated data of the core with lead target	
Neutron generation intensity in target, 1/s	$1{,}21 \cdot 10^{14}$
Neutrons escaped to the core, 1/s	$1{,}14 \cdot 10^{14}$
Total energy release in target, kW	0,94
Mass of loaded fuel UO_2-PuO_2, kg	396,8
K_{eff}	0,951
Lifetime of prompt neutrons, s	$2{,}4 \cdot 10^{-5}$
Effective share of delayed neutrons, %	0,373
Energy release in fuel, kW	26,1
Total energy release in installation, kW	28,5
Neutron multiplication factor *)	22,6
Neutron generation intensity in the core,, 1/s	$2{,}57 \cdot 10^{15}$
Maximum neutron flux density in the core at the power 28,5 kW, 1/(cm^2·s):	
With energy from 20 to 1,0 MeV	$5{,}83 \cdot 10^{11}$
With energy from 1,0 MeV to 0,1 MeV	$1{,}62 \cdot 10^{12}$
With energy from 1,0 KeV to 100 KeV	$7{,}13 \cdot 10^{11}$
With energy from 0 to 20 MeV	$2{,}92 \cdot 10^{12}$
Average density of neutron flux in the core at the power 28,5 kW, 1/(cm^2·s):	
With energy from 0 to 20 MeV	$1{,}7 \cdot 10^{12}$
Calculated data of the core with tungsten target	
Number of FA	132
Neutron generation intensity in target, 1/s	$1{,}14 \cdot 10^{14}$
Neutrons escaped to the core, 1/s	$1{,}04 \cdot 10^{14}$
Total energy release in target, kW	1,01
Mass of loaded fuel UO_2-PuO_2, kg	390,9
K_{eff}	0,9526

Table 6.1, continued

Description	Value
Energy release in fuel, kW	23,8
Total energy release in installation, kW	26,1
Neutron multiplication factor *)	23,1
Neutron generation intensity in the core, 1/s	$2{,}4 \cdot 10^{15}$
Lifetime of prompt neutrons, s	$2{,}24 \cdot 10^{-5}$

*)A total quantity of neutrons generated in the core at the expense of fuel fission and reactions (n,2n) and (n,3n) per one neutron escaping from target.

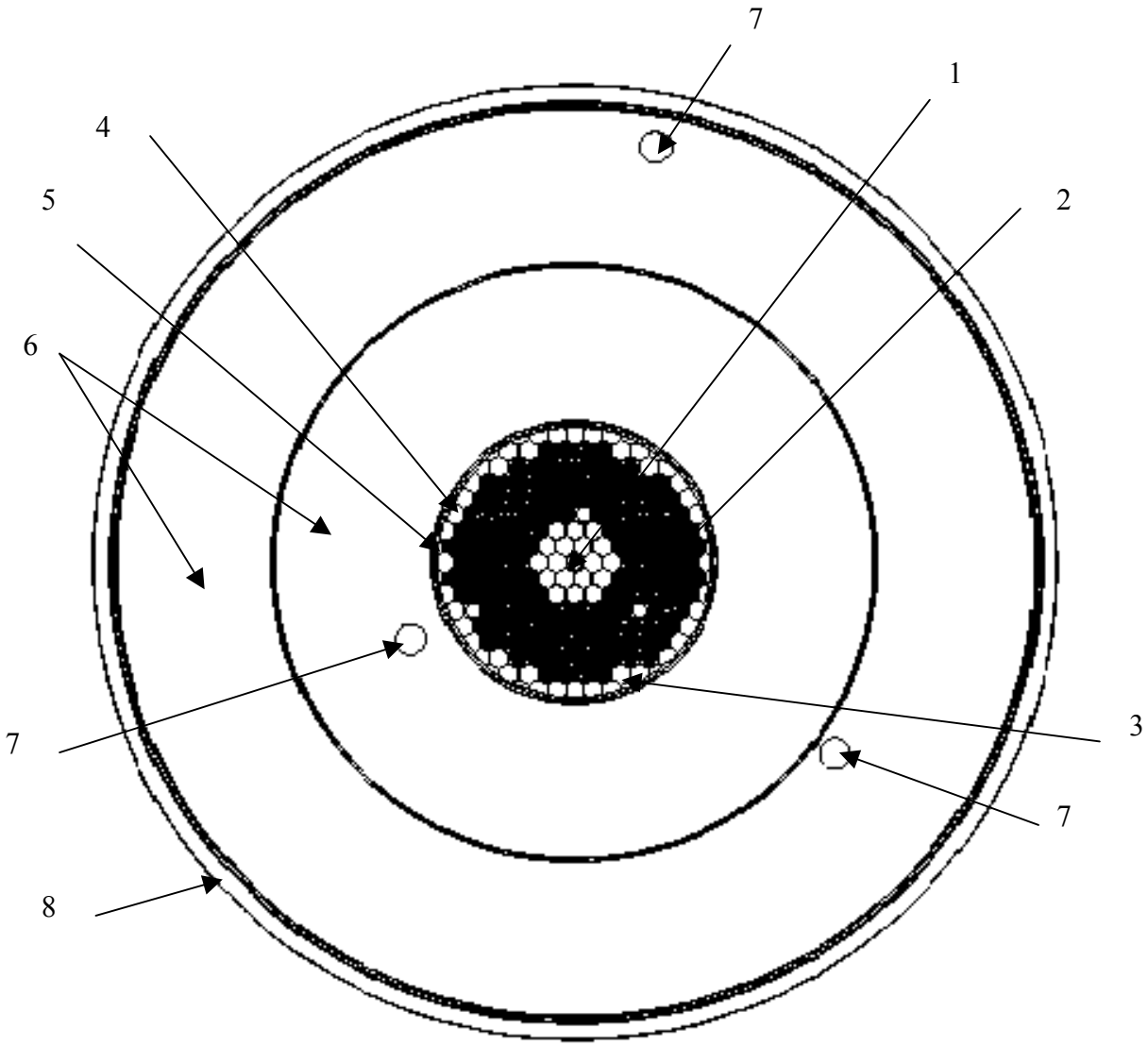

1 - target
2 – FA
3 – hexagonal lead block
4 – steel displacer
5 – blanket housing
6 – side reflector (lead)
7 – Vertical experimental channel
8- boron carbide absorbent screen

Figure 6.1 – Horizontal section of calculated model of SAD variant with lead target

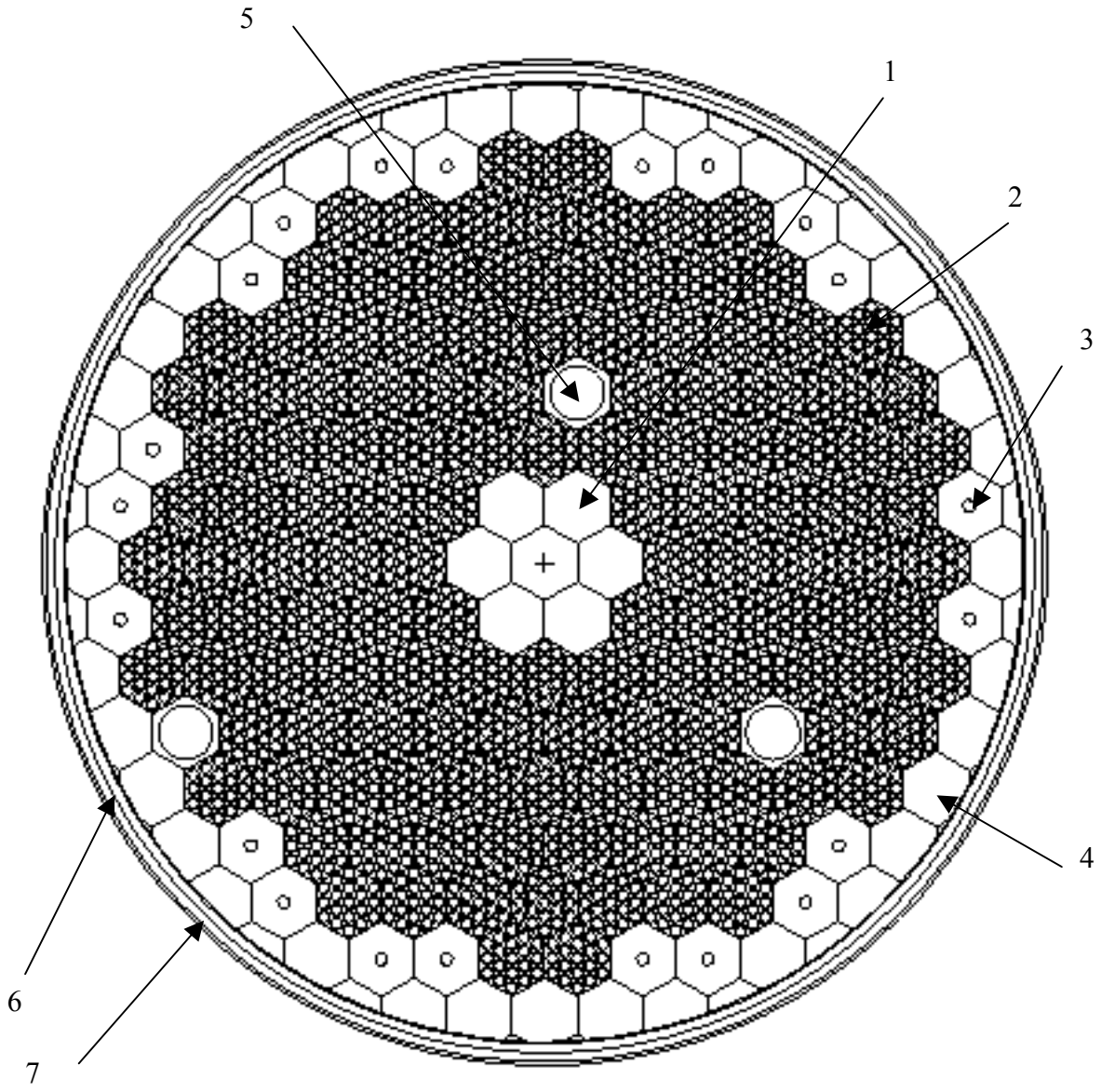

1 - target
2 - FA
3 – hexagonal lead block
4 – steel displacer
5 – vertical experimental channel
6 – blanket housing
7 – air gap

Figure 6.2 – Horizontal section of calculated model of SAD variant with tungsten target

6.3 Energy release distribution in constructs

6.3.1 Total energy release in the core and constructs

In subcritical installation with an external (not at the expense of chain fission reaction) neutron source, the heat power, determined by fuel fission, depends on neutron generation intensity of a source and of the K_{eff} level. Calculation modeling of a subcritical core with external source yields, at source values and $K_{eff,}$ given in Table 6.1, the fission power in the core, which is equal to 28,5 kW for the variant with lead target and 26,1 kW for the variant with tungsten target. The smaller power in the variant with tungsten target is mainly caused by a lesser number of neutrons escaping from target to blanket.

Table 6.2 demonstrates energy release distribution in main constructs of the SAD, caused by nuclear fuel fission in the core. Attention should be payed to the following. Energy release in target, given in Table 6.2, reflects one component only: energy release from gamma-ray quantum absorbing and scattering, which are produced at fuel fission and absorption of neutrons with an energy below 20 MeV by constructs. This energy release is relatively evenly distributed across the target section, the height profile corresponds to energy release profile in the fuel (see 6.3.2). The second component caused by proton beam passing through target material and, which has a substantially higher value and space irregularity, is described in 6.3.3.

Table 6.2 – Energy release in main constructs of the installation at operation in nominal mode, W

Construct	Lead target	Tungsten target
Fuel and fuel element cladding	26100	23800
Target	97	147
Lead displacers in the core	43	101
Steel displacers in the core	140	95
Steel housing of the core	22	16
Lead reflector	565	538
Boron carbide layer	195	162
Concrete layer	709	590
Other constructs	629	651
Installation as a whole	28500	26100

As mentioned above, the power of installation is determined by the neutron source and K_{eff}. Generally, this dependence can be determined in the following way:

$$W_t = N_n \cdot K_n \cdot K_{eff} \cdot q_f / (\nu \cdot (1 - K_{eff})) \qquad (6.1)$$

N_n – intensity of neutrons escaping from target to blanket,

K_n – neutron source value coefficient, reflects better fission properties (energy spectrum, place of birth) of source neutrons as compared with fission neutrons, born in the core ,

$K_{эфф}$ – effective multiplication factor of neutrons in the core,

q_f – one fission energy,

ν - number of neutrons born per one fission.

Using initial data from Table.6.2 and formula (6.1), we can calculate values of K_n for variants with lead and tungsten target and obtain dependences for determination of power, released at fuel fission in the core, for a case, when K_{eff} differs from values given in Table 6.1:

Lead target - $W_t = 1468 \cdot K_{eff}/(1- K_{eff})$ [W], (6.2)

Tungsten target - $W_t = 1299 \cdot K_{eff}/(1- K_{eff})$ [W]. (6.3)

These dependences are shown graphically in Fig. 6.3.

Table 6.3 – Initial data for calculation of source neutron value coefficient K_n

Parameter	**Lead target**	**Tungsten target**
Heat power of the core W_t, kW	28,5	26,1
Intensity of neutrons escaping from target to blanket N_n, 1/c	$1{,}143 \cdot 10^{14}$	$1{,}035 \cdot 10^{14}$
K_{eff}	0,951	0,9526
One-fission energy q_f, J	$3{,}2 \cdot 10^{-11}$	$3{,}2 \cdot 10^{-11}$
Number of neutrons born per one fission ν (^{239}Pu), relative unit.	2,95	2,95
Source neutron value coefficient K_n, relative unit.	1,184	1,157

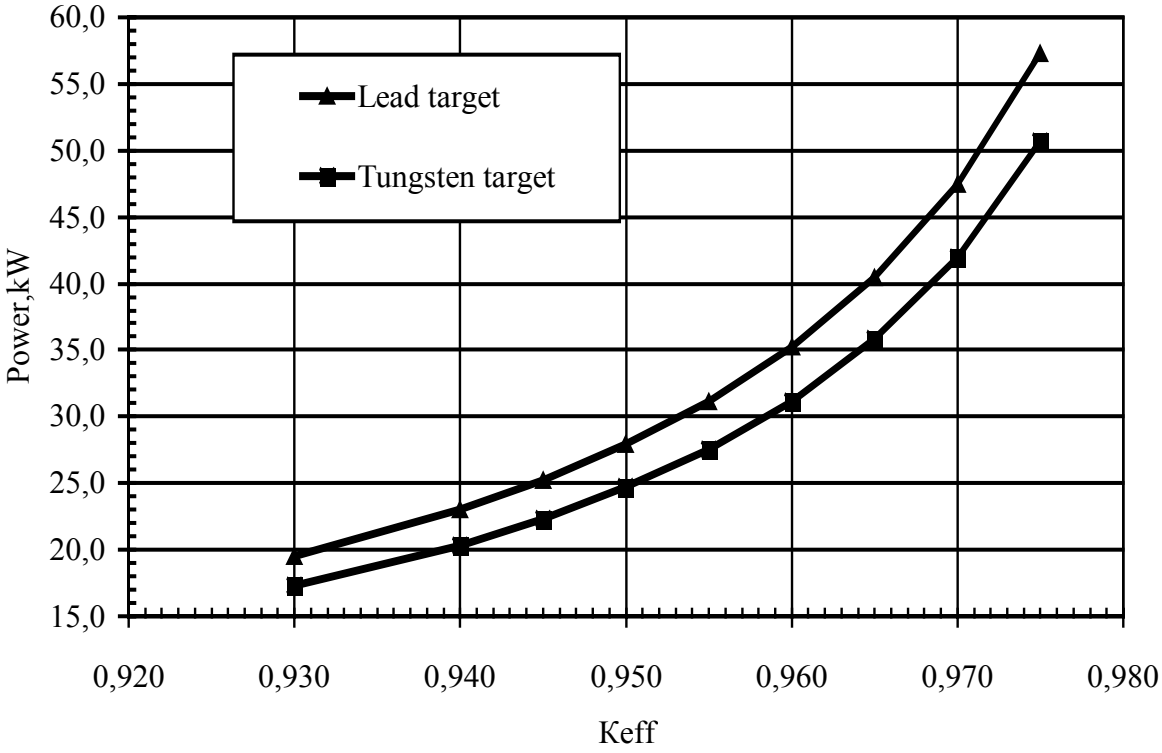

Figure 6.3. – Dependence of power, released at fuel fission in the core, in case, when K_{eff} differs from values given in Table.6.2.

6.3.2 Energy release distribution in the core

Energy release calculations in the core and its surroundings at active proton beam were carried out with the use of MCNP program, into which were input, besides a detailed description of design of the SAD, space—energy neutron distribution, produced by proton beam on the target (6.4). In the cause of calculations, total fission energy, including the energy of delayed gamma-ray quanta and neutrons as well as the energy of gamma-ray quanta, produced at neutron interaction with reactor constructs was taken into account. All results were normalized for a number of neutrons escaping from side surface of the target to the

core during 1s. For a variant with lead target, it is equal to $1{,}143 \cdot 10^{14}$ n/s, and for variant with tungsten target it is equal to $1{,}035 \cdot 10^{14}$ n/s. Radial energy release distribution in the core and height distribution in the maximally strained FA were calculated.

Energy release distribution across the core in radial direction was calculated for the segment, including approx. 1/6 FA (Fig. 6.4, 6.5). Total energy release in fuel and fuel element claddings for each FA chosen were obtained. For the variant with lead target, the FA power in the core changes from 167 W to 221 W, for the variant with tungsten target – from 154 W to 207 W.

Height energy release distribution was calculated for the most strained FA. Its location in the core is represented in Fig. 6.6. This FA was divided in the calculation model in 10 layers of 5.8 cm each and total energy release in each layer was calculated. Calculation results normalized for a maximum value are given in Table 6.6.

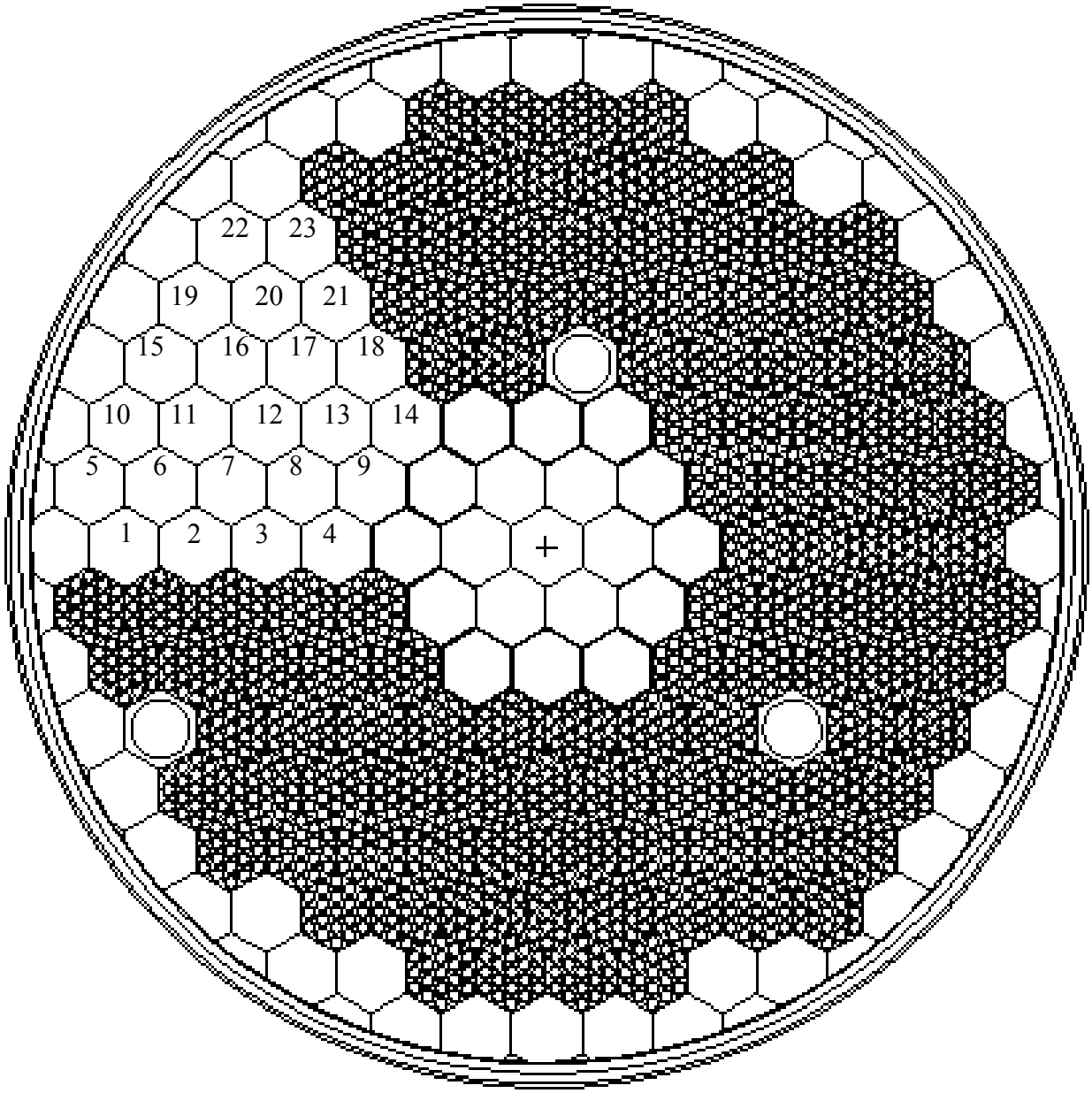

Figure 6.4 – Location cartogram of FA, chosen for energy release calculation in the core variant with lead target.

FA numbers from Table 6.4 are numerated on the cartogram.

Table 6.4 – Total energy release in fuel and fuel element cladding of selected FA of the core with lead reflector

FA number	Energy release in fuel, W	Energy release in fuel element claddings, W
1	176,8	1,00
2	194	1,19
3	209	1,28
4	218,3	1,24
5	166,2	0,80
6	184,9	1,10
7	200,9	1,25
8	213,5	1,30
9	220,4	1,17
10	171,9	0,89
11	189,4	1,15
12	204,3	1,27
13	214,9	1,29
14	220,3	1,18
15	175,2	0,92
16	190,9	1,16
17	204,4	1,25
18	213,5	1,29
19	174,7	0,91
20	189,1	1,12
21	200,5	1,21
22	171,6	0,82
23	184	1,02

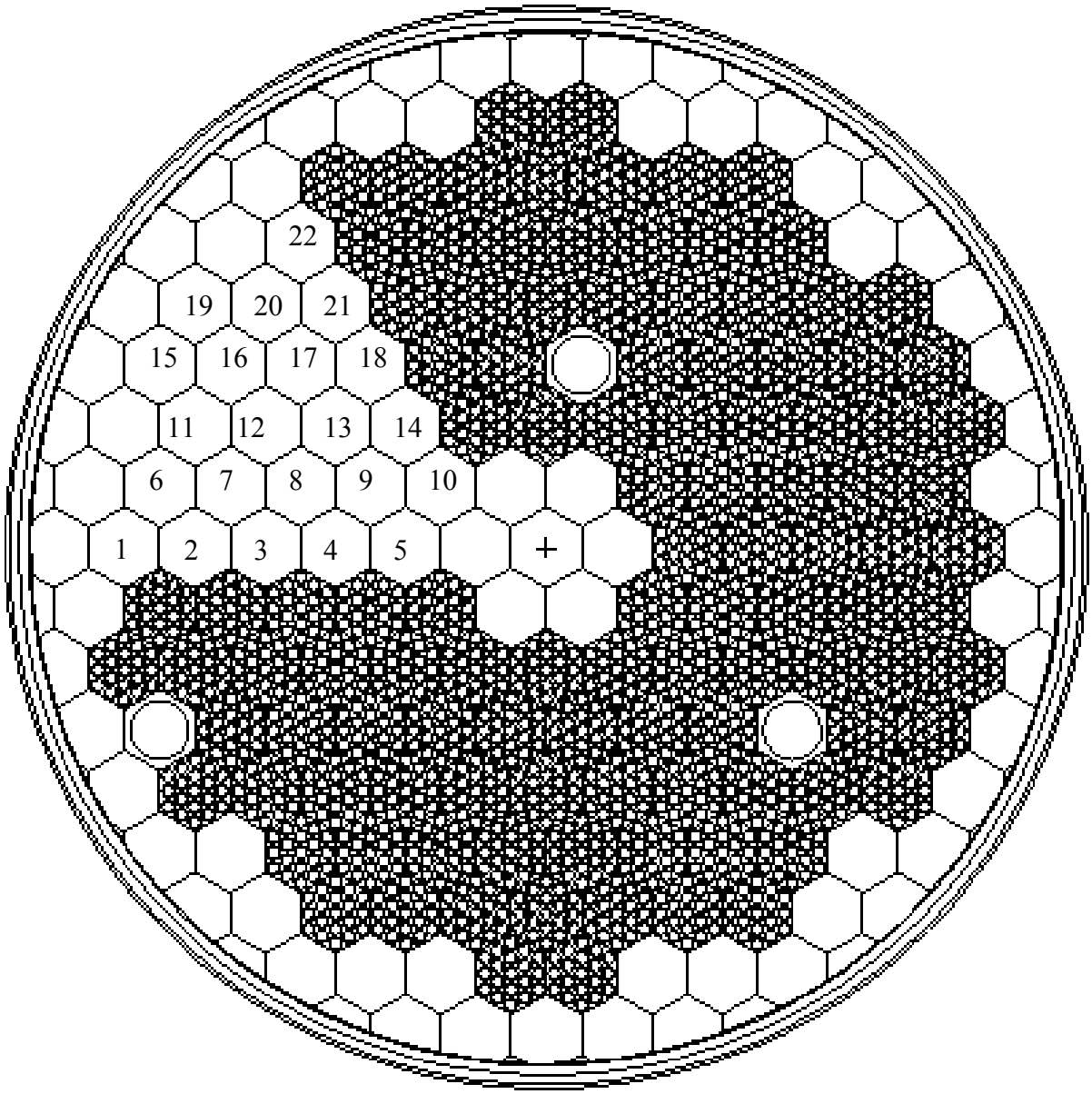

Figure 6.5 – Location cartogram of FA, chosen for energy release calculation in the core variant with tungsten target.

FA numbers from Table 6.5 are numerated on the cartogram.

Table 6.5 – Total energy release in fuel and fuel element cladding of selected FA of the core with tungsten reflector

FA number	Energy release in fuel, W	Energy release in fuel element claddings, W
1	155,3	0,81
2	170,3	1,08
3	184,1	1,20
4	195,9	1,28
5	204,4	1,31
6	162,4	0,91
7	176,7	1,14
8	190,5	1,26
9	200,1	1,31
10	205,9	1,28
11	166,7	1,00
12	180,6	1,17
13	192,1	1,26
14	200,4	1,32
15	153,3	0,81
16	167,3	1,06
17	180,4	1,17
18	191,2	1,26
19	153,3	0,80
20	166	0,99
21	176,8	1,15
22	162	0,90

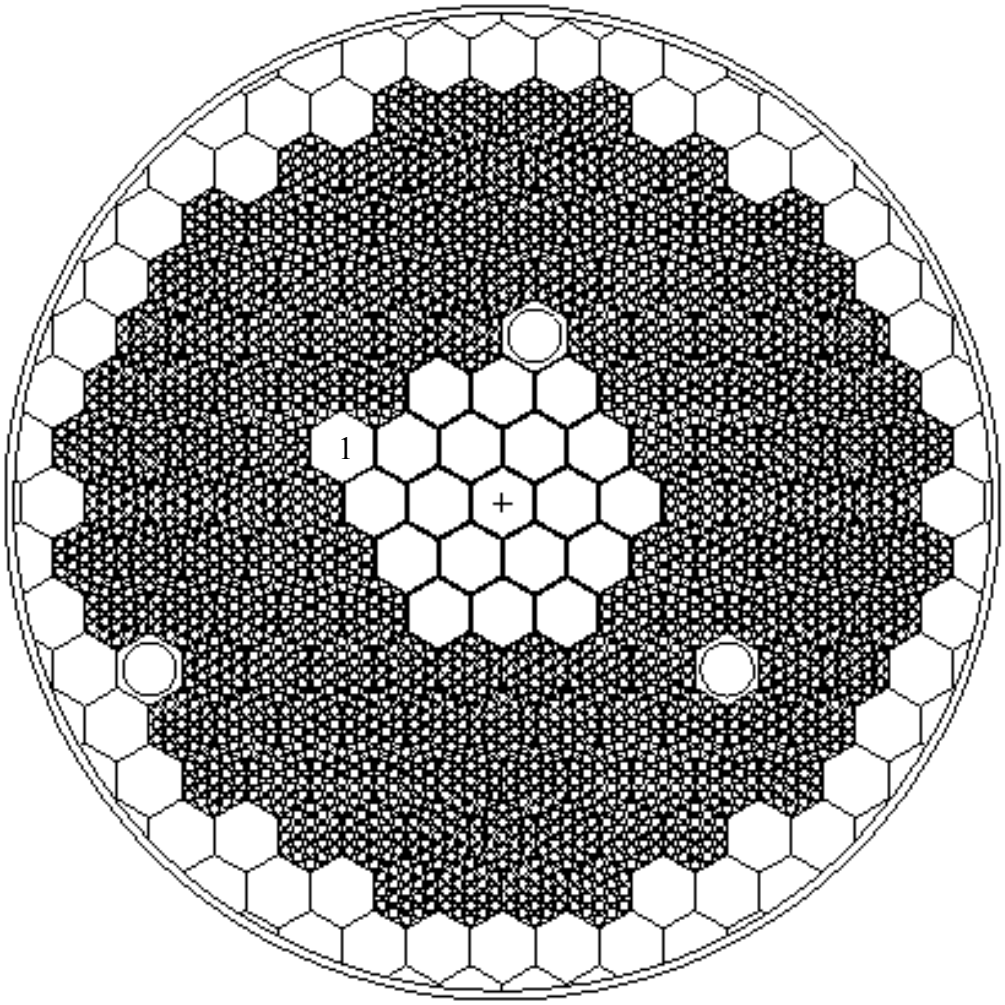

Figure 6.6 – Location of most energy strained FA in the core
1- most enrgy-strained FA.

Table 6.6 – Distribution of energy release (formed for maximum value) depending on height in the most strained FA

Layer height coordinate of FA, cm*)	**Energy release, relative unit**
0 ÷ 5,8	0,643
5,8 ÷ 11,6	0,782
11,6 ÷ 17,4	0,908
17,4 ÷ 23,2	0,976
23,2 ÷ 29	1,000
29,0 ÷ 34,8	0,975
34,8 ÷ 40,6	0,917
40,6 ÷ 46,4	0,811
46,4 ÷ 52,2	0,696
52,2 ÷ 58	0,561

*) Height counting out starts from the low end of fuel column.

6.3.3 Energy release in target at irradiation by proton beam

Lead target

Lead target is made of 13 elements. In the center of target there is an element uniting 7 hexagonal prisms, it is surrounded at the periphery by 12 hexagonal prisms, the “wrench” size is 3,45 cm, mounting pitch is 3,6 cm. All target elements are filled with lead of a density 11.15 g/cm^3. There is a hollow channel 10 cm long in the bottom part of central element, it is intended for proton beam inlet into target. Proton beam is put in the target bottom-up.

In the prepared calculation model, the whole target was divided into horizontal layers 2 cm high. The central target element was divided into radial layers 0.5 cm thick (Fig..6.7). It was assumed for calculation purposes that proton energy is 660 MeV, beam power is 1 kW, effective beam diameter is 3 cm, power distribution across beam section is given in Table 6.7.

As a result of calculation it was obtained that a power of 840 W is released in target under the action of protons. Space distribution of energy release in target is given in Table 6.8. An average amount of energy release in target elements under calculation (radial layers of prescribed size and 2 cm high) are given. An average value along hexagonal prism 2 cm high is given for 12 external hexagonal prisms. The results show that beam energy is completely absorbed in axial layer approx. 40 cm thick (coordinates 10÷50 cm in Table 6.8). There is practically no energy release at farther distances.

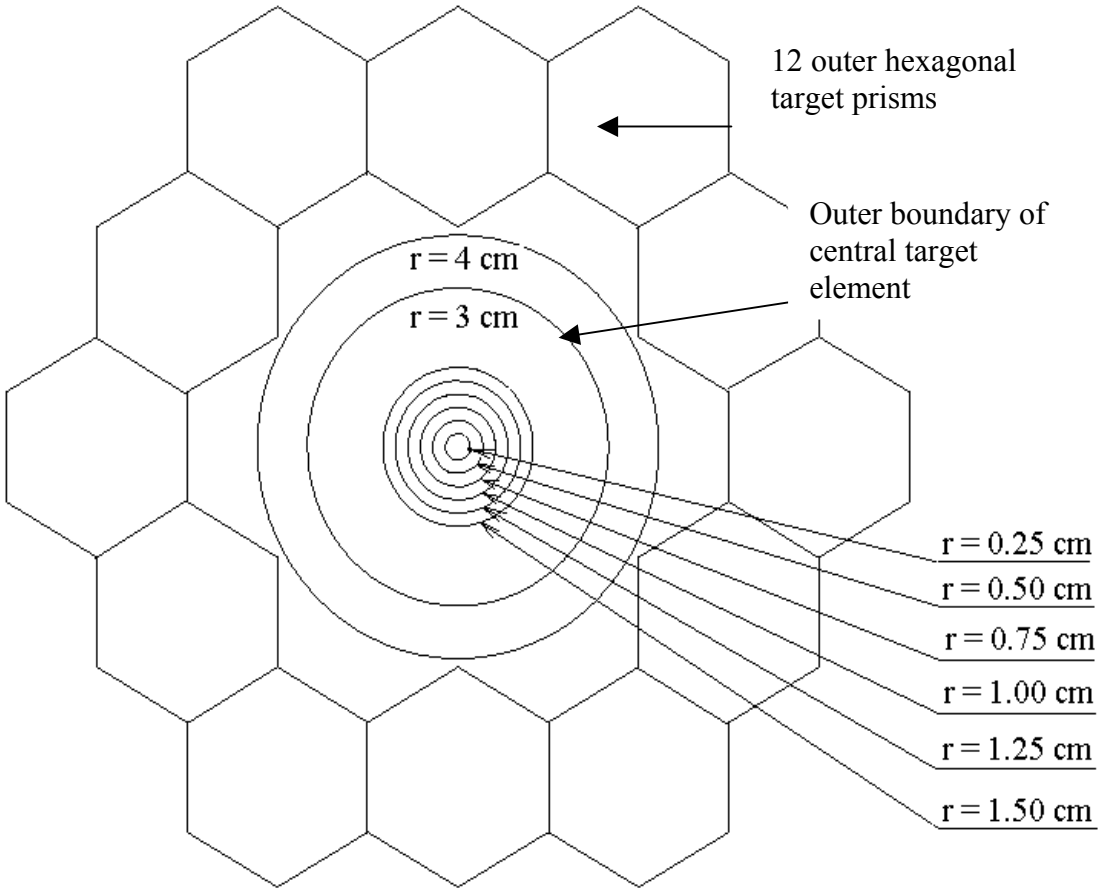

Figure 6.7 – Horizontal target section of calculated target model.

Table 6.7 – Proton beam intensity distribution

Radial layer, cm	Beam intensity share, %	Specific power, W/cm^2
0÷0,25	27,3	1390
0,25÷0,50	24,5	416
0,50÷0,75	19,7	201
0,75÷1,0	14,1	103
1,0÷1,25	9,1	51,5
1,25÷1,50	5,3	24,5

Table 6.8 – Space distribution of specific energy release in lead target, W/cm^3

Vertical coordinate, cm	Outer boundary of radial layer, cm				
	0,25	0,5	0,75	1,0	1,25
0÷2	0,00E+00	0,00E+00	0,00E+00	0,00E+00	0,00E+00
2÷4	0,00E+00	0,00E+00	0,00E+00	0,00E+00	0,00E+00

4÷6	0,00E+00	0,00E+00	0,00E+00	0,00E+00	0,00E+00
6÷8	0,00E+00	0,00E+00	0,00E+00	0,00E+00	0,00E+00
8÷10	0,00E+00	0,00E+00	0,00E+00	0,00E+00	0,00E+00
10÷12	4,80E+01(*	1,66E+01	8,10E+00	4,29E+00	2,26E+00
12÷14	3,93E+01	1,62E+01	7,89E+00	4,27E+00	2,32E+00
14÷16	2,90E+01	1,53E+01	7,33E+00	3,98E+00	2,18E+00
16÷18	2,02E+01	1,33E+01	7,00E+00	3,78E+00	2,07E+00
18÷20	1,36E+01	1,05E+01	6,54E+00	3,67E+00	2,03E+00
20÷22	8,92E+00	7,73E+00	5,59E+00	3,52E+00	2,06E+00
22÷24	5,95E+00	5,47E+00	4,36E+00	3,10E+00	2,04E+00
24÷26	4,08E+00	3,87E+00	3,29E+00	2,59E+00	1,85E+00
26÷28	2,82E+00	2,72E+00	2,48E+00	2,02E+00	1,59E+00
28÷30	2,00E+00	1,97E+00	1,81E+00	1,58E+00	1,31E+00
30÷32	1,43E+00	1,43E+00	1,36E+00	1,23E+00	1,05E+00
32÷34	1,06E+00	1,07E+00	1,03E+00	9,32E-01	8,58E-01
34÷36	8,20E-01	8,17E-01	7,76E-01	7,47E-01	6,88E-01
36÷38	6,48E-01	6,51E-01	6,46E-01	6,24E-01	5,70E-01
38÷40	5,95E-01	6,06E-01	6,17E-01	5,72E-01	5,44E-01
40÷42	4,09E-01	4,35E-01	4,32E-01	4,15E-01	3,87E-01
42÷44	1,99E-03	4,29E-03	1,87E-03	2,87E-03	3,10E-03
44÷46	2,85E-03	2,88E-03	1,50E-03	1,58E-03	2,36E-03
46÷48	1,02E-03	1,37E-03	7,16E-04	1,24E-03	1,46E-03
48÷50	1,86E-04	1,65E-03	1,02E-03	9,87E-04	9,12E-04
50÷52	1,67E-03	1,25E-03	6,89E-04	3,78E-04	4,15E-04
52÷54	2,38E-05	4,97E-04	1,07E-03	4,78E-04	4,24E-04
54÷56	1,26E-04	4,33E-04	1,10E-03	3,73E-04	7,04E-04
56÷58	1,45E-03	4,77E-04	6,92E-04	5,15E-04	6,13E-04

*) 4,80E+01 = $4{,}80 \cdot 10^{1}$

Table 6.8, continued

Vertical coordinate, cm	Outer boundary of radial layer, cm				
	1,5	3,0	4,0	Outer boundary	Outer hexahedrons
0÷2	0,00E+00	4,66E-04	1,27E-04	1,07E-04	8,30E-05
2÷4	0,00E+00	1,02E-03	2,54E-04	1,40E-04	1,18E-04
4÷6	0,00E+00	2,12E-03	6,64E-04	3,17E-04	1,87E-04
6÷8	0,00E+00	5,82E-03	1,30E-03	8,13E-04	3,25E-04
8÷10	0,00E+00	1,63E-02	3,50E-03	1,39E-03	5,16E-04
10÷12	1,10E+00(*	6,35E-02	1,01E-02	3,73E-03	1,12E-03
12÷14	1,17E+00	1,28E-01	2,52E-02	8,57E-03	2,29E-03
14÷16	1,13E+00	1,61E-01	3,91E-02	1,56E-02	4,00E-03
16÷18	1,08E+00	1,79E-01	4,76E-02	2,13E-02	6,04E-03
18÷20	1,09E+00	1,91E-01	4,88E-02	2,33E-02	7,62E-03
20÷22	1,14E+00	2,12E-01	4,93E-02	2,54E-02	8,76E-03
22÷24	1,23E+00	2,45E-01	4,93E-02	2,56E-02	9,29E-03
24÷26	1,24E+00	2,87E-01	4,93E-02	2,52E-02	9,52E-03
26÷28	1,17E+00	3,26E-01	5,31E-02	2,51E-02	9,44E-03
28÷30	1,03E+00	3,52E-01	6,34E-02	2,46E-02	9,52E-03
30÷32	8,72E-01	3,62E-01	7,93E-02	2,66E-02	9,29E-03
32÷34	7,37E-01	3,52E-01	9,90E-02	3,19E-02	8,99E-03
34÷36	6,19E-01	3,35E-01	1,18E-01	3,99E-02	9,37E-03
36÷38	5,19E-01	3,19E-01	1,35E-01	5,17E-02	1,07E-02
38÷40	5,02E-01	3,36E-01	1,70E-01	7,39E-02	1,58E-02
40÷42	3,61E-01	2,38E-01	1,13E-01	5,69E-02	1,36E-02
42÷44	2,29E-03	1,95E-03	1,61E-03	1,49E-03	1,04E-03
44÷46	1,83E-03	1,45E-03	1,31E-03	1,15E-03	8,38E-04
46÷48	1,32E-03	1,11E-03	9,30E-04	9,50E-04	7,85E-04
48÷50	4,89E-04	8,09E-04	8,53E-04	8,02E-04	6,39E-04
50÷52	3,84E-04	6,53E-04	6,38E-04	6,47E-04	5,35E-04
52÷54	7,50E-04	6,22E-04	4,58E-04	5,03E-04	4,14E-04
54÷56	4,49E-04	5,11E-04	3,56E-04	3,92E-04	3,18E-04
56÷58	3,68E-04	3,88E-04	2,61E-04	2,68E-04	2,63E-04

*) 1,10E+00 = $1{,}10 \cdot 10^{0}$

Tungsten target

Tungsten target is made of one element uniting 7 hexagonal prisms of the "wrench" size equal to 3,6 cm. The target is made of tungsten alloy VNZh 95 (W - 95%; Ni – 3,5%; Fe – 1,5%)with a density 18,0 g/cm^3. There is a hollow channel 10 cm long in the bottom part of central element, it is intended for proton beam inlet into target. Proton beam is put in the target bottom-up.

In the prepared calculation model, the whole target was divided into horizontal layers 2 cm high and radial layers 0.5 cm thick (Fig..6.8). It was assumed for calculation purposes that proton energy is 660 MeV, beam power is 1 kW, effective beam diameter is 3 cm, power distribution across beam section is given in Table 6.7.

As a result of calculation it was obtained that a power of 861 W is released in target under the action of protons. Space distribution of energy release in target is given in Table 6.9. An average amount of energy release in target elements under calculation (radial layers of prescribed size and 2 cm high) are given. The results show that beam energy is completely absorbed in axial layer approx. 36 cm thick (coordinates 10÷46 cm in Table 6.9). There is practically no energy release at farther distances.

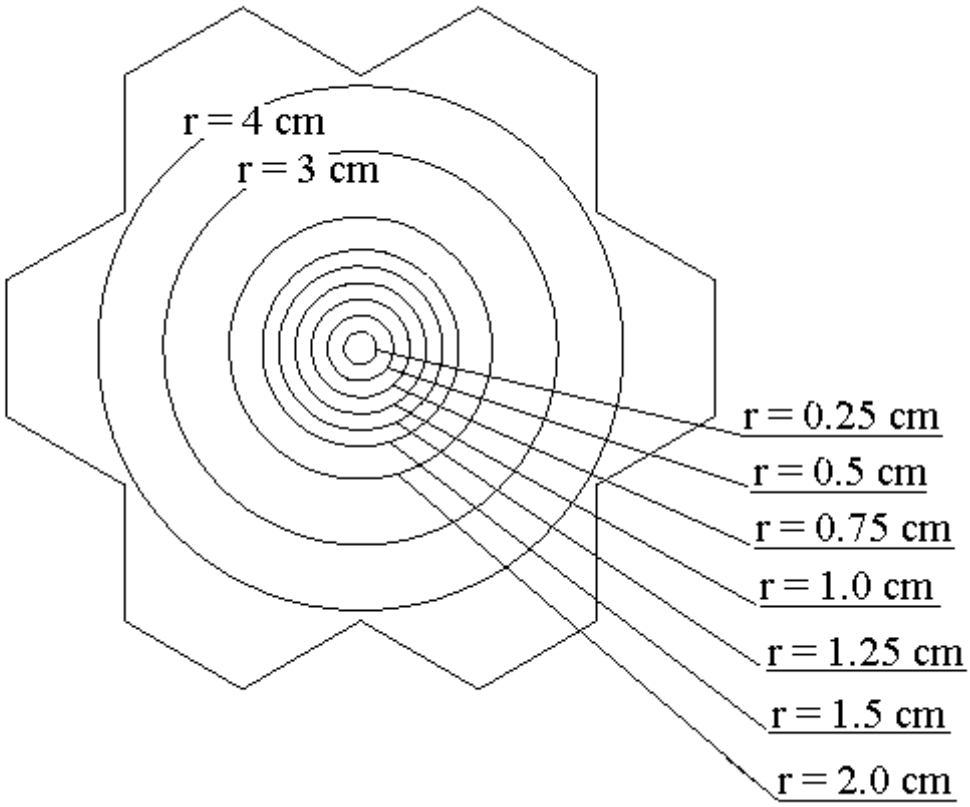

Figure 6.8 – Horizontal target section of calculated tungsten target model.

Table 6.9 – Space distribution of specific energy release in tungsten target, W/cm^3

Vertical coordinate, cm	Outer boundary of radial layer, cm				
	0,25	0,5	0,75	1,0	1,25
0÷2	0,00E+00	0,00E+00	0,00E+00	0,00E+00	0,00E+00
2÷4	0,00E+00	0,00E+00	0,00E+00	0,00E+00	0,00E+00
4÷6	0,00E+00	0,00E+00	0,00E+00	0,00E+00	0,00E+00
6÷8	0,00E+00	0,00E+00	0,00E+00	0,00E+00	0,00E+00
8÷10	0,00E+00	0,00E+00	0,00E+00	0,00E+00	0,00E+00
10÷12	7,79E+01(*	2,73E+01	1,34E+01	7,12E+00	3,75E+00
12÷14	5,97E+01	2,52E+01	1,24E+01	6,80E+00	3,69E+00
14÷16	4,00E+01	2,22E+01	1,10E+01	6,05E+00	3,33E+00
16÷18	2,49E+01	1,76E+01	9,84E+00	5,43E+00	2,97E+00
18÷20	1,48E+01	1,23E+01	8,24E+00	4,98E+00	2,81E+00
20÷22	8,93E+00	8,04E+00	6,23E+00	4,33E+00	2,73E+00
22÷24	5,67E+00	5,31E+00	4,49E+00	3,43E+00	2,47E+00
24÷26	3,65E+00	3,55E+00	3,19E+00	2,66E+00	2,09E+00
26÷28	2,55E+00	2,53E+00	2,43E+00	2,12E+00	1,77E+00
28÷30	1,91E+00	2,02E+00	1,98E+00	1,76E+00	1,55E+00
30÷32	6,22E-03	1,35E-02	9,46E-03	9,37E-03	8,82E-03
32÷34	6,95E-03	5,87E-03	6,45E-03	6,05E-03	5,25E-03
34÷36	6,95E-03	4,24E-03	3,37E-03	2,69E-03	4,03E-03
36÷38	2,38E-03	2,96E-03	3,90E-03	1,76E-03	2,33E-03
38÷40	1,27E-03	2,19E-03	1,79E-03	1,87E-03	2,13E-03
40÷42	1,55E-03	1,03E-03	1,14E-03	1,31E-03	6,08E-04
42÷44	2,79E-03	1,08E-03	1,27E-03	1,42E-03	1,13E-03
44÷46	2,05E-03	8,40E-04	9,62E-04	6,73E-04	7,34E-04
46÷48	3,61E-04	2,56E-03	6,51E-04	6,84E-04	5,23E-04
48÷50	3,18E-04	4,11E-04	3,74E-04	3,84E-04	6,91E-04
50÷52	0,00E+00	2,58E-04	1,53E-04	1,56E-04	1,61E-04
52÷54	6,51E-04	9,40E-05	3,80E-05	4,45E-04	1,72E-04
54÷56	0,00E+00	3,50E-05	2,19E-04	2,96E-04	2,26E-04
56÷58	0,00E+00	0,00E+00	1,64E-04	8,03E-06	1,99E-04

*) 7,79E+01 = 7,79·10^1,

Table 6.9, contimued

Vertical coordinate, cm	Outer boundary of radial layer, cm				
	1,5	2,0	3,0	4,0	Outer boundary
0÷2	0,00E+00	9,91E-04	2,45E-04	1,42E-04	1,07E-04
2÷4	0,00E+00	3,77E-03	5,80E-04	3,10E-04	2,46E-04
4÷6	2,23E-05	5,65E-03	1,41E-03	5,99E-04	3,39E-04
6÷8	7,34E-05	1,74E-02	4,17E-03	1,47E-03	7,53E-04
8÷10	1,68E-04(*	5,57E-02	1,26E-02	3,43E-03	1,52E-03
10÷12	1,82E+00	2,27E-01	4,74E-02	1,07E-02	3,73E-03
12÷14	1,88E+00	4,51E-01	1,23E-01	3,20E-02	9,62E-03
14÷16	1,74E+00	5,36E-01	1,60E-01	5,28E-02	1,77E-02
16÷18	1,61E+00	5,88E-01	1,76E-01	6,52E-02	2,40E-02
18÷20	1,57E+00	6,43E-01	1,78E-01	6,96E-02	2,84E-02
20÷22	1,63E+00	7,29E-01	1,90E-01	6,69E-02	2,84E-02
22÷24	1,66E+00	8,44E-01	2,26E-01	6,25E-02	2,53E-02
24÷26	1,57E+00	9,23E-01	2,84E-01	6,61E-02	2,12E-02
26÷28	1,46E+00	9,72E-01	3,72E-01	8,41E-02	1,81E-02
28÷30	1,30E+00	9,35E-01	4,07E-01	9,60E-02	1,61E-02
30÷32	8,52E-03	7,13E-03	6,97E-03	4,93E-03	3,76E-03
32÷34	5,34E-03	5,06E-03	4,55E-03	3,88E-03	3,10E-03
34÷36	3,48E-03	2,99E-03	2,77E-03	2,75E-03	2,13E-03
36÷38	3,13E-03	2,57E-03	2,46E-03	2,00E-03	1,49E-03
38÷40	1,85E-03	1,65E-03	1,44E-03	1,51E-03	1,23E-03
40÷42	1,24E-03	1,38E-03	1,20E-03	9,25E-04	7,05E-04
42÷44	1,02E-03	1,01E-03	9,06E-04	6,08E-04	5,68E-04
44÷46	1,13E-03	7,28E-04	7,09E-04	5,46E-04	4,11E-04
46÷48	5,69E-04	6,64E-04	4,83E-04	4,58E-04	4,48E-04
48÷50	4,89E-04	3,17E-04	2,34E-04	3,09E-04	2,79E-04
50÷52	1,22E-04	2,22E-04	1,93E-04	1,86E-04	2,16E-04
52÷54	1,60E-04	2,22E-04	1,71E-04	1,77E-04	2,57E-04
54÷56	3,99E-04	1,83E-04	1,52E-04	1,14E-04	1,07E-04
56÷58	1,89E-04	1,63E-04	1,52E-04	1,52E-04	1,20E-04

*) 1,68E-04=$1{,}68 \cdot 10^{-4}$

6.3.4 Energy release in the core after proton beam is switched off

The case was considered, where proton beam switches off after 300 hours of continuous operation. All this period the fission power in the core was 28,5 kW. After proton beam is switched off, energy release in the core is caused by two components:

1) fission products decay (variable component);

2) plutonium isotopes decay (constant component).

To determine variable component, the method /6.8/ was used supposing that plutonium-239 only is fissionable in the core. At fuel load given in Table 6.1, plutonium isotopes decay yields a steady energy release 230 W. Calculation results of components and total residual energy release in the core is given in Table.6.10.

Table 6.10 – Energy release in the core after proton beam is switched off

Time lag	Residual energy release of fission products in fractions of nominal power, %	Residual energy release of fission products, kW	Residual energy release in the core, kW
1 s	4,97	1,372	1,602
2 s	4,744	1,309	1,539
3 s	4,574	1,262	1,492
4 s	4,439	1,225	1,455
5 s	4,328	1,195	1,425
10 s	3,958	1,092	1,322
30 s	3,35	0,925	1,155
1 min	2,961	0,817	1,047
2 min	2,581	0,712	0,942
3 min	2,377	0,656	0,886
5 min	2,142	0,591	0,821
10 min	1,832	0,506	0,736
20 min	1,507	0,416	0,646
30 min	1,324	0,365	0,595

Table 6.10, contimued

Time lag	Residual energy release of fission products in fractions of nominal power, %	Residual energy release of fission products, kW	Residual energy release in the core, kW

1 hour	1,013	0,280	0,510
2 hours	0,784	0,216	0,446
3 hours	0,6812	0,188	0,418
10 hours	0,4554	0,126	0,356
1 day	0,327	0,0903	0,320
2 days	0,2477	0,0684	0,2984
3 days	0,2099	0,0579	0,288
5 days	0,1674	0,0462	0,276
10 days	0,1147	0,0317	0,262
30 days	0,0491	0,0136	0,244

6.3.4 Energy release in target after proton beam is switched off

The case for lead and tungsten target was considered, where proton beam switches off after 300 hours of continuous operation. All this period the beam has nominal data: proton energy 660 MeV, power 1 kW. After proton beam is switched off, energy release in the core is caused by three components:

1) decay of nuclides produced in high energy nuclear reactions;
2) decay of nuclides produced at neutron absorption with an energy below 20 MeV;
3) gamma-ray quantum absorption produced in the core at fission products decay

Calculation of components 1 and 2 was carried out for composition of lead and tungsten alloys given in Tables 6.11, 6.12.

Table 6.11 – Lead alloy composition

Element	Weight fraction, %
Pb	99,985
Ag	0,001
Cu	0,001
Zn	0,001

Bi	0,006
As	0,0005
Sn	0,0005
Sb	0,001
Fe	0,001
Mg+Ca+Na	0,003

Table 6.12 – Tungsten alloy composition

Element	Weight fraction, %
W	95
Ni	3,5
Fe	1,5

To determine component 1 on the basis of calculations, executed by the program LAHET, a nuclide production velocity as a result of high energy processes during 1 second of target irradiation was obtained. Based on that production velocity, equilibrium concentrations for short-lived nuclides were obtained:

$$N_i=G_i/\lambda_i,,$$

where N_i – equilibrium nuclide concentration,

G_i – isotope production velocity during 1 s,

λ_i – decay constant of this isotope.

Thus, the quantity of radioactive nuclei for the moment of proton beam switching off was evaluated. Nuclides with half-life time below 1000 hours were taken into

account. Energy release from the decay of formed nuclides was conducted with the program FISPACT [7].

FISPACT allows to calculate the change of nuclides composition of various materials at irradiation in neutron flux and during the time lag without irradiation. After irradiation is stopped, all decays of radioactive nuclei are calculated, and energy of all decays with the exception of energy, brought away by neutrinos, is included in total energy release.

To determine the component 2, a calculation of radioactive nuclides accumulation in target under neutron flux with an energy below 20 MeV for 300 hours and subsequent time lag without irradiation was carried out. Neutron flux density in target was obtained by means of SAD calculation modeling with the program MCNP at nominal power (Table 6.1).

The component 3 was determined in the following way. Residual energy release in the core, caused by fission products decay, is given in Table 6.8. The MCNP yielded that energy equal to 5% of gamma-ray energy release component in the core fuel at nominal power operation (at target irradiation by nominal proton beam) is released in the target. Gamma-ray quanta are supposed to carry all energy produced as a result of fission products decay and this energy is distributed in constructs in the same way as at nominal mode operation. I.e., 5,3% of residual energy release power in the core is released in lead target, and 7,5% - in tungsten target (upper estimate).

All three energy release components in lead and tungsten targets after proton beam is switched off are given in Tables 6.13 and 6.14. For both targets, energy release is mainly (over 80%) is caused by gamma-ray quantum absorption produced in fuel. At that, energy release in tungsten target is approx. 30% higher than that in the lead target.

Table 6.13 – Energy release components in lead target after proton beam is switched off

Time lag	High energy processes (component 1), W	Low energy processes (component 2), W	Absorption of gamma-ray quanta from the core (component 3), W	Total energy release in target, W
1 s	1,051	0,5511	72,716	74,32
2 s	1,050	0,3502	69,377	70,78
3 s	1,048	0,2652	66,886	68,20
4 s	1,047	0,2291	64,925	66,20
5 s	1,045	0,2138	63,335	64,59
10 s	1,041	0,2021	57,876	59,12
30 s	1,030	0,2003	49,025	50,25
1 min.	1,018	0,1988	43,301	44,52
2 min.	1,002	0,1965	37,736	38,93
3 min.	0,990	0,1944	34,768	35,95
5 min.	0,969	0,1904	31,323	32,48
10 min.	0,935	0,1810	26,818	27,93
20 min.	0,893	0,1641	22,048	23,11
30 min.	0,865	0,1490	19,345	20,36
1 hour	0,803	0,1119	14,840	15,75
2 hours	0,718	0,0642	11,448	12,23
3 hours	0,659	0,0380	9,964	10,66
10 hours	0,464	0,0042	6,678	7,15
1 day	0,325	0,0020	4,786	5,11
2 days	0,240	0,0014	3,625	3,87
3 days	0,197	0,0010	3,069	3,27
5 days	0,147	0,0007	2,449	2,60
10 days.	0,090	0,0004	1,680	1,77
30 сут.	0,024	0,0002	0,721	0,74

Table 6.14 – Energy release components in tungsten target after proton beam is switched off

Time lag, sec	High energy processes (component 1), W	Low energy processes (component 2), W	Absorption of gamma-ray quanta from the core (component 3), W	Total energy release in target, W
1 s	0,7496	3,463	95,051	99,26
5 s	0,7481	3,134	82,773	86,65
10s	0,7472	2,901	75,697	79,34
30 s	0,7449	2,644	64,069	67,46
1 min.	0,7423	2,583	56,629	59,95
2 min.	0,7382	2,522	49,362	52,62
3 min.	0,7347	2,482	45,460	48,68
5 min.	0,7286	2,438	40,966	44,13
10 min	0,7145	2,403	35,037	38,15
20 min	0,6837	2,388	28,821	31,89
30 min	0,6528	2,377	25,322	28,35
1 hour	0,5831	2,345	19,374	22,30
2 hours	0,5130	2,282	14,994	17,79
3 hours	0,4765	2,222	13,028	15,73
10 hours	0,3583	1,850	8,710	10,92
1 day	0,2529	1,301	6,254	7,81
2 days.	0,1789	0,751	4,737	5,67
3 days	0,1428	0,475	4,014	4,63
5 days	0,1024	0,268	3,202	3,57
10 days	0,0586	0,193	2,194	2,45
30 days	0,0185	0,159	0,939	1,12

6.4 Neutron generation intensity in target and core

6.4.1 Lead target

With program LAHET and lead target calculation model described in 6.3.3, neutron generation intensity in target at nominal proton beam data (Tables 6.1, 6.6) and intensity distribution across target calculation zones were obtained..

As a result of calculations it was concluded that $1{,}21 \cdot 10^{14}$ n/s are born in the target under the action of protons , $1{,}143 \cdot 10^{14}$ n/s escape from target to blanket through the side surface.. Integral target data and neutron generation space distribution in target as normalized per one proton are given in Tables 6.15.and 6.16.

Table 6.16 shows a total number of neutrons born in target calculation zones (radial layers of prescribed size and 2 cm high). The results demonstrate that neutrons are effectively produced in axial layer approx. 30 cm thick along proton travel direction (coordinates 10÷40 cm in Tables 6.16). 79,2% of neutrons are produced in central target element, and 10,2% of neutrons are produced in 12 external prisms..

Table 6.15 – Integral target data (as normalized per 1 incident proton)

Total number of neutrons produced	12,95
Number of neutrons escaped from target	12,73
Number of neutrons escaped from target through bottom end surface	0,43
Number of neutrons escaped from target through upper end surface	0,08
Number of neutrons escaped from target through side surface	12,22
Total energy of neutrons produced, MeV	196,5
Total energy of neutrons escaped from target, MeV	103,2

Table 6.16 – Number of neutrons produced in calculation zones in lead target, neutrons per 1 proton

Vertical coordinate, cm	Outer boundary of radial layer, cm				
	0,25	0,5	0,75	1,0	1,25
0÷2	0,00E+00	0,00E+00	0,00E+00	0,00E+00	0,00E+00
2÷4	0,00E+00	0,00E+00	0,00E+00	0,00E+00	0,00E+00
4÷6	0,00E+00	0,00E+00	0,00E+00	0,00E+00	0,00E+00
6÷8	0,00E+00	0,00E+00	0,00E+00	0,00E+00	0,00E+00
8÷10	0,00E+00	0,00E+00	0,00E+00	0,00E+00	0,00E+00
10÷12	3,51E-01(*	3,56E-01	2,82E-01	2,10E-01	1,41E-01
12÷14	2,81E-01	3,29E-01	2,78E-01	2,00E-01	1,36E-01
14÷16	1,92E-01	3,04E-01	2,35E-01	1,81E-01	1,24E-01
16÷18	1,27E-01	2,52E-01	2,20E-01	1,68E-01	1,17E-01
18÷20	8,58E-02	1,97E-01	1,94E-01	1,57E-01	1,12E-01
20÷22	5,07E-02	1,38E-01	1,65E-01	1,43E-01	1,11E-01
22÷24	3,47E-02	9,39E-02	1,22E-01	1,20E-01	1,01E-01
24÷26	2,21E-02	6,21E-02	8,27E-02	9,85E-02	8,61E-02
26÷28	1,28E-02	3,84E-02	6,06E-02	6,93E-02	6,90E-02
28÷30	9,65E-03	2,72E-02	4,11E-02	5,14E-02	5,27E-02
30÷32	5,59E-03	1,92E-02	2,76E-02	3,45E-02	3,95E-02
32÷34	4,46E-03	1,12E-02	1,87E-02	2,24E-02	3,11E-02
34÷36	2,43E-03	7,58E-03	1,20E-02	1,61E-02	2,01E-02
36÷38	1,54E-03	4,84E-03	7,98E-03	1,01E-02	1,34E-02
38÷40	7,73E-04	3,50E-03	5,84E-03	7,36E-03	8,66E-03
40÷42	3,92E-04	8,56E-04	1,77E-03	2,05E-03	3,00E-03
42÷44	1,03E-04	3,95E-04	4,88E-04	8,40E-04	8,10E-04
44÷46	9,29E-05	4,71E-04	3,45E-04	4,22E-04	8,36E-04
46÷48	8,96E-05	8,96E-05	5,64E-05	3,78E-04	3,88E-04
48÷50	0,00E+00	1,96E-04	3,92E-04	3,05E-04	2,72E-04
50÷52	0,00E+00	2,66E-05	1,73E-04	1,53E-04	1,26E-04
52÷54	3,98E-05	6,64E-05	1,69E-04	2,39E-04	1,23E-04
54÷56	0,00E+00	2,32E-05	1,43E-04	8,30E-05	2,16E-04
56÷58	2,32E-05	6,31E-05	5,64E-05	6,64E-05	2,49E-04

*) 3,51E-01 = $3{,}51 \cdot 10^{-1}$

Table 6.16, continued

Vertical coordinate, cm	Outer boundary of radial layer, cm				
	1,5	3,0	4,0	Outer boundary	Outer hexahedrons
0÷2	0,00E+00	1,19E-03	7,50E-04	8,99E-04	3,98E-03
2÷4	0,00E+00	1,85E-03	1,58E-03	1,24E-03	5,32E-03
4÷6	0,00E+00	2,89E-03	2,64E-03	2,27E-03	8,47E-03
6÷8	0,00E+00	6,70E-03	4,12E-03	4,00E-03	1,32E-02
8÷10	0,00E+00	1,49E-02	8,76E-03	6,62E-03	2,00E-02
10÷12	8,46E-02(*	5,12E-02	1,84E-02	1,31E-02	3,30E-02
12÷14	8,26E-02	9,52E-02	3,32E-02	2,03E-02	4,90E-02
14÷16	8,24E-02	1,22E-01	4,50E-02	2,95E-02	6,40E-02
16÷18	7,61E-02	1,37E-01	4,96E-02	3,43E-02	7,74E-02
18÷20	7,22E-02	1,46E-01	5,57E-02	3,48E-02	8,59E-02
20÷22	7,21E-02	1,53E-01	5,16E-02	3,79E-02	8,79E-02
22÷24	7,75E-02	1,67E-01	5,14E-02	3,69E-02	8,96E-02
24÷26	7,20E-02	1,84E-01	4,96E-02	3,57E-02	8,91E-02
26÷28	6,62E-02	1,89E-01	4,85E-02	3,17E-02	8,04E-02
28÷30	5,18E-02	1,83E-01	5,03E-02	3,12E-02	7,93E-02
30÷32	3,82E-02	1,72E-01	5,32E-02	2,83E-02	7,54E-02
32÷34	3,01E-02	1,51E-01	5,25E-02	2,96E-02	6,64E-02
34÷36	2,20E-02	1,25E-01	5,23E-02	2,84E-02	6,32E-02
36÷38	1,48E-02	9,51E-02	4,74E-02	2,71E-02	5,80E-02
38÷40	1,02E-02	6,33E-02	3,79E-02	2,35E-02	5,04E-02
40÷42	2,46E-03	2,35E-02	1,52E-02	1,31E-02	3,72E-02
42÷44	1,09E-03	8,74E-03	7,36E-03	8,59E-03	2,85E-02
44÷46	5,71E-04	6,36E-03	5,73E-03	6,43E-03	2,35E-02
46÷48	5,38E-04	4,49E-03	4,21E-03	4,77E-03	1,91E-02
48÷50	2,06E-04	3,45E-03	3,44E-03	4,09E-03	1,58E-02
50÷52	2,22E-04	3,12E-03	2,81E-03	2,86E-03	1,29E-02
52÷54	4,25E-04	2,21E-03	2,36E-03	3,05E-03	9,98E-03
54÷56	1,66E-04	2,18E-03	1,79E-03	2,00E-03	8,67E-03
56÷58	1,99E-04	1,89E-03	1,20E-03	1,78E-03	6,71E-03

*) 8,46E-02 = $8{,}46 \cdot 10^{-2}$

6.4.2 Tungsten target

With program LAHET and lead target calculation model described in 6.3.3, neutron generation intensity in target at nominal proton beam data (Tables 6.1, 6.6) and intensity distribution across target calculation zones were obtained..

As a result of calculations it was concluded that $1{,}14 \cdot 10^{14}$ n/s are born in the target under the action of protons , $1{,}04 \cdot 10^{14}$ n/s escape from target to blanket through the side surface.. Integral target data and neutron generation space distribution in target as normalized per one proton are given in Tables 6.17.and 6.18.

Table 6.18 shows a total number of neutrons born in target calculation zones (radial layers of prescribed size and 2 cm high). The results demonstrate that neutrons are effectively produced in axial layer approx. 20 cm thick along proton travel direction (coordinates 10÷30 cm in Table 6.18).

Table 6.17 – Integral target data (as normalized per 1 incident proton)

Total number of neutrons produced	12,07
Number of neutrons escaped from target	11,11
Number of neutrons escaped from target through bottom end surface	0,163
Number of neutrons escaped from target through upper end surface	0,004
Number of neutrons escaped from target through side surface	10,95
Total energy of neutrons produced, MeV	196,0
Total energy of neutrons escaped from target, MeV	91,6

6.4.3 The core

The calculations show that 22,6 and 23,1 neutrons are produced, at the expense of fuel fission, in the core with lead (K_{eff}=0,951) and tungsten (K_{eff}=0,953) target per one neutron escaping from the target correspondingly. Taking into account the intensity of neutrons escaping from the target, this provides a neutron generation intensity in the core equal to $2{,}57 \cdot 10^{15}$ 1/s for the lead target and $2{,}4 \cdot 10^{15}$ 1/s for tungsten target. The maximum neutron flux density in the core with lead target is:

With energy from 20 MeV to 1,0 MeV - $5{,}83 \cdot 10^{11}$ 1/(cm^2·s);

With energy from 1,0 MeV to 0,1 MeV - $1{,}62 \cdot 10^{12}$ 1/(cm^2·s);

With energy from 1,0 keV to 100 keV - $7{,}13 \cdot 10^{11}$ 1/(cm^2·s);

With energy from 0 to 20 MeV - $2{,}92 \cdot 10^{12}$ 1/(cm^2·s).

The average neutron flux density in the core is $1{,}7 \cdot 10^{12}$ 1/(cm^2·s). Corresponding values for the core with tungsten target are 9% lower.

Detailed diagrams of energy dependence of neutron flux density in the core are given in section 6.6.

To carry out strength calculations of the core constructs and its closest surroundings, fast neutron fluence was calculated based on maximum flux density in the core with lead target (maximum estimate). During the total service life of installation of 10000 hours at full power, the fast neutron fluence (energy ower 0,1

MeV) is $7{,}9 \cdot 10^{19}$ 1/cm^2. Fast neutron fluence was also calculated for the steel end membrane of vacuum duct of accelerator. That membrane is located along the central axis 44 cm below the central plane of the core. Fast neutron fluence (energy over 0,1 MeV) will be, during the service life of installation, $2{,}0 \cdot 10^{19}$ 1/cm^2.

To evaluate the resistance of rubber sealing of the core and experimental channel, absorbed radiation dose at the places of sealing, situated at a distance of 47,8 cm (core housing) and 58,1 cm (experimental channel) was calculated. At given points, the absorbed dose is equal to 1,1 Gy and 7,1 Gy (1 Gy= J/kg) correspondingly. And the dose is determined mainly by gamma-ray quanta (contribution 88% and 85% correspondingly).

Table 6.18 – Number of neutrons, produced in calculation zones of tungsten target, neutrons per 1 proton

Vertical Coordinate, cm	Outer boundary of radial layer, cm				
	0,25	0,5	0,75	1,0	1,25
0÷2	0,00E+00	0,00E+00	0,00E+00	0,00E+00	0,00E+00
2÷4	0,00E+00	0,00E+00	0,00E+00	0,00E+00	0,00E+00
4÷6	0,00E+00	0,00E+00	0,00E+00	0,00E+00	0,00E+00
6÷8	0,00E+00	0,00E+00	0,00E+00	0,00E+00	0,00E+00
8÷10	0,00E+00	0,00E+00	0,00E+00	0,00E+00	0,00E+00
10÷12	5,00E-01	5,11E-01	4,12E-01	3,05E-01	2,12E-01
12÷14	3,55E-01(*	4,38E-01	3,66E-01	2,83E-01	1,98E-01
14÷16	2,24E-01	3,70E-01	3,05E-01	2,41E-01	1,73E-01
16÷18	1,30E-01	2,80E-01	2,54E-01	2,04E-01	1,44E-01
18÷20	7,02E-02	1,78E-01	1,97E-01	1,67E-01	1,29E-01
20÷22	4,20E-02	1,05E-01	1,28E-01	1,33E-01	1,11E-01
22÷24	2,24E-02	6,01E-02	8,30E-02	8,92E-02	8,58E-02
24÷26	1,10E-02	3,35E-02	5,12E-02	5,85E-02	5,85E-02
26÷28	6,33E-03	1,93E-02	2,87E-02	3,58E-02	4,07E-02
28÷30	1,56E-03	4,93E-03	7,74E-03	1,07E-02	1,18E-02
30÷32	4,37E-04	7,56E-04	1,54E-03	2,14E-03	2,46E-03
32÷34	2,30E-04	4,70E-04	1,17E-03	1,49E-03	2,14E-03
34÷36	1,44E-04	4,04E-04	6,78E-04	7,96E-04	1,21E-03
36÷38	6,30E-05	4,59E-04	3,33E-04	5,33E-04	7,26E-04
38÷40	1,85E-05	3,30E-04	2,85E-04	4,22E-04	7,33E-04
40÷42	8,15E-05	1,63E-04	3,07E-04	2,63E-04	2,30E-04
42÷44	5,56E-05	1,07E-04	6,67E-05	2,56E-04	4,11E-04
44÷46	0,00E+00	1,00E-04	9,63E-05	1,11E-04	2,93E-04
46÷48	0,00E+00	9,63E-05	2,70E-04	5,93E-05	3,41E-04
48÷50	1,48E-05	3,70E-05	1,00E-04	1,48E-04	2,00E-04
50÷52	0,00E+00	7,78E-05	2,22E-05	8,52E-05	5,93E-05
52÷54	0,00E+00	0,00E+00	2,22E-05	8,89E-05	1,11E-05
54÷56	0,00E+00	9,26E-05	1,85E-05	1,22E-04	1,48E-05
56÷58	1,85E-05	0,00E+00	2,22E-05	0,00E+00	1,85E-05

*) 3,55E-01 = $3{,}55 \cdot 10^{-1}$

Table 6.18, continued

Vertical Coordinate, cm	Outer boundary of radial layer, cm				
	1,5	2,0	3,0	4,0	Outer boundary
0÷2	0,00E+00	4,77E-04	1,20E-03	1,44E-03	1,67E-03
2÷4	0,00E+00	1,38E-03	1,79E-03	2,15E-03	2,33E-03
4÷6	0,00E+00	1,42E-03	3,43E-03	3,31E-03	3,69E-03
6÷8	0,00E+00	3,48E-03	6,74E-03	7,00E-03	6,41E-03
8÷10	0,00E+00	9,17E-03	1,73E-02	1,45E-02	1,27E-02
10÷12	1,29E-01	4,81E-02	5,06E-02	3,56E-02	2,56E-02
12÷14	1,25E-01	8,85E-02	1,00E-01	6,34E-02	4,43E-02
14÷16	1,11E-01	1,03E-01	1,22E-01	8,46E-02	5,86E-02
16÷18	1,01E-01	1,11E-01	1,26E-01	9,15E-02	6,42E-02
18÷20	8,71E-02(*	1,08E-01	1,21E-01	8,95E-02	6,63E-02
20÷22	8,27E-02	1,04E-01	1,14E-01	8,16E-02	6,41E-02
22÷24	7,22E-02	9,99E-02	1,09E-01	7,09E-02	5,11E-02
24÷26	5,71E-02	8,94E-02	1,03E-01	6,14E-02	4,79E-02
26÷28	3,94E-02	6,73E-02	9,29E-02	5,28E-02	3,71E-02
28÷30	1,26E-02	2,51E-02	4,19E-02	3,49E-02	2,88E-02
30÷32	3,33E-03	8,05E-03	2,06E-02	2,18E-02	2,15E-02
32÷34	2,59E-03	5,01E-03	1,39E-02	1,56E-02	1,47E-02
34÷36	1,03E-03	3,34E-03	8,94E-03	1,13E-02	1,14E-02
36÷38	1,10E-03	2,39E-03	6,36E-03	8,28E-03	8,63E-03
38÷40	5,78E-04	1,82E-03	4,74E-03	5,53E-03	5,88E-03
40÷42	3,19E-04	1,01E-03	3,30E-03	4,10E-03	4,52E-03
42÷44	3,70E-04	8,96E-04	2,58E-03	3,48E-03	3,41E-03
44÷46	3,07E-04	6,89E-04	2,14E-03	2,19E-03	2,49E-03
46÷48	1,56E-04	6,26E-04	1,24E-03	1,67E-03	1,93E-03
48÷50	1,22E-04	3,59E-04	6,48E-04	1,38E-03	1,41E-03
50÷52	1,63E-04	2,41E-04	5,89E-04	8,44E-04	1,22E-03
52÷54	1,04E-04	2,48E-04	5,89E-04	9,70E-04	7,93E-04
54÷56	3,33E-05	9,63E-05	5,07E-04	7,41E-04	8,59E-04
56÷58	9,26E-05	1,74E-04	2,70E-04	5,11E-04	6,44E-04

*) 8,71E-02 = $8{,}71 \cdot 10^{-2}$

6.5 Reactivity balance at changes in the core and reflector

Reactivity changes at changes in the core are calculated for the variant with lead target. For regular (operation) state of the core, K_{eff}=0,951 (Table 6.1). At such deep subcriticality, there is no need to provide the installation with emergency protection controls. [8].

6.5.1 Reactivity changes at start load forming

In assumed core composition, 134 FA and 7 lead displacers at periphery are loaded in the core. At core forming, displacers can be partly or completely replaced for FA (or FA replaced for displacers), if measured subcriticality of the regular load does not coincide with designed value. Calculation results of dependence of the change of K_{eff} on the quantity of loaded FA at lowered lid of the core and upper end reflector are given in Table 6.19:

$$\Delta K_{eff} = K_{eff}(N) - K_{eff}(134),$$

where K_{eff} (N) and K_{eff} (134) – are values of K_{eff} at loading of N and 134 FA in the core.

If all lead displacers are replaced for FA, i.e. 141 FA are located in the core, this will increase the K_{eff} for 1,49% (K_{eff}=0,965) . At that, the level K_{eff}=0,98 will not be exceeded.

The FA effectivity of each row is calculated, i.e. the. ΔK_{eff} at removal of FA (air is in place of removed FA). The lid of the core and upper end reflector

are in regular state. The location of removable FA is given in Figure 6.9, calculation results are given in table.6.20. Effectivity of FA is from 0,33 to 0,46%.

Table 6.19 – Change of K_{eff} at replacement of lead displacers for FA at core periphery

Number of FA/lead displacers	ΔK_{eff}
132/8	-0,0067
133/8	-0,0037
134/7	0
135/6	0,0019
136/5	0,0042
138/3	0,0084
141/0	0,0149

Table 6.20 – Change of K_{eff} at removal of FA from the core

Number of a cell with FA (Fig.6.9)	ΔK_{eff}
1	-0,0046
2	-0,0046
3	-0,00434
4	-0,00428
5	-0,0033

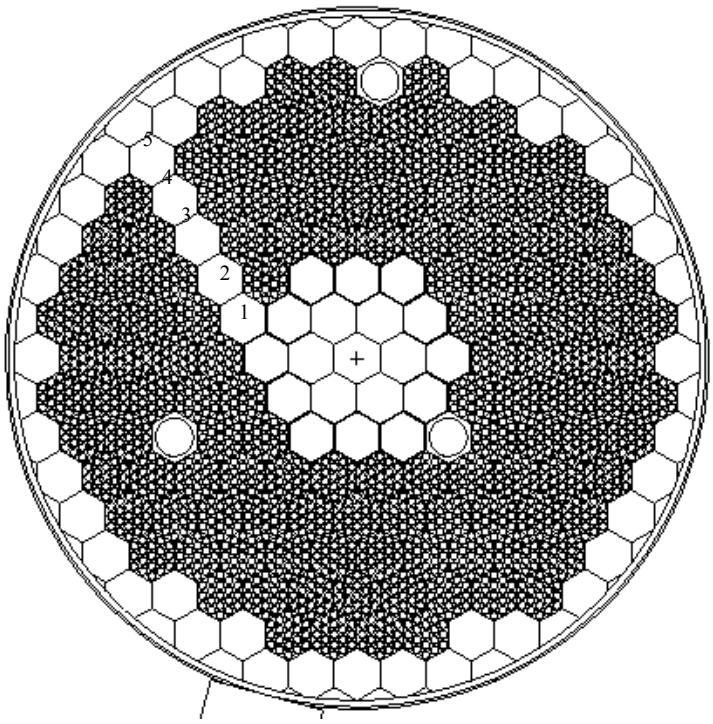

Figure 6.9 – Location of FA, which can be removed from the core.
1-5 - numbers of removable FA from Table 6.19

6.5.2 Reactivity change at filling of experimental channels

After regular load of the core is formed, the core closes with lid, upper end reflector and protective plugs. A reactivity change of the core is possible in this position only in case if experimental channels in the core and side reflector get filled. Because mass-dimensional data of samples are not determined, let us consider two hypothetical variants to evaluate the upper limit of possible influence on reactivity:

1) 100% of internal volume of experimental channel is filled with boron carbide;

2) a regular FA is inserted in experimental channel.

The second variant is not possible for experimental channels in the core, because outer dimensions of FA are larger than internal channel diameter. The calculations assumed that experimental channel was dismantled and FA was installed in its place in the grid. The results of calculation are given in Table 6.21. Vertical experimental channels are numbered from the core center to periphery. The channels 1-3 are situated in the core (Fig.6.10), the channels 4-6 are located in lead reflector (Fig. 6.11). Even if FA are located in all experimental channels, the value K_{eff} is 0,966, and this does not exceed the threshold value 0,98 (emergency protection channels and emergency protection controls are not required, item.2.19 [7]).

Table 6.21 – Change of K_{eff} at location of materials in vertical experimental channels

Filling of Experimental channels	Channel number					
	1	2	3	4	5	6
with	ΔK_{eff}					
B_4C of density 1,1 g/cm^3	-0,0041	-0,0031				

Table 6.21, continued

Filling of experimental Channels with	Channel number					
	1	2	3	4	5	6
B_4C of density 1,7	-0,0062	-0,0054				

g/cm^3						
FA in one channel	0,0042	0,0042	0,0033	0,0021	0,0004	0,0004
FA in channels 1-3	0,0121					
FA in channels 4-6				0,0022		

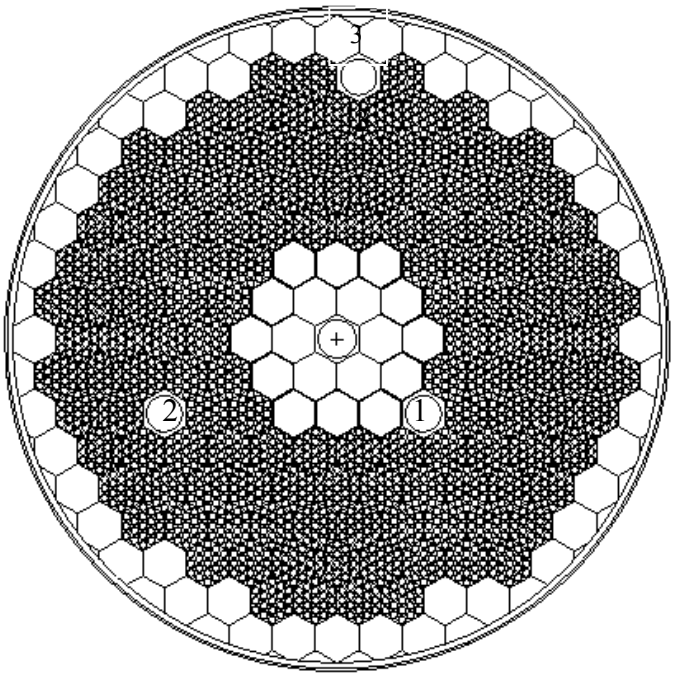

Figure 6.10 – Location of vertical experimental channels in the core
1-3 - numbers of experimental channels

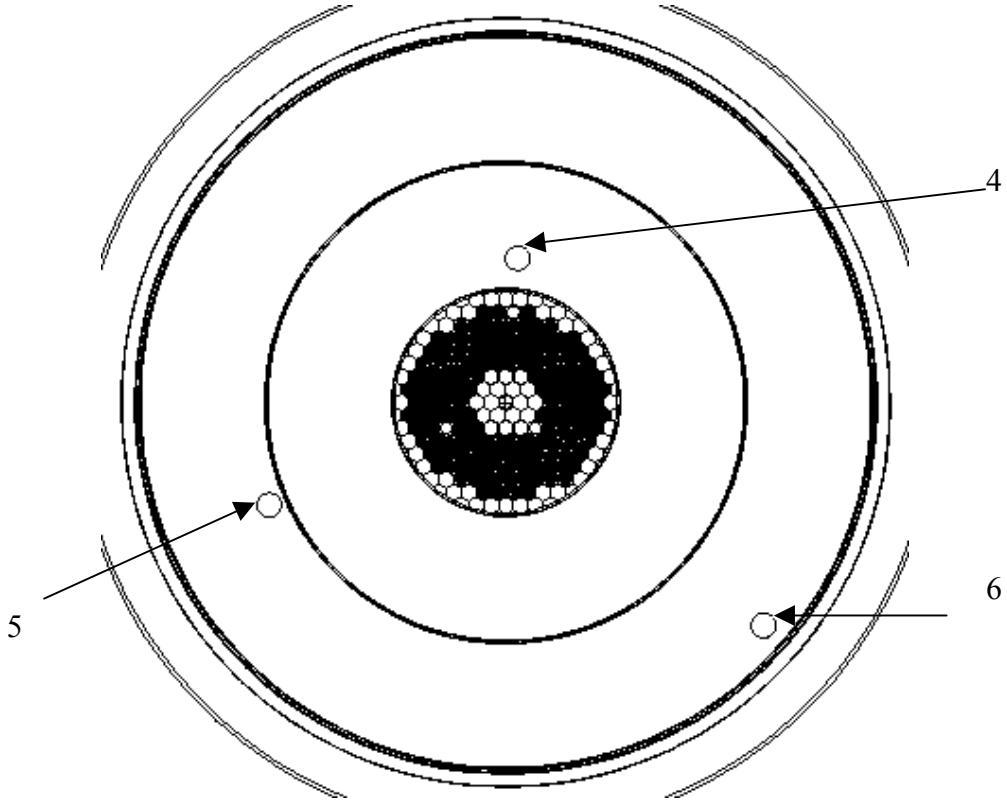

Figure 6.11 – Location of vertical experimental channels in side reflector of the core.
4-6 - numbers of experimental channels.

6.5.3 Flooding the core and experimental channels with water

SAD is an installation with neutron flux density spectrum close to that of fast neutron reactors. Correspondingly, a possibility of getting inside of large masses of neutron-delaying materials, first of all water, should be excluded in such a core. This is realized in SAD by assumed design solutions.(see chapter 12). To demonstrate a necessity of such solutions, the below calculations were carried out.

For variant with lead target, hypothetical situations with flooding the core and experimental channels in the core with water were considered, and following results were obtained:

1) K_{eff}= 1,221 for a case, when all air duct in the core and experimental channels are flooded with water;
2) K_{eff}= 0,962 for a case, when channel 1 only is filled with water (Fig. 6.10);
3) K_{eff}= 0,961 for a case, when channel 2 only is filled with water ;
4) $K_{эфф}$= 0,956 for a case, when channel 3 only is filled with water ;
5) $K_{эфф}$= 0,975 for a case, when channels 1,2 and 3 are is filled with water .

The results show that the requirement to exclude penetration of water into the core is a justified requirement. At that, flooding experimental channels only does not cause supercritical states.

6.6 Neutron flux density in experimental channels

An important consumer feature of SAD is value and energy distribution (spectrum) of neutron flux density in experimental channels. These values are calculated for all channels. Figures 6.12, 6.13 show energy dependences of neutron flux densities in all vertical channels of the core and reflector for lead target variant. Values averaged against internal channel volume at core level (height 58 cm) are given. At that, height distribution corresponds to height distribution of energy release in fuel. (see Table 6.8). Summary values for neutron flux density values in channels 1-6 are $2{,}43\cdot10^{12}$ 1/(cm^2·s), $2{,}21\cdot10^{12}$ 1/(cm^2·s), $1{,}85\cdot10^{12}$ 1/(cm^2·s), $1{,}47\cdot10^{12}$ 1/(cm^2·s), $1{,}15\cdot10^{12}$ 1/(cm^2·s), $8{,}96\cdot10^{11}$ 1/(cm^2·s), correspondingly. Flux density in the beginning part of horizontal channels is given in Table 6.22. For the variant with tungsten target, the corresponding values are 9% lower, which is caused by a lesser heat power of installation (Table 6.1).

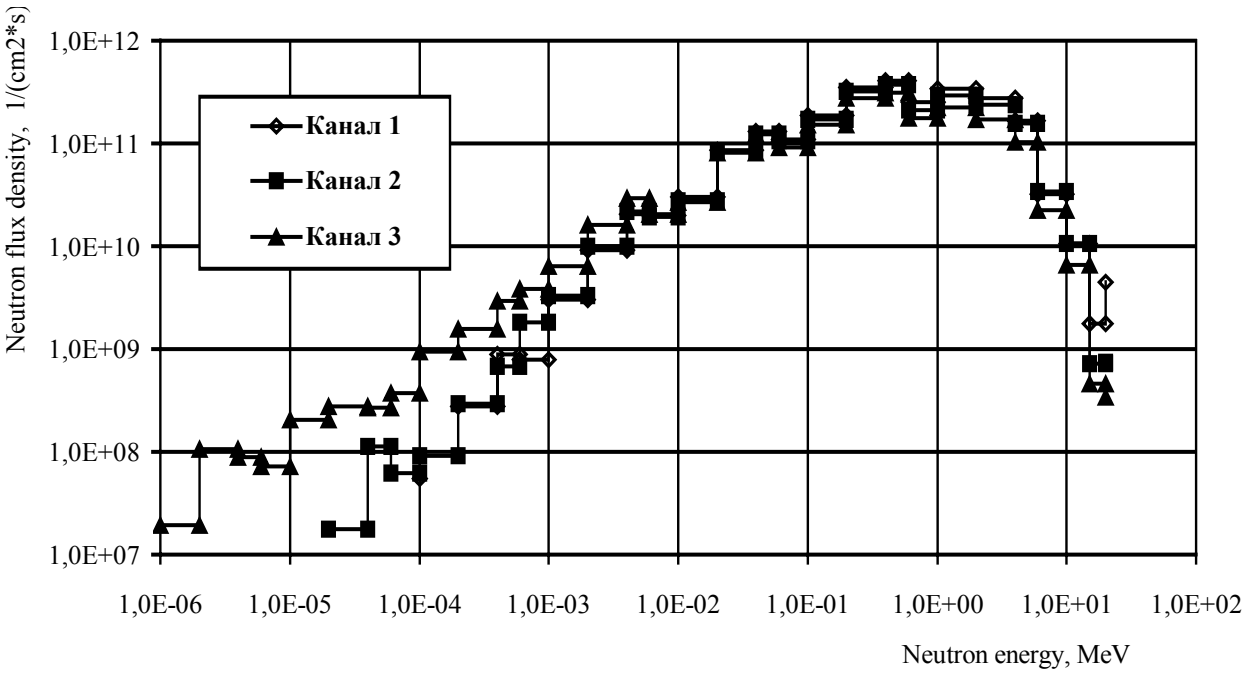

Figure 6.12 – Neutron flux density in core experimental channels

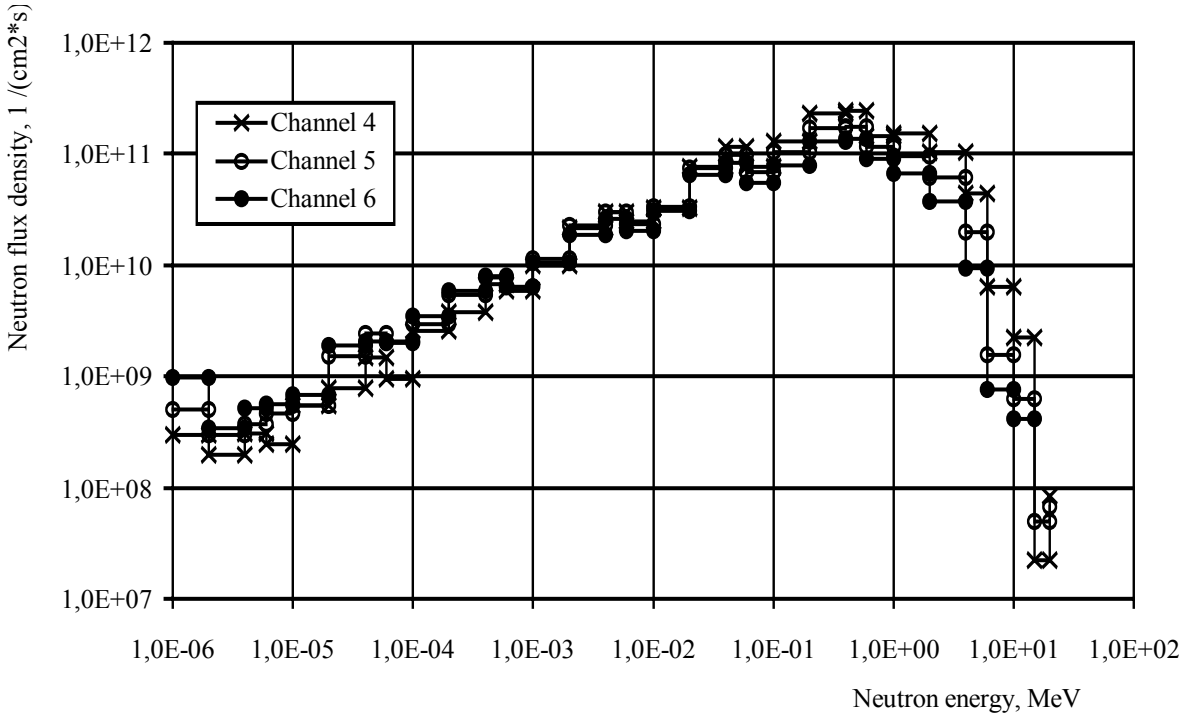

Figure 6.13 – Neutron flux density in experimental channels in reflector

Table 6.22 – Neutron flux densities in the beginning part of upper, central and bottom horizontal channels

Neutron enegry (MeV)	Upper channel	Central channel	Bottom channel
$1{,}0\cdot10^{-6}$	$7{,}68\cdot10^{9}$	$4{,}26\cdot10^{8}$	$1{,}04\cdot10^{10}$
$2{,}0\cdot10^{-6}$	$1{,}89\cdot10^{9}$	$3{,}35\cdot10^{8}$	$2{,}67\cdot10^{9}$
$4{,}0\cdot10^{-6}$	$2{,}06\cdot10^{9}$	$5{,}78\cdot10^{8}$	$2{,}49\cdot10^{9}$
$6{,}0\cdot10^{-6}$	$1{,}39\cdot10^{9}$	$6{,}98\cdot10^{8}$	$1{,}53\cdot10^{9}$
$1{,}0\cdot10^{-5}$	$2{,}00\cdot10^{9}$	$1{,}01\cdot10^{9}$	$2{,}14\cdot10^{9}$
$2{,}0\cdot10^{-5}$	$3{,}63\cdot10^{9}$	$1{,}81\cdot10^{9}$	$3{,}02\cdot10^{9}$
$4{,}0\cdot10^{-5}$	$3{,}84\cdot10^{9}$	$2{,}57\cdot10^{9}$	$3{,}85\cdot10^{9}$
$6{,}0\cdot10^{-5}$	$2{,}88\cdot10^{9}$	$1{,}97\cdot10^{9}$	$3{,}03\cdot10^{9}$
$1{,}0\cdot10^{-4}$	$4{,}66\cdot10^{9}$	$3{,}85\cdot10^{9}$	$4{,}14\cdot10^{9}$
$2{,}0\cdot10^{-4}$	$8{,}10\cdot10^{9}$	$6{,}79\cdot10^{9}$	$6{,}56\cdot10^{9}$
$4{,}0\cdot10^{-4}$	$9{,}14\cdot10^{9}$	$9{,}71\cdot10^{9}$	$7{,}73\cdot10^{9}$
$6{,}0\cdot10^{-4}$	$5{,}50\cdot10^{9}$	$7{,}93\cdot10^{9}$	$5{,}63\cdot10^{9}$
$1{,}0\cdot10^{-3}$	$8{,}66\cdot10^{9}$	$1{,}25\cdot10^{10}$	$8{,}87\cdot10^{9}$
$2{,}0\cdot10^{-3}$	$1{,}26\cdot10^{10}$	$2{,}48\cdot10^{10}$	$1{,}40\cdot10^{10}$
$4{,}0\cdot10^{-3}$	$1{,}43\cdot10^{10}$	$3{,}19\cdot10^{10}$	$1{,}56\cdot10^{10}$
$6{,}0\cdot10^{-3}$	$8{,}73\cdot10^{9}$	$2{,}19\cdot10^{10}$	$1{,}01\cdot10^{10}$
$1{,}0\cdot10^{-2}$	$1{,}27\cdot10^{10}$	$3{,}29\cdot10^{10}$	$1{,}49\cdot10^{10}$
$2{,}0\cdot10^{-2}$	$2{,}50\cdot10^{10}$	$6{,}50\cdot10^{10}$	$2{,}90\cdot10^{10}$
$4{,}0\cdot10^{-2}$	$3{,}20\cdot10^{10}$	$9{,}58\cdot10^{10}$	$3{,}75\cdot10^{10}$
$6{,}0\cdot10^{-2}$	$2{,}11\cdot10^{10}$	$7{,}24\cdot10^{10}$	$2{,}48\cdot10^{10}$
$1{,}0\cdot10^{-1}$	$2{,}85\cdot10^{10}$	$1{,}05\cdot10^{11}$	$3{,}48\cdot10^{10}$
$2{,}0\cdot10^{-1}$	$4{,}45\cdot10^{10}$	$1{,}83\cdot10^{11}$	$5{,}63\cdot10^{10}$
$4{,}0\cdot10^{-1}$	$4{,}73\cdot10^{10}$	$1{,}99\cdot10^{11}$	$6{,}11\cdot10^{10}$
$6{,}0\cdot10^{-1}$	$2{,}90\cdot10^{10}$	$1{,}24\cdot10^{11}$	$3{,}77\cdot10^{10}$
1,0	$1{,}71\cdot10^{10}$	$1{,}20\cdot10^{11}$	$2{,}56\cdot10^{10}$
2,0	$7{,}14\cdot10^{9}$	$7{,}94\cdot10^{10}$	$1{,}24\cdot10^{10}$
4,0	$9{,}66\cdot10^{8}$	$3{,}11\cdot10^{10}$	$2{,}66\cdot10^{9}$
6,0	$7{,}77\cdot10^{7}$	$4{,}61\cdot10^{9}$	$1{,}52\cdot10^{8}$
10,0	$1{,}32\cdot10^{7}$	$1{,}37\cdot10^{9}$	$6{,}58\cdot10^{7}$
15,0	$1{,}12\cdot10^{7}$	$1{,}10\cdot10^{8}$	$4{,}38\cdot10^{7}$
20,0	$8{,}33\cdot10^{6}$	$1{,}37\cdot10^{8}$	$2{,}24\cdot10^{7}$
Всего:	$3{,}63\cdot10^{11}$	$1{,}24\cdot10^{12}$	$4{,}39\cdot10^{11}$

6.7 Neutron flux density at location of power monitoring sensors

Neutron flux density at location of power monitoring sensors was calculated. These sensors are situated in the concrete of biological shielding at a distance of 153,5 cm of the core central axis. It is located in a cavity filled with graphite, and a channel of 10 cm in diameter is available in the center of cavity. Based on preliminary calculations, a graphite layer thickness of 10 cm was chosen.

The calculations (Table 6.23) showed that thermal neutron flux density level (with energy below 1 eV) is equal to $2{,}7 \cdot 10^{6}$ $1/(cm^2 \cdot s)$ at heat power of the core 28,5 kW.

Table 6.23 – Energy distribution of neutron flux density in detector

Upper boundary of energy group, MeV	Neutron flux density, $1/cm^2 s$
$1{,}0 \cdot 10^{-6}$	$2{,}12 \cdot 10^{6}$
$1{,}0 \cdot 10^{-5}$	$9{,}70 \cdot 10^{4}$
$1{,}0 \cdot 10^{-4}$	$1{,}32 \cdot 10^{5}$
$1{,}0 \cdot 10^{-3}$	$4{,}53 \cdot 10^{4}$
$1{,}0 \cdot 10^{-2}$	$2{,}20 \cdot 10^{5}$
$1{,}0 \cdot 10^{-1}$	$1{,}03 \cdot 10^{4}$
1,0	$1{,}02 \cdot 10^{5}$
10	$4{,}87 \cdot 10^{3}$
20	$3{,}40 \cdot 10^{2}$
Sum	$2{,}73 \cdot 10^{6}$

6.8 Procedure of fuel loading in the core at physical start-up of installation SAD

Fuel is loaded in the core and operation value of K_{eff} is achieved in accordance with requirements item 7.2 [8].

Initial state of installation SAD prior to fuel loading procedure:

- All SAD equipment elements are mounted, including bottom and side reflectors, core and target cooling duct and so on.;
- Lead target is placed in regular position,
- Lead and steel displacers and FA simulators are put in the core; outer dimensions of the FA simulators are identical to regular FA, they have upper and bottom constructions identical to regular FA, which are connected with 7 steel rods repeating outer geometry of fuel elements, they are located along central axis and in vertices of six angles;
- Start-up neutron source with an intensity approximately 10^7 1/s is installed in one of vertical experimental channels of the core .

Fuel is loaded in the core by serial replacement of simulators for regular fuel assemblies. At first stage of fuel loading, the core lid and upper end reflector are missing. Loading is executed in serial steps. First not more than 10% of regular loading of the core is loaded. After readout of monitoring devices of neutron flux density, a second fuel lot is loaded, which should be not bigger than the first lot. Further each following fuel lot to be loaded should not exceed 25% of remaining

FA amount up to full core loading in the quantity of 134 FA. After each fuel lot loading, the neutron flux density control devices are read out and diagram 1/N is plotted (item.7.2.4 [8]). 4 hexagonal rows of the core, containing, all together, 106 FA, are loaded to the described procedure.. The lid and upper reflector are mounted after that and neutron flux density control devices are read out. At the second stage the core lid and upper reflector are installed after loading each lot of FA. Neutron flux density control devices are read out in the state without lid and reflector and in the state with lid and reflector installed. FA are loaded in serial lots of 6, 5, 4, 3, 2, 2, and six times 1 FA each.

The character of K_{eff} change at fuel loading stages in the core is given in Table 6.24. At all fuel loading stages, the K_{eff} does not exceed the value 0,98.

After fuel loading, practically achieved value of K_{eff} is determined experimentally. ения работ будут определены в программе и методике физического пуска SAD. will be determined in the program and method of physical start-up of SAD installation.

If, for any reason, the required value K_{eff}=0,95 is not achieved at loading of 134 FA in the core, then there is a possibility to increase K_{eff} , by replacing 7 lead displacers for FA. At that, При этом можно увеличить K_{eff} can be increased by 0,015, on the average, a loading of 1 FA increases the K_{eff} by 0,00213.

After correction of K_{eff} , the core is closed and no change in its composition during the work with lead target is foreseen. The core composition is changed after replacement of lead target for the tungsten target.

After fuel is loaded in the core, no special neutron source to monitor the state of the core is required. Total regular fuel load generates about $(3\div5)\cdot10^6$ neutrons per second at the expense of spontaneous fission of plutonium-240 and at the expense of fission neutron multiplication in subcritical system (approximately 20). Total neutron generation intensity in the core is approximately $(6\div10)\ 10^7$ 1/s.

Table 6.24 – Calculation of K_{eff} change at FA loading in the core

Number of loaded FA	**R_{eff}**	**Standard deviation**
Stage 1		
17(*	0,2712	0,00012
41	0,4863	0,00018
70	0,6681	0,00022
106	0,8326	0,00026
Stage 2		
106 (the core lid and upper reflector are in their regular places)	0,8507	0,00026
112	0,8737	0,00019
118	0,8955	0,00019
124	0,9174	0,00019
130	0,9379	0,00019
131	0,9411	0,00019
132	0,9447	0,00019
133	0,9477	0,00019

134	0,9514	0,00020

*) All fuel assemblies are supposed to have the same fuel composition, which corresponds to that given in Table 6.1.

6.9 Conclusion

The section contains results of neutron-physical calculation research, executed to substantiate design solutions and safety of SAD running. The section describes:

- Energy release distribution in SAD constructs for core variants with lead and tungsten targets;
- Energy release in core and target after proton accelerator beam is switched off;
- K_{eff} change of the core for various initial events;
- neutron generation intensity in lead and tungsten targets under the action of proton beam;
- fuel loading procedure into the core.

Volume and content of results represented allow to substantiate the accuracy of design solutions and to confirm the necessity of observing nuclear safety requirements at SAD installation.

7 Results of thermohydraulic calculations

7.1 Introduction

Thermohydraulic calculations of cooling of subcritical blanket SAD are executed in accordance with technical assignment requirements (Appendix A), results of neutron-physical calculations (section 6) for a design, presented in design documentation SAD.00.000.

A direct-flow cooling scheme of the core with lead target, given in Figure 7.1, is realized in the installation. The ducts of lead target and core are parallel channels with a joint mixture chamber at outlet section. Pressure differences in cooling ducts connected in parallel, are the same. This is achieved by means of throttle devices in core cooling loop. Coolant discharge distribution among cooling ducts is executed by regulating armature at outlet section and target duct.

Cylinder housing of blanket located in biological shielding, made of iron-serpentinite concrete, is designed for location of replaceable targets, subcritical multiplying blanket, as well as for organizing air coolant flow for their cooling. Central part of lead target is cooled autonomously through pipeline Dpass = 24mm.

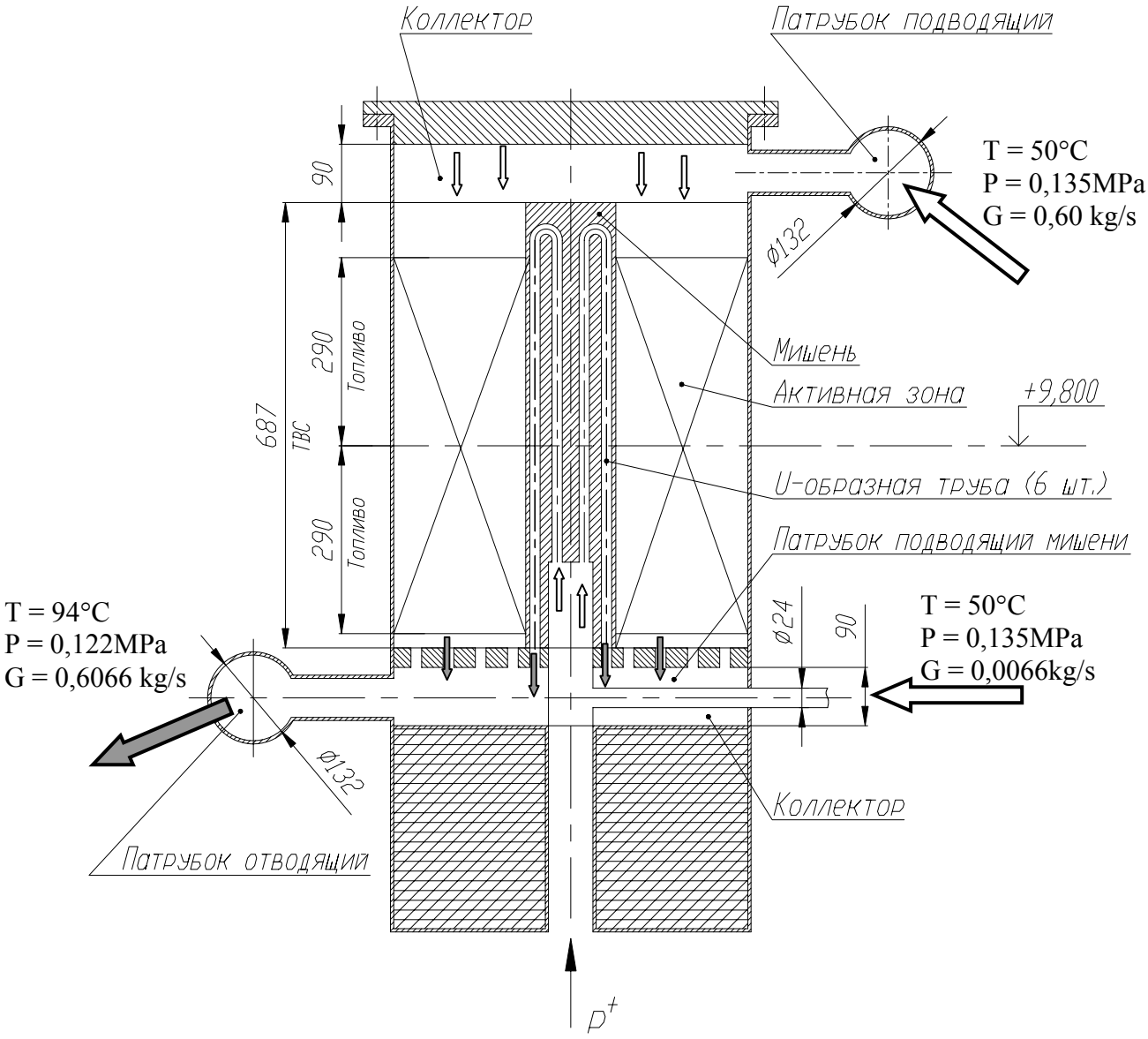

collector, fuel, fuel,exit branch, inlet branch, target, core, U-shaped pipe (6 ps)

Figure 7.1 - Cooling scheme of the core with lead target

target inlet branch, collector

№ подл.	Подпись и дата	Взам. инв. №	Инв. № дубл.	Подпись и дата

Лист

with discharge 0.00662 kg/s to pressure chamber and further, through six U-shaped pipes ∅ 6×0.5mm, inundated in lead, to outlet core cooling duct and twelve periphery blocks of lead target.

The core and tungsten target are cooled by supplying the coolant through the pipeline Dpass=200mm via rectangular section box to pressure collector and further, through the core to exit box and then to outlet pipeline.

The core is collected from FA installed vertically. Lead blocks are installed in cells not occupied by FA. A FA is composed of 18 fuel elements. Structurally, a rod-type fuel element is a cylindrical cladding made of stainless steel, where a fuel column consisting of pellets of mixed uranium dioxide and plutonium. Fuel pellets are a continuous mixture, without internal hole. The ends of cladding are sealed by welding top and bottom steel end pieces (gags). The bottom end piece is placed in the bottom FA spacer grid and fixed there by means of welding.. Fuel pellet column is drawn in by a spring holder. The internal volume of fuel element is filled with high purity helium. Outer surface of the cladding is spiraled with ellipse-shaped spacer wire (0,6 x 1,3 mm).

The FA are installed on support plate of blanket housing across a rectilinear triangle grid with a pitch of 36 mm.

Structurally, each fuel assembly consists of:

- 18 fuel elements;
- bearing rod;
- bottom spacer grid;
- upper flange with cover;
- hold head for reloading tool.

Bearing FA element is bearing rod, to which bottom spacer grid, upper flange with cover and FA head are welded. The bottom spacer grid forms the fuel

elements bundle in rectilinear triangular grid with a pitch of 7,6 mm. This grid has six holes with a diameter of 3,5 mm for passing air, these holes when FA is placed on the support plate of blanket housing do coincide with holes in the plate, which are 4,0 mm in diameter.

For the purpose of thermohydraulic calculations, the following values of maximum admissible parameters were assumed:

- fuel element temperature - 250°C *)

- lead target temperature - 250°C

-tungsten target temperature - 300°C

Remark: *) Calculations showed that temperature difference in fuel element cross-section does not exceed 2,5°C.

Thermohydraulic calculations of core and target are carried out with the use of cell code POOCHOK BM-SWEEP-1 [9] and Russian commercial three-dimensional code FLOW VISION [10]. Specific character of autonomous lead target cooling required the application of three-dimensional code, while methods of averaging flow data in FA cross-section or cells between fuel elements could be sufficient for thermohydraulic data calculation of the core. Adiabatic conditions were taken at the target-core boundary, what yielded a conservative estimate of maximum target temperature.

The tungsten target is cooled with general coolant flow of the core. In this connection, a necessity arises to solve a dual problem: core – target. That problem

was solved by means of code FLOW VISION. The core calculation was carried out according to one-temperature model of porous body, implemented in the code FLOW VISION. For tungsten target, heat conductivity equation was solved by means of the same code. Obtained heat flows on side surface of the target were used in the cell calculation of the core, which to some extend was a duplicate calculation to that using the porous body model. It should be noted, that cell calculation allows, in the framework of averaged models, to calculate more precisely the flow data in the field of non-heated surfaces, non-regular cells etc.

The cell calculation of the core was carried out in two stages. At the first stage, calculation for 1/12 symmetrical part of core cross-section was executed. At that, FA were considered as cells. At the second stage, a calculation of FA, where fuel element temperature was maximal, was carried out. FA cross-section was divided in cells, formed by fuel elements. As distinct from the first stage, azimuth heat spread in fuel elements was taken into account at the second stage.

After thermohydraulic calculations for nominal power, maximum temperature values of cooling loop elements under consideration of parameter deviations from nominal values were estimated.

7.2 Core with lead target

7.2.1 Calculation model

Cell-by-cell calculation of the core with lead target is executed with program POOCHOK BM-SWEEP [9], designed for thermohydraulic calculation of gas-cooled rod assemblies supplemented with algorithm allowing to account for azimuth heat spreads in fuel elements.

According to algorithm of the program POOCHOK BM-SWEEP, the core section is divided in cells, thermophysical flow parameters (mass velocity, temperature) within those cells are assumed to be constant. The core is considered as a system of parallel communicating channels; a balance equation taking into account their interaction is written for each such channel. A cell numbered k is characterized by passing surface F_k, , wet perimeters of solid cell-forming surfaces Π_k^j, relative pitch between fuel elements $(S/d)_k$, hydraulic diameter $d_{Г,\ k}$. A cell numbered k is adjacent to a cell n, divided by specific perimeter $П_{kn}$. The flow of mass W_{kn} from cell n to cell k is conditionally considered positive, if the flow is directed from cell n to cell k, and negative – in the opposite case. τ_{kn} and q_{kn} are the from-cell-to-cell transfer of motion and heat correspondingly. A flow with discharge m_k and heat content i_k. moves through the cell under consideration. Friction on the wall with perimeter Π_k^j is designated as τ_k^j, and heat flow density as q_k^j.

Mass balance, motion and energy quantity equations have, for the cell k, the form :

$$\frac{dm}{dz} = \sum W_{kn} \tag{7.5}$$

$$\frac{1}{F_k} \cdot \frac{d}{dz} \cdot \left(\frac{m_k^2}{\rho_k} \right) + F_k \cdot \frac{dp_k}{dz} = \sum_n W_{kn} \cdot J_{kn} + \sum_n \tau_{kn} \cdot \Pi_{kn} - \sum_j \tau_k^j \cdot \Pi_k^j \tag{7.6}$$

$$\frac{d}{dz} \left[\left(i_k + \frac{m_k^2}{2\rho_k^2 \cdot F_k^2} \right) \cdot m_k \right] = \sum_n \left(i + \frac{u^2}{2} \right)_{kn} \cdot W_{kn} + \sum_n q_k \cdot \Pi_{kn} + \sum_j q_k^j \cdot \Pi_k^j \tag{7.7}$$

Where $k = 1, 2, \ldots N$;

$W_{kn} + W_{nk} = 0$,

at $W_{kn} < 0$ $J_{kn} = u_k$, $Q_{kn} = i_k + \frac{1}{2} u_k^2$,

at $W_{kn} > 0$ $J_{kn} = u_n$, $Q_{kn} = i_n + \frac{1}{2} u_n^2$, $u_k = \frac{m_k}{\rho_k \cdot F_k}$.

It is assumed that within the core

$$p_1 = p_2 = \ldots p_n = idem, \tag{7.8}$$

$$\rho = \frac{p}{RT},$$

where R – is gas constant.

Equation terms (7.6), (7.7), characterizing channel-to-channel transfer of motion and heat quantity, are proportional to difference of velocities (or heat contents) in cells:

$$\tau_{kn} = \beta_{kn}^M \cdot \overline{\rho u} \cdot (u_n - u_k)$$

$$q_{kn} = \beta_{kn}^q \cdot \overline{\rho u} \cdot (i_n - i_k),$$

where β_{kn}^M, β_{kn}^q are coefficients of channel-to-channel transfer of motion and heat quantity, correspondingly.

Shear stress on the wall with perimeter Π_k^j is expressed through hydraulic resistance coefficient to friction ς_k^j and dynamic pressure:

$$\tau_k = \zeta_k^j \cdot \frac{\rho_k \cdot u_k^2}{8}.$$

Heat transfer coefficient α_k, required for temperature field calculation in fuel element is connected with Nusselt number Nu_k:

$$\alpha_k = Nu_k \cdot \frac{\lambda_k}{d_{\Gamma,k}}$$

The system of equations (7.5) – (7.7) is solved with initial conditions

$$m_k(z = 0) = m_{k,\,вх},$$

$$p_k(z = 0) = p_{вх},$$

$$i_k(z = 0) = i_{вх}.$$

Transversal convective transfers are in the process of iteration equalizing of pressure gradients for a particular cell in order to meet the condition (7.8). The system of equations (7.5) – (7.7) is solved with numerical Eulerian method with converting. Algorithm details of the program POOCHOK BM-SWEEP are given in [9].

The applied approximate method of calculations of heat azimuth spread in fuel element is based on assumption of cladding temperature constancy across its thickness and on solution of one-dimensional differencial equation for each cladding section i:

$$\frac{d^2T_i}{dl_i^2} - \lambda_i \cdot T_i = H_i\ , \qquad (7.9)$$

where l_i is local azimuth coordinate, counted from the beginning of section i;

$$\lambda_i = \frac{\alpha_i}{\frac{\lambda_{cp}}{r_2} \cdot \ln\left(\frac{r_2}{r_0}\right)} \; ;$$

$$H_i = -\frac{\alpha_i \cdot T_{cp,i}}{\frac{\lambda_{cp}}{r_2} \cdot \ln\left(\frac{r_2}{r_0}\right)} \; ;$$

where α_i, $T_{cp,\,i}$ are heat transfer coefficient and coolant temperature in section i, correspondingly

λ_{cp} – average heat conductivity coefficient of the cladding;

r_2, r_0 –outer and internal radii of the cladding, correspondingly.

General solution of equation (7.9) takes the form for temperature:

$$T_i = -\frac{H_i}{\lambda_i} + C_{1,i} \cdot Ch(\sqrt{\lambda_i} \cdot l_i) + C_{2,i} \cdot Sh(\sqrt{\lambda_i} \cdot l_i)$$

and its derivative with respect to l_i:

$$\frac{dT_i}{dl_i} = C_{1,i} \cdot \sqrt{\lambda_i} \cdot Sh(\sqrt{\lambda_i} \cdot l_i) + C_{2,i} \cdot \sqrt{\lambda_i} \cdot Ch(\sqrt{\lambda_i} \cdot l_i) \; ,$$

where $C_{1,i}$, $C_{2,i}$ are constant coefficients, defined from boundary conditions.

At solution of equation (7.9), two cases may have place: symmetry condition and periodicity condition.

The symmetry condition yields the following equations to determine coefficients:

$$\begin{gathered} C_{1,i} \cdot 0 + C_{2,i} \cdot 1 = 0 \\ C_{1,N} \cdot \sqrt{\lambda_i} \cdot Sh(\sqrt{\lambda_N} \cdot L_N) + C_{2,N} \cdot \sqrt{\lambda_N} \cdot Ch(\sqrt{\lambda_N} \cdot L_N) = 0 \end{gathered} \qquad (7.10)$$

where l_i – is length of section i,

N – number of sections.

The periodicity condition gives:

$$-C_{1,1} + C_{1,N} \cdot \sqrt{\lambda_N} \cdot Sh(\sqrt{\lambda_N} \cdot L_N) + C_{2,N} \cdot \sqrt{\lambda_N} \cdot Ch(\sqrt{\lambda_N} \cdot L_N) = \frac{H_N}{\lambda_N} - \frac{H_1}{\lambda_1}, \quad (7.11)$$

$$C_{1,N} \cdot \sqrt{\lambda_N} \cdot Sh(\sqrt{\lambda_N} \cdot L_N) + C_{2,N} \sqrt{\lambda_N} \cdot Ch(\sqrt{\lambda_N} \cdot L_N) - C_{2,1} \sqrt{\lambda_1} = 0$$

Condition of mating temperature and its gradient at the boundary of sections i-1 and i give additionally $2(N\text{-}1)$ conditions for defining $C_{1,i}$ and $C_{2,i}$.

$$C_{1,i-1} \cdot Ch(\sqrt{\lambda_{i-1}} \cdot L_{i-1}) - C_{1,i} + C_{2,i-1} \cdot Sh(\sqrt{\lambda_{i-1}} \cdot L_{i-1}) = \frac{H_{i-1}}{\lambda_{i-1}} - \frac{H_i}{\lambda_i} \quad (7.12)$$

The $2N$ system of linear equations (7.10), (7.12) or (7.11), (7.12) was solved by Gauss method.

The average heat flow density value at the cladding section i was calculated by formula:

$$q_i = q_{cp,j} + \frac{\alpha_i}{L_i \sqrt{\lambda_i}} \cdot \left[C_{1,i} \cdot Sh(\sqrt{\lambda_i} \cdot L_i) + C_{2,i} \cdot \left(Ch(\sqrt{\lambda_i} \cdot L_i) - 1 \right) \right],$$

where $q_{cp,j}$ –is average heat flow on the surface of fuel element j.

Azimuth heat spread in fuel were taken into account approximately by way of heat conductivity coefficient increase of the cladding for correction coefficient $K_П$:

$$\lambda_{ср,\ эф} = \lambda_{ср} \cdot K_П, \quad (7.13)$$

Where the expression for $K_П$ will be given in the following section.

Maximal temperatures are calculated for each cell k:

of outer surface of fuel element:

$$T_{об} = T_{ср} + \frac{q_k^j}{\alpha_k} ,$$

of internal surface of cladding:

$$T_{вн} = T_{об} + \frac{q_k^j \cdot r_2}{\lambda_{об}} \cdot \ln\left(\frac{r_2}{r_1}\right),$$

of outer surface of fuel :

$$T_o = T_{вн} + \frac{q_k^j}{2 \cdot \lambda_{He}} \cdot \delta_{He},$$

of fuel center:

$$T_{0,\,Ц} = T_0 + \frac{q_V \cdot (r_1 - \delta_{He})^2}{4\lambda_0} ,$$

where r_2, r_1 – are outer and internal radii of the cladding correspondingly;

δ_{He} – gas gap thickness;

α_k – heat transfer coefficient;

q_k^j - average heat flow density in section k taking into account azimuth heat spreads in fuel element;

q_V – density of volumetric energy release in fuel;

λ_0 – fuel heat conductivity coefficient;

$T_{ср}$ –coolant temperature.

7.2.2 Closing dependences

7.2.2.1 Hydraulic friction coefficient ς_T for laminar flow is calculated by formulas [11]:

pipe $\varsigma_T = 64/\mathrm{Re}$;

flat gap $\varsigma_T = 96/\mathrm{Re}$;

triangular cell of rod bundle $\varsigma_T = \dfrac{64 \cdot (0{,}41 + 1{,}9\sqrt[3]{s/d - 1})}{\mathrm{Re}}$;

square cell of rod bundle $\varsigma_T = \dfrac{64 \cdot (0{,}41 + 1{,}9\sqrt{s/d - 1})}{\mathrm{Re}}$.

7.2.2.2 Hydraulic friction coefficient ς_T for turbulent flow (Re ≥ 2200) is calculated by formulas [11]:

pipe $\varsigma_T = \dfrac{0{,}3164}{\mathrm{Re}^{0{,}25}}$;

flat gap $\varsigma_T = \dfrac{1{,}08 \cdot 0{,}3164}{\mathrm{Re}^{0{,}25}}$;

rod bundle cell $\varsigma_T = \dfrac{0{,}21}{\mathrm{Re}^{0{,}25}} \cdot \left[1 + \left(\dfrac{s}{d} - 1\right)\right]^{0{,}32}$.

Form factor for FA is calculated by formula:

Laminar flow $K_{TBC} = \dfrac{\varsigma_{TBC}}{\varsigma_{mp}} = \left[\sum_{j=1}^{M} \dfrac{F_j}{F_{TBC}} \cdot \left(\dfrac{d_{\Gamma,\,j}}{d_{\Gamma,\,TBC}}\right)^2 \cdot K_j^{-1}\right]^{-1}$,

Turbulent flow $K_{TBC} = \dfrac{\varsigma_{TBC}}{\varsigma_{mp}} = \left[\sum_{j=1}^{M} \dfrac{F_j}{F_{TBC}} \cdot \left(\dfrac{d_{\Gamma,j}}{d_{\Gamma,\,TBC}}\right)^{5/7} \cdot K_j^{-4/7}\right]^{-7/4}$

where ς_{mp} – friction coefficient in pipe;

j – cell number;

M – number of cells;

F_j, F_{TBC} – square of cell j and FA, correspondingly;

$d_{\Gamma,j}$, $d_{\Gamma,\,TBC}$ – hydraulic diameter of cell j and FA, correspondingly;

K_j – form factor of cell j.

7.2.2.3 Local hydraulic resistance coefficient is calculated by dependences [11]:

at sudden contraction $\varsigma_M = 0{,}5 \cdot \left(1 - \dfrac{F_M}{F_\delta}\right)$;

at sudden expansion $\varsigma_M = 1{,}1 \cdot \left[1 - \left(\dfrac{F_M}{F_\delta}\right)^2\right]$;

where F_M, F_δ -are transversal areas in narrow and broad sections correspondingly,

90°-turn

$$\varsigma_M = 0{,}41;$$

180°-turn

$$\varsigma_M = 0{,}6.$$

At Re < 10^4 , a correction for Raynolds number influence is introduced [11].

7.2.2.4 Interchannel mixing coefficients β_{kn}^M and β_{kn}^q are calculated by recommendations for assemblies with wire ribs [12]:

$$\beta_{kn}^M = \beta_{kn}^q = 0{,}15 \cdot \frac{d_{\Gamma,kn}}{h},$$

where h winding pitch, hydraulic diameter $d_{\Gamma,kn}$ – calculated by average parameters of two adjacent cells k and n.

7.2.2.5 Nusselt number for laminar flow is determined by formulas [13]:

pipe $Nu = 4{,}36,$

flat gap $Nu = 4{,}86,$

rod bundle cell $Nu = 6.$

7.2.2.6 Nusselt number for turbulent flow is determined by formulas [14]:

pipe, ring gap, rod assembly cell:

$$Nu = 0{,}023 \cdot Re^{0{,}8} \cdot Pr^{0{,}4},$$

where Pr – Prandtl number;

7.2.2.7 Correction coefficient value

Correction coefficient value $K_П$ in expression (7.13) is found from equality condition of generalized similarity factors [14]: for fuel element, consisting of cladding, fuel and gas gap, on the one hand, and cladding with a prescribed constant heat flow from internal surface, on the other hand:

$$K_П = \varepsilon_{K,0} \cdot \frac{1+x}{1-x},$$

where $\varepsilon_{K,0}$ – is a generalized parameter of heat simulator of fuel element, which can be determined by formula :

$$\varepsilon_{K,0} = \frac{\lambda_{об}}{\lambda_f} \cdot \frac{1+x+(\sigma+1)(1-x)-m_1[(1+x)+(\sigma-1)(1-x)]}{1-x+(\sigma+1)(1-x)-m_1[(1-x)+(\sigma-1)(1+x)]}$$

The following designations are used here:

λ_f – heat conductivity coefficient of air coolant;

$\lambda_{об}$ – heat conductivity coefficient of the cladding;

$x = \left(\frac{r_1}{r_2}\right)^{2k}$;

r_1 – external radius of the cladding;

r_2 – internal radius of the cladding;

k – fundamental harmonic number (for triangular cell $k = 6$);

$m_1 = \frac{\lambda_{об} - \lambda_o}{\lambda_{об} + \lambda_0}$;

λ_o – fuel heat conductivity coefficient;

$\sigma = k\,\lambda_{об} \cdot Ф / r_1$,

$\Phi = \delta_г/\lambda_т$ – thermal resistance of helium gap.

7.2.2.8 Heat physical properties of helium coolant are calculated by formulas [13]:

heat capacity $c_p = 5193$ J/(kg·K),

density $\rho = \dfrac{p}{2077,23 \cdot (T + 273)}$,

heat conductivity coefficient $\lambda = 0,1383 \cdot \left(\dfrac{T + 273}{273}\right)^{0,706}$,

dynamic viscosity $\mu = 1,866 \cdot 10^{-5} \cdot \left(\dfrac{T + 273}{273}\right)$.

7.2.2.9 Heat physical properties of air are calculated by formulas [13]:

heat capacity $c_p = 1000,4 + (T - 20) \cdot 0,132$,

density $\rho = \dfrac{p}{283,2 \cdot (T + 273)}$,

heat conductivity coefficient $\lambda = 24,42 \cdot 10^{-3} \cdot \left(\dfrac{T + 273}{273}\right)^{0,82}$,

dynamic viscosity $\mu = 17,16 \cdot 10^{-6} \cdot \left(\dfrac{T + 273}{273}\right)^{0,68}$.

7.2.2.10 Heat conductivity coefficient of fuel element materials are assumed the following:

steel cladding $\lambda_{Fe} = 11,2$ W/(m·K)

fuel $\lambda_0 = 3,68 - 0.0023 \cdot T$ W/(m·K)

7.2.2.11 Heat conductivity coefficient of tungsten is calculated by formulas [13]:

$$\lambda = 134{,}2 - 0{,}0157 \cdot T \text{ W/(m·K) at } T < 2700 \text{ K},$$

$$\lambda = 91{,}8 \text{ W/(m·K) at T} > 2700 \text{ K}$$

7.2.3 Initial data

Heat hydraulic cell-by-cell calculation of the core was carried out for the following initial data:

Heat power of the core (fuel + fuel element cladding), kW	26.1
Cooling coolant	air
Coolant pressure at core inlet, Mpa	0.135
Coolant discharge, kg/s	0,6
Coolant temperature at core inlet, °C	50
Core height, m	0,58
FA number	134
Number of fuel elements in FA	18
Outer diameter of fuel element, mm	6,9
Steel cladding thickness, mm	0,4
Nominal value of gas gap, mm	0,075
Pitch of triangular grid of fuel elements, mm	7,6

Distribution of relative energy release by core length is given in Table 7.1.

Table 7.1 – Distribution of relative energy release by core height

Z, mm	0.0	0.049	0.05	0.108	0.166	0.224	0.282	0.340	0.398
K_z	10^{-7}	10^{-7}	0.69130	0.8635	1.02085	1.1354	1.18945	1.18945	1.1414

Table 7.1, continued

Z, mm	0.456	0.514	0.572	0.630
K_z	1.05020	0.91850	0.76500	0.59820

Cell-by-cell thermohydraulic calculation of the core at first stage was carried out for 1/12 of symmetric part. Calculation area is shown in Figure 7.2. It includes 16 cells, (FA and gaps between target blocks are taken as cells) and 32 links between selected cells. Relative values of energy release by FA are also given in Fig. 7.2 . Geometrical parameters of 8 cell groups are given in Table 7.2: F_i – passing area of a cell, Π_j – wet perimeters.

Table 7.2 – Geometrical parameters of cell groups

Group number	Number of cells, included in group	Area, mm^2	Perimeter, m	
			1	2
1	5, 7, 8, 11, 12	396,99	0,39018	0,081367
2	4, 6, 9, 10	198,49	0,19509	0,040684
3	2	428,16	0,39018	0,081367
4	3	214,08	0,19509	0,040684
5	14, 15	396,99	0,39018	0,122946
6	16	396,99	0,39018	0,14372
7	13	198,49	0,19509	0,051076
8	1	74,9937	0,1004588	0

Values of local coefficients of hydraulic resistance, referring to FA passing area, are the following:

At inlet to FA – 15.4,

At outlet from FA – 196.

At the second stage, the cell-by-cell thermohydraulic calculation was carried out for ½ of FA symmetric part, where fuel element cladding temperature is maximal. Calculation area is shown in Fig. 7.3. It includes 23 cells, 11 fuel elements and 30 links between selected cells. Energy release in FA cross-section is assumed uniform. Geometrical cell parameters are given in Table 7.3..

Table 7.3 – Geometrical parameters of cell group

Group number	Cell numbers, included in group	Area, mm^2	Perimeter, m			
			1	2	3	4

1	4, 5, 9, 10, 13, 14, 18, 19	5,9631	3,6128e-3	3,6128e-3	3,6128e-3	1,6425e-3
2	6, 17	2,9816	3,6128e-3	1,8064e-3	8,2130e-4	0
3	1, 3, 11, 20, 21, 23	17,7090	5,4193e-3	5,4193e-3	1,6425e-3	0
4	2, 12, 22	7,1556	3,6128e-3	5,4750e-4	0	0
5	7, 16	2,9816	3,6128e-3	2,6277e-3	0	0
6	8, 15	5,9631	3,6128e-3	3,6128e-3	5,2553e-3	0

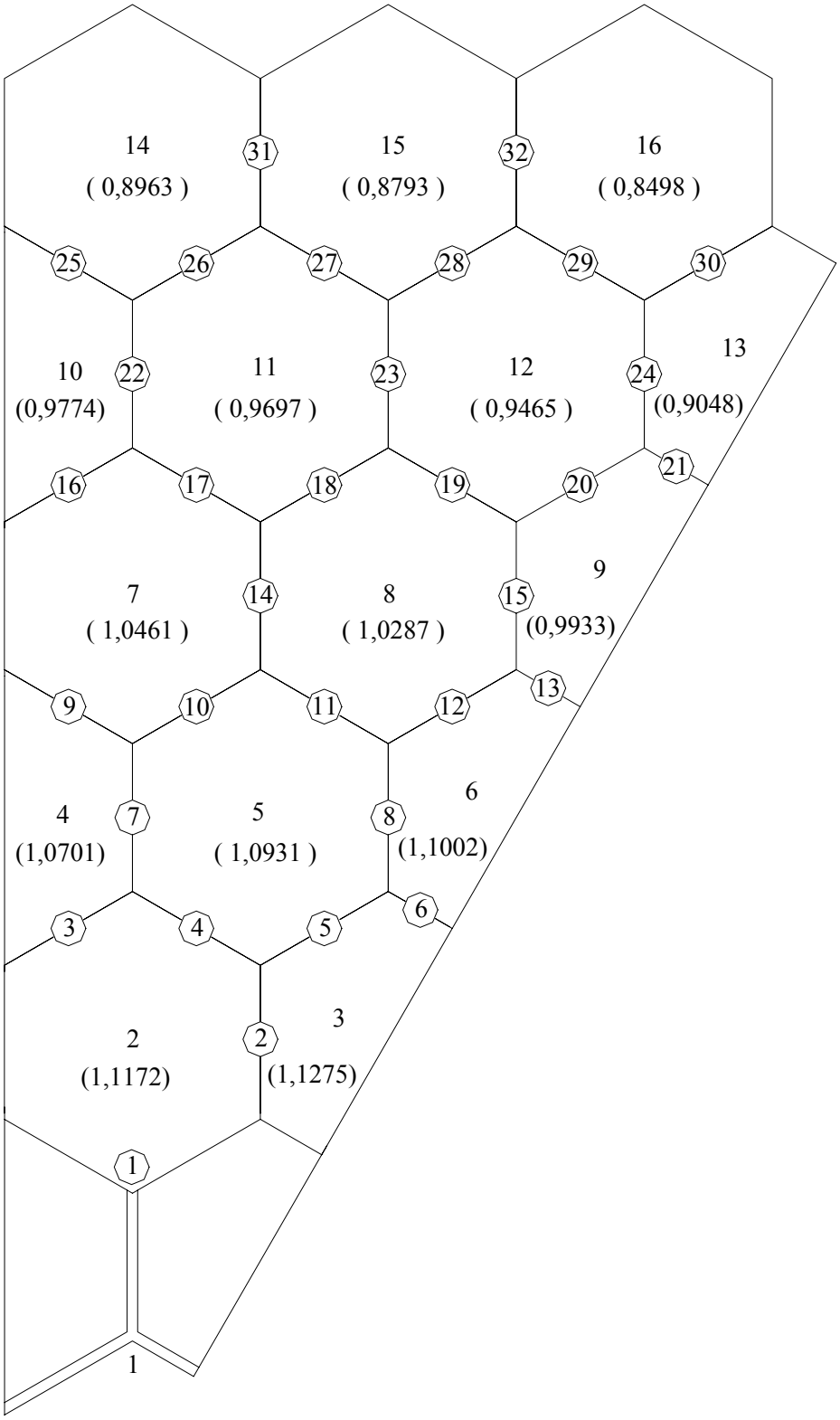

Figure 7.2 – Calculation area at stage 1.

Подпись и дата | Инв. № дубл. | Взам. инв. № | Подпись и дата | Инв. № подл.

Лист

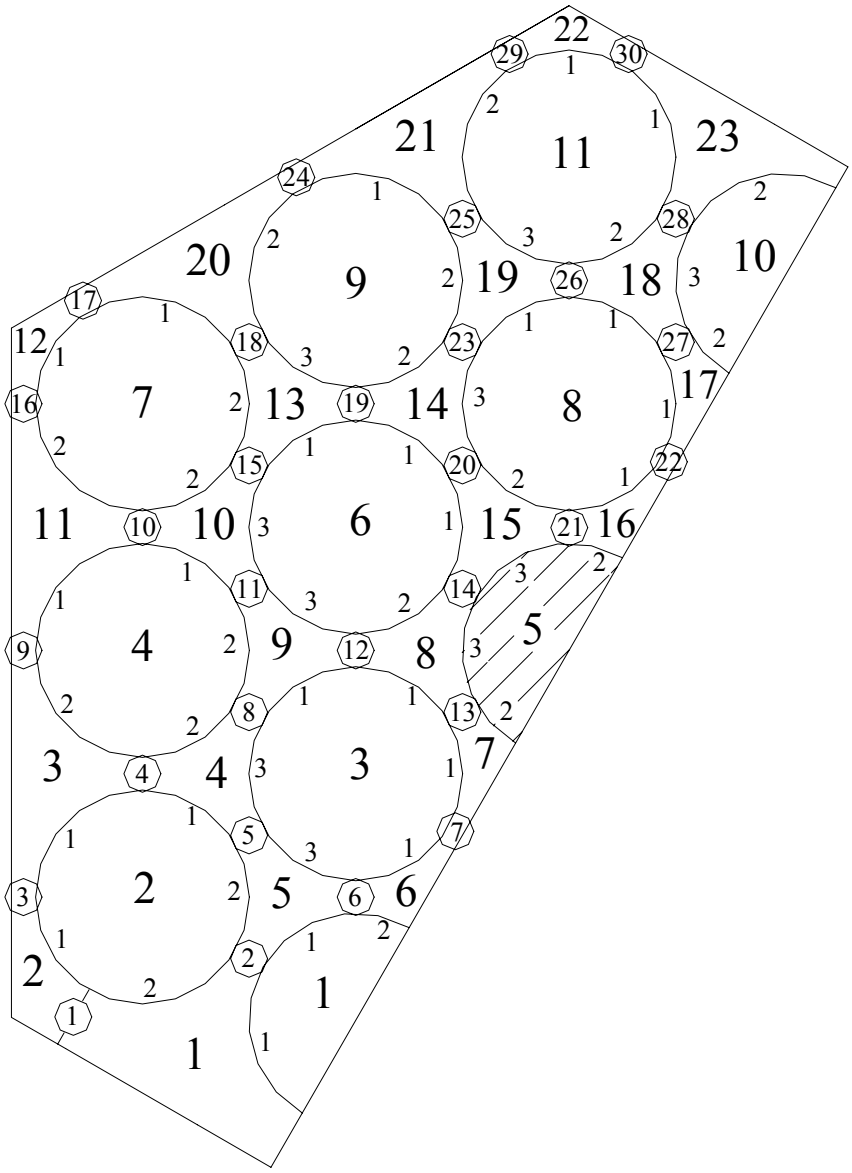

Figure 7.3 – Calculation area at stage 2.

7.2.4 Calculation results without parameter deviations

First let us consider the calculation results at stage 1. Coolant temperature distribution by core height in “cold” cell (No.2). average cross-section distribution, temperature distribution in “hot” cell (No.6), as well as temperature distributions of outer surface of cladding in cell No. 6, where they run up to maximal value, are shown in Fig. 7.4. Average heating of coolant in the core is 44°C. Minimal coolant temperature value at core outlet was 90,2°C, maximal value was 97,1°C.

The maximal temperature value of cladding is reached in cross-section, which is situated at the distance about 572 mm from outlet to the core and is 111°C. Maximal temperature difference in fuel element cross-section is below 2,5°C. That is why we can suppose that fuel element temperature is determined by outer surface of the cladding. Coolant temperature distribution cartogram and cell cladding temperature distribution in the core cross-section, where cladding temperature runs up to maximal value (z = 572 mm) are given in Fig. 7.5. The Fig.7.5 shows also distributions at the core outlet.

As can be seen from Fig. 7.4 and 7.5, irregularity of coolant temperature distribution in the core cross-section does not exceed 8°C.

Coolant velocity distribution in “cold” (No.2) and “hot” (No.6) cells as well as in target gaps (No.1) are given in Fig. 7.6. Coolant velocity distribution cartogram at core outlet is shown in Fig. 7.7.

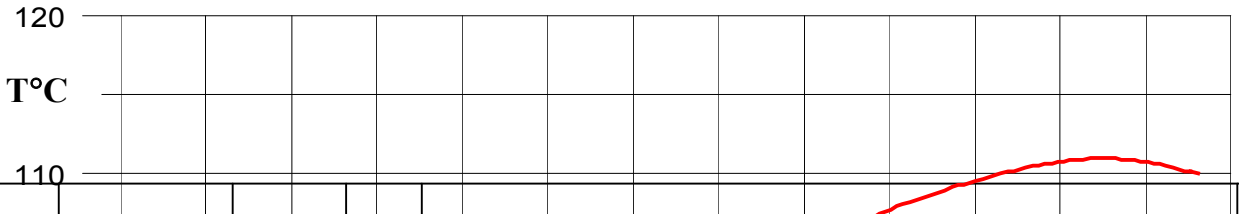

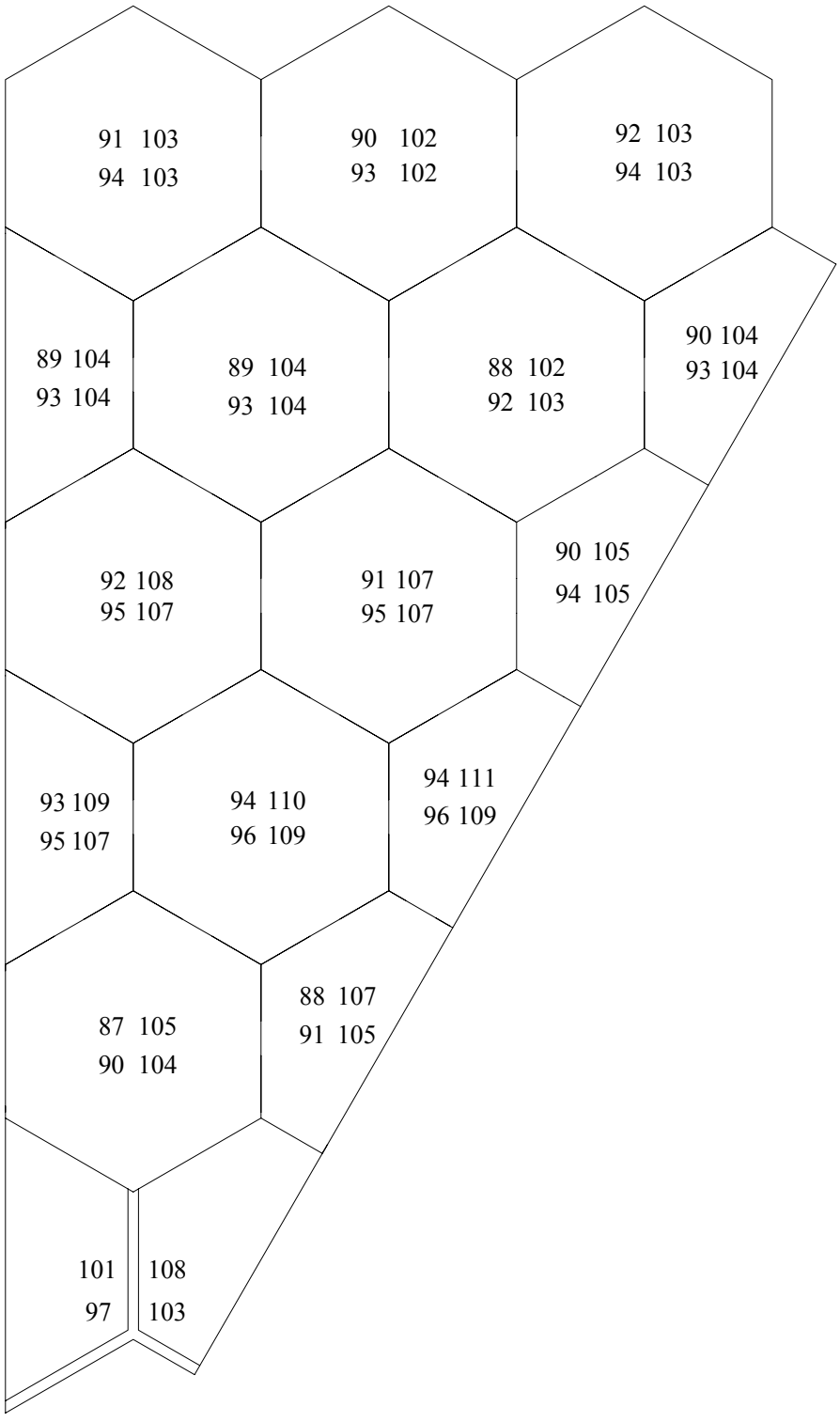

Figure 7.5 – Cartogram of coolant and cladding temperature distribution by cells in core cross-section, where cladding temperature runs up to

Maximal value (z = 572 mm),as well as at core outlet.

Column 1 – coolant temperature, column 2 - cladding temperature;

Line 1- section (z = 572 mm), line 2 – at core outlet.

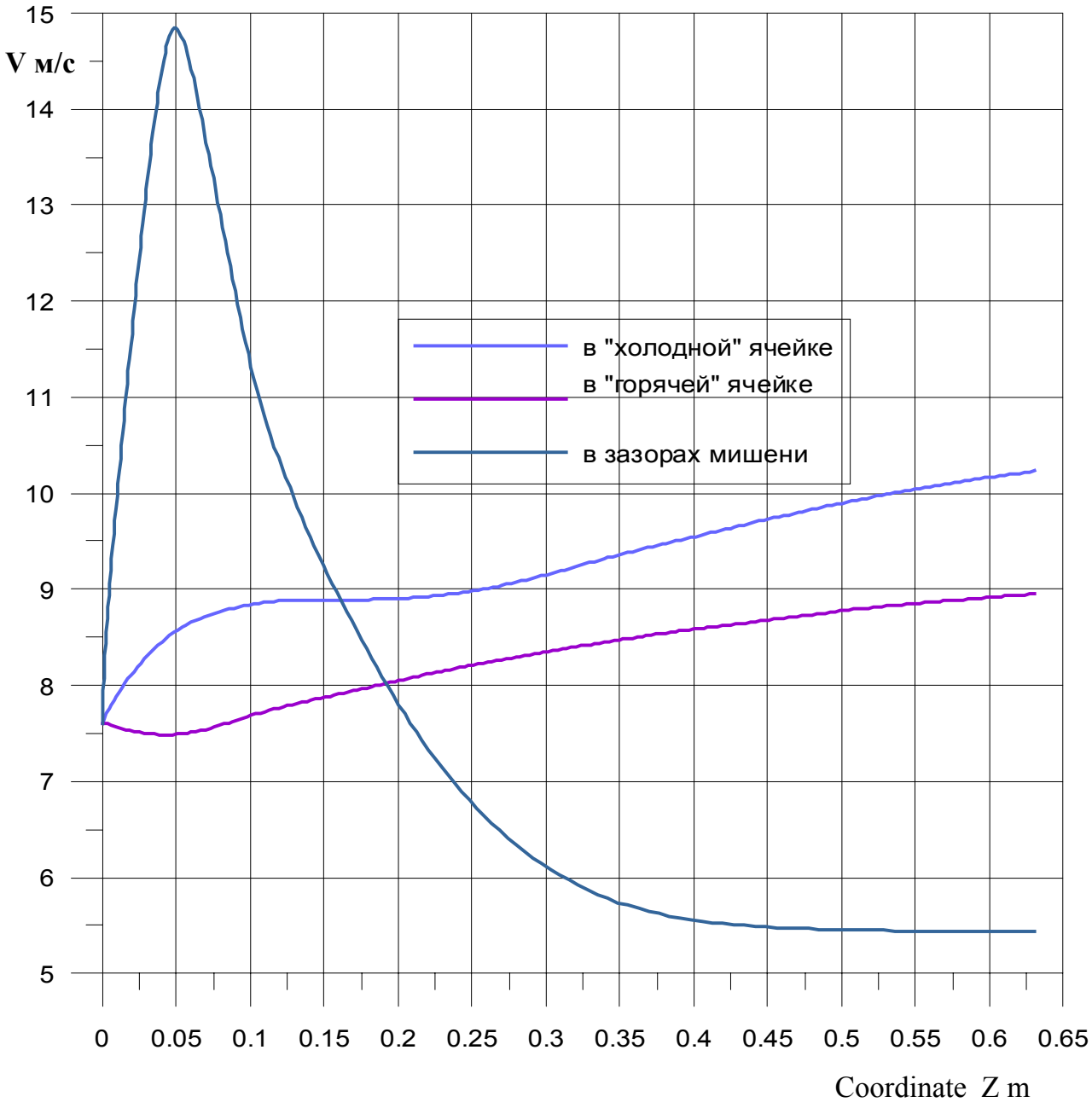

Figure 7.6 – Coolant velocity distribution in
- «cold» cell;
- «hot» cell;
- target gaps

(variant with lead target).

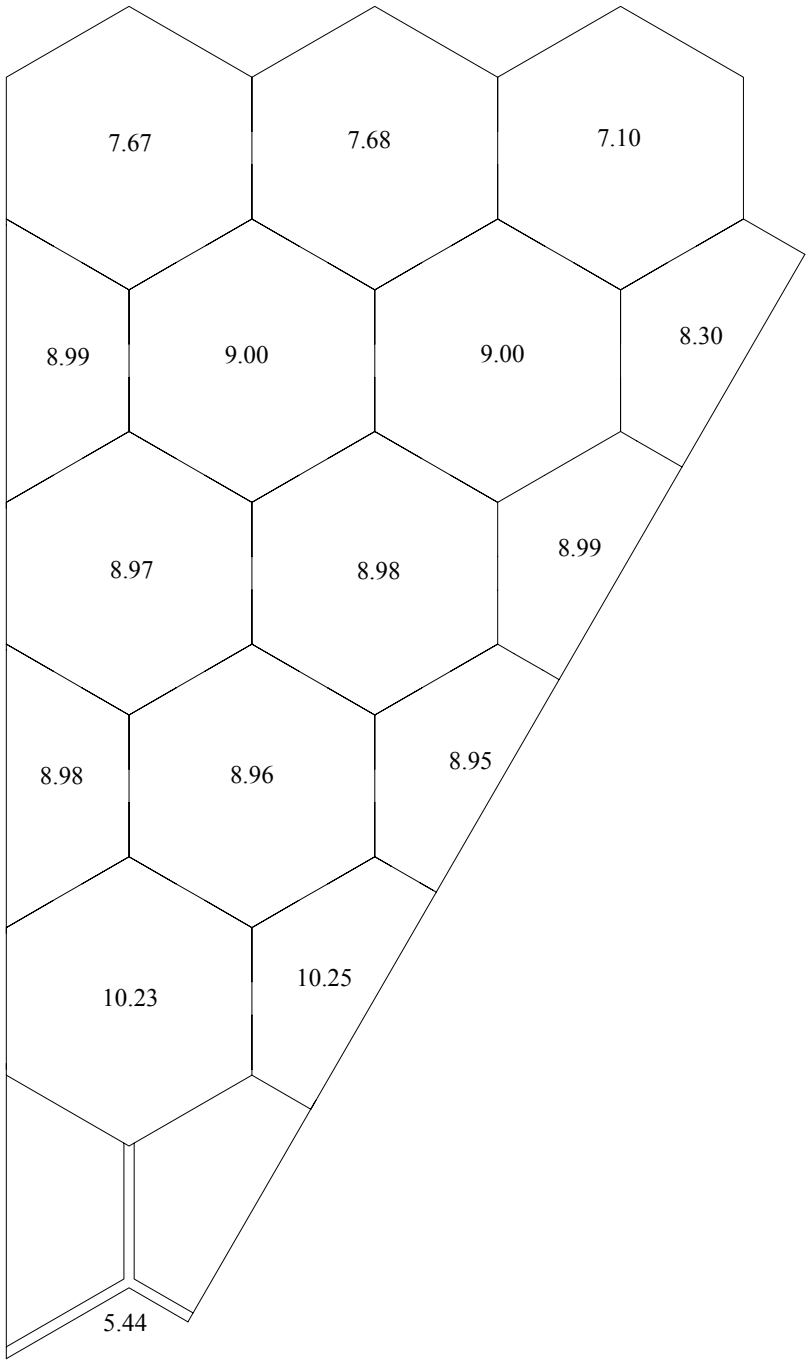

Figure 7.7 – Cell coolant velocity distribution cartogram at core outlet (variant with lead target)

Coolant velocity through FA is in the range 7÷10.3 m/s. As can be seen from Figure 7.6, coolant velocity at core inlet, due to flow throttling in FA spacer grids, increases in target gaps up to 15 m/s, then it falls to 5,4 m/s. Average value of coolant velocity along the target gaps is 8,9 m/s. This velocity value was used in thermohydraulic calculations of the target.

Flow mode by local Raynolds number Re_i in FA was in transitional area to turbulent flow (1200÷2400). Hydraulic losses in the core sections were:

Core inlet, kPa - 0.66

Fuel element part of the core, kPa - 0.51

Core outlet, kPa - 8.55

Total losses, kPa - 9.72

The results of thermohydraulic calculation at second stage for FA (cell No.6), where fuel element cladding temperature runs up to maximum value at first stage, are illustrated in Figures 7.8÷7.10. . Coolant temperature distribution by core height in “cold” cell (No.11). average cross-section distribution, temperature distribution in “hot” cell (No16), and fuel element temperature distribution (No.9), are shown in Fig. 7.8. Irregularity of coolant temperature in FA cross-section is 39°C, and this exceeds nearly six times the irregularity of average temperature distribution in FA in the core cross-section. The indicated irregularity of coolant temperature in FA is explained by availability of two types of cells: triangular (in FA center) and square (at FA periphery) with various areas of cross-section and

hydraulic diameters. Coolant velocity distribution cartogram at FA outlet is shown in Figure 7.9. It can be seen on cartogram that the velocity is higher in square cells than in triangular cells and runs up to 12 m/s.

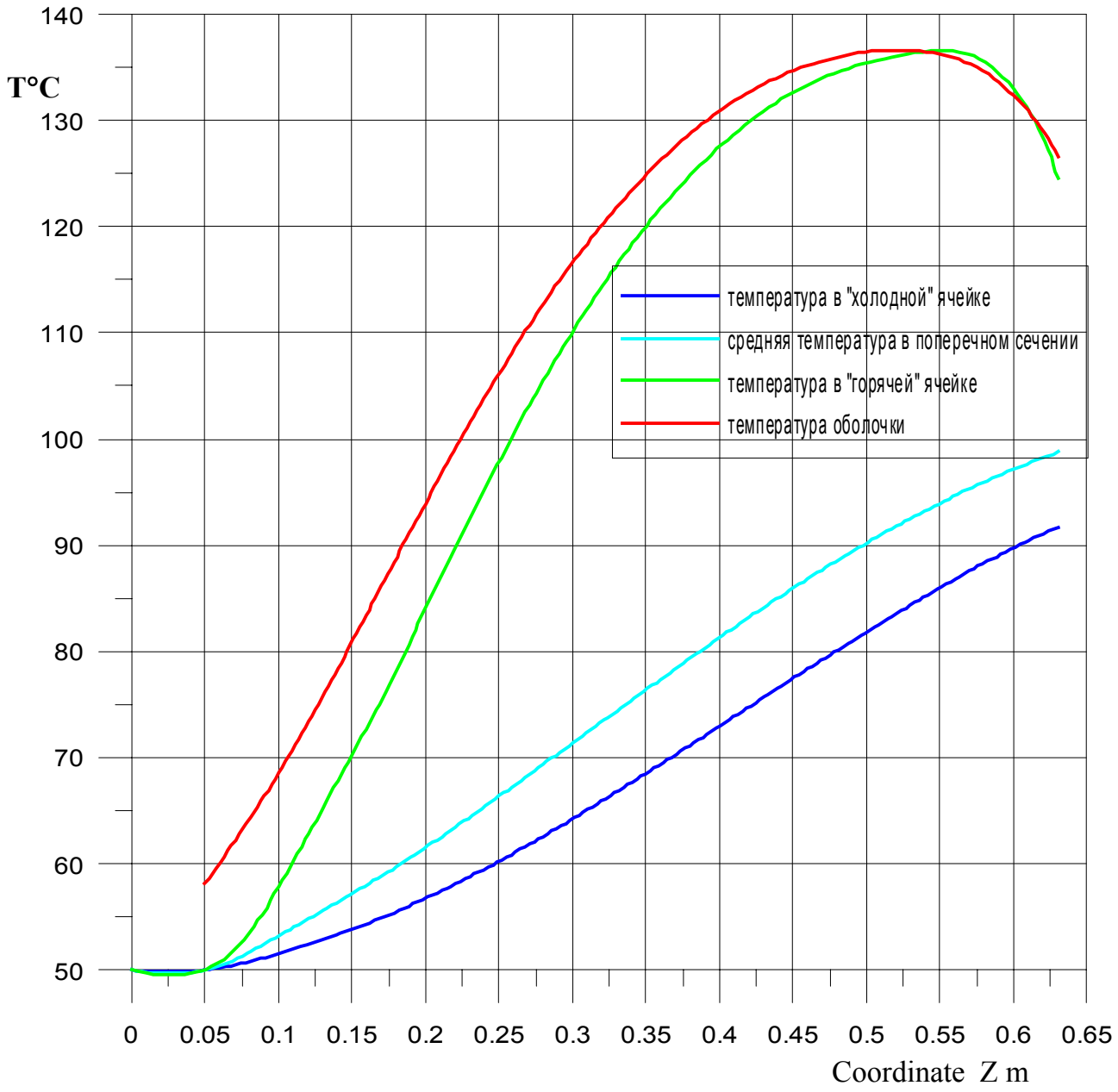

Figure 7.8 – Core height distribution of coolant temperature and fuel element temperature (variant with lead target).

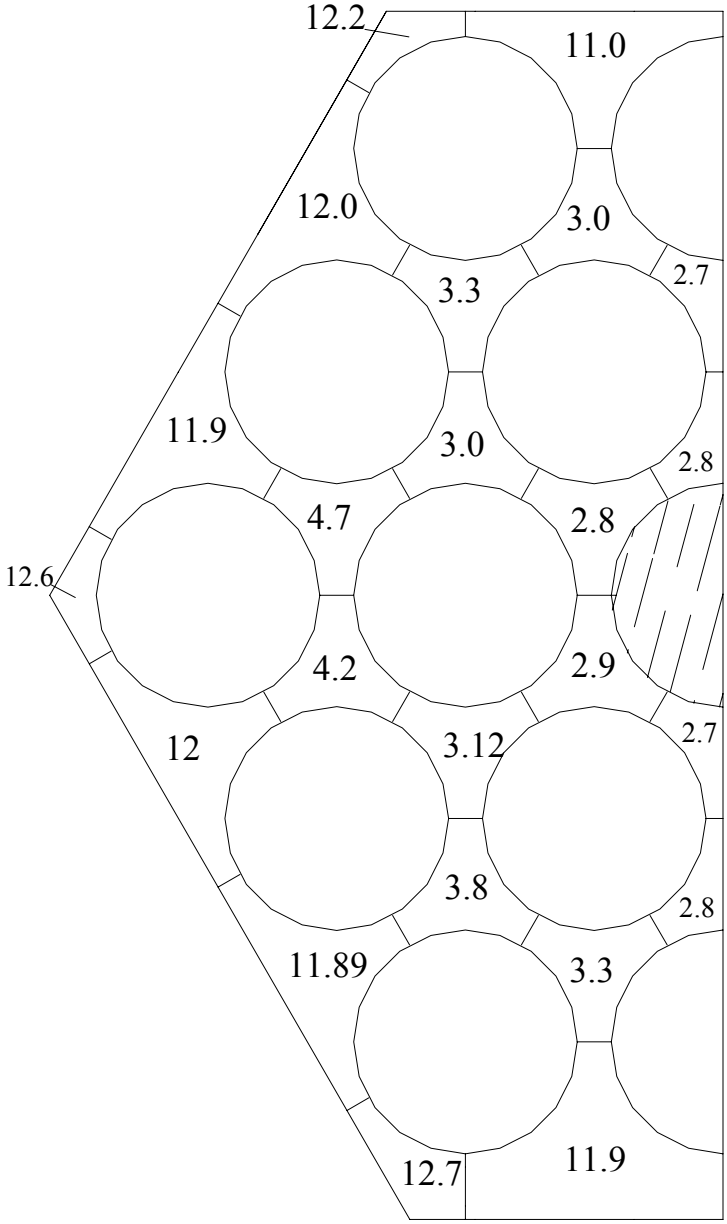

Figure 7.9 –Coolant velocity distribution cartogram in cells at outlet from FA (variant with lead target)

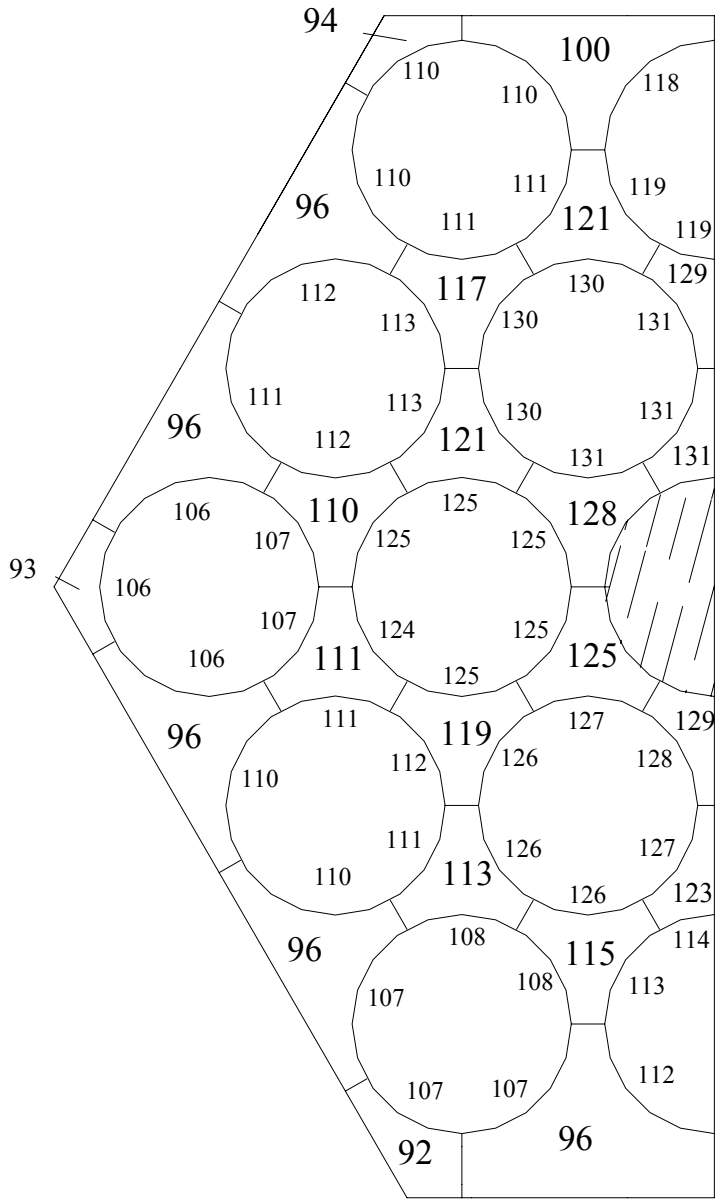

Figure 7.10 –Coolant and fuel element cladding temperature distribution cartogram at outlet cross-section (variant with lead target)

Coolant and fuel element cladding temperature distribution cartogram at outlet section is given in Figure 7.10. As distinct from from first stage calculations, the fuel element cladding temperature maximum was observed at core outlet in fuel element No.8 and it amounted to 131°C, what was 20°C higher than at first stage. The change of temperature maximum state of fuel element cladding can be explained by substantial influence of azimuth spreads in fuel element. Azimuth temperature irregularity of fuel element cladding does not exceed 1°C.

7.2.5 Calculation results with parameter deviations

Really, a temperature of various reactor elements is a random function of coordinates and time. It is due to the fact that actual conditions of heat release and heat removal at any core point at any time moment differ from conditions given as nominal owing to the influence of various random values. To take them into account, a coefficient system called overheating factors is introduced. According to [15], a maximum value of some parameter versus its nominal value is called overheating factor F_i . A difference of F from one characterises a relative error of the parameter.

According to [15], overheating factors for the core are introduced for temperature difference in two areas: that of coolant F_b, close-to-wall layer F_t. For example, if temperature difference in fuel element is below 2,5°C, there is no need to take into account overheating factors for cladding, gas gap and fuel.

Aoverheating factor influence is analyzed by limit method, in accordance with that method the resulting overheating factor has the form:

$$F_i = 1 + \sum_{k=1}^{S} \left(F_{i,k} - 1 \right) ,$$

where S – is a number of all factors to be taken into account;

i – overheating factor number;

k – random effect number.

The following maximum values are calculated, taking into account overheating factors for the core:

outlet temperature of coolant

$$T_{f,m} = T_{f,0} + \Delta t_{f,0} \cdot F_b$$

fuel element outer surface temperature

$$T_{об,m} = T_{f,0} + \Delta t_{f,0} \cdot F_b + \Delta t_{t,0} \cdot F_q \cdot F_t$$

where $\Delta t_{f,0}$, $\Delta t_{t,0}$ are temperature differences calculated without taking into account the overheating factors, correspondingly for coolant and close-to-wall layer;

$T_{f,0}$ – coolant temperature at core inlet.

Table 7.4 gives overheating factor values for disturbed parameters as a function of a set of various error sources as well as full overheating factor for maximum temperature value of fuel.

Table 7.4 – Overheating factors for the core

No.	Error sources	Coolant	Close-to-wall layer	Heat flow
1.	Fuel element diameter	1,1		
2.	Fuel element grid pitch	1,2		

3.	Hydraulic resistance	1,1		
4.	Fuel density in the core part	1,01		1,01
5.	Physical constant precision	1,01		1,01
6.	Energy release distribution	1,1		1,1
7.	Coolant heat capacity	1,002		
8.	Coolant heat conductivity		1,03	
9.	Precision of heat transfer formulas		1,2	
10.	Coolant discharge through core	1,1		
11.	Coolant temperature at core inlet	1,05		
	Total factor *F*	1,672	1,23	1,12

Calculation results showed that maximum fuel element temperature value taking into account parameter deviations (overheating factors) is 178°C, and this does not exceed maximum permissible value, equal to 250°C.

7.3 Lead target

7.3.1 Calculation model

Thermohydraulic data of lead target, which is cooled autonomously by pumping the coolant through six U-shaped pipes, were calculated by means of three-dimensional code FLOW VISION. An advantage of three-dimensional codes if compared with averaging methods consists in the fact that three-dimensional codes do not need to assume dependences for averaging coefficients (friction, heat transfer coefficients etc.). These coefficients are themselves products of three-dimensional calculations. At the same time, it does not mean that three-dimensional models using turbulent models do not require some closing coefficients. However, the universality of these coefficients is substantially broader than of those in averaged models.

FLOW VISION CODE is based on solution of Navier-Stokes equations in vector form:

$$\frac{\partial(\rho V)}{\partial\tau}+\nabla(\rho V\times V)=-\nabla P+\nabla(\mu\nabla V)+(1-\frac{\rho_{ref}}{\rho})g\rho \qquad (7.14)$$

$$\nabla V=0 \qquad (7.15)$$

and energy equation:

$$\frac{\partial h}{\partial\tau}+\nabla(V\cdot h)=\frac{1}{\rho}\nabla(\frac{\lambda}{Cp}\nabla h)+q_v. \qquad (7.16)$$

the following designations are assumed in equations (7.14)÷(7.16):

V – velocity vector in Cartesian coordinate system x, y, z;

τ – tiem;

P – pressure;

h – enthalpy of fluid;

ρ – density of fluid;

ρ_{ref} – reference value of fluid density;

μ – dynamic fluid viscosity;

c_p – теплоемкость жидкости;

λ – fluid heat conductivity coefficient;

q_v – volumetric density of energy release.

Turbulent fluid flow model used in the code FLOW VISION, is based on standard turbulence model κ - ε, where turbulent viscosity μ_t is expressed through κ and ε in the following way:

$$\mu_t = c_\mu \cdot \rho \frac{k^2}{\varepsilon},$$

where κ– is turbulent energy;

ε - turbulent energy dissipation velocity.

The values κ and ε are found from solution of equations:

$$\frac{\partial k}{\partial \tau} + \nabla(V \cdot k) = \frac{1}{\rho}\nabla((\mu + \frac{\mu_t}{\sigma_K})\nabla k) + \frac{G}{\rho} - \varepsilon, \qquad (7.17)$$

$$\frac{\partial \varepsilon}{\partial \tau} + \nabla(V \cdot \varepsilon) = \frac{1}{\rho}\nabla((\mu + \frac{\mu_t}{\sigma_\varepsilon})\nabla \varepsilon) + \frac{\varepsilon}{k}(C_1 \frac{G}{\rho} - C_2 \varepsilon), \qquad (7.18)$$

$$G = \mu_t \frac{\partial V_i}{\partial x_j}(\frac{\partial V_i}{\partial x_j} + \frac{\partial V_j}{\partial x_i}), \quad i, j = 1,2,3$$

Parameter values of the model κ - ε are assumed as follows:

$\sigma_\kappa = 1.0$; $\sigma_\varepsilon = 1.3$; $C\mu = 0.09$; $C_1 = 1.44$; $C_2 = 1.92$.

Equations (7.14)÷(7.18) are solved for time span (τ_n, τ_{n+1}) with the following equation approximation:

In solid state

$$\frac{(TCf)^{n+1} - (TCf)^n}{\tau} = \frac{1}{PC}\nabla_h(DC\nabla_h f^{n+1}) + SST \qquad (7.19)$$

in fluid

$$\frac{(TCf)^{n+1} - (TCf)^n}{\tau} = (1-\sigma)\nabla^{(k,s)}(CC\vec{V}f^n) + \sigma\nabla^{(k,s)}(CC\vec{V}f^{n+1}) =$$
$$= \frac{1}{PC}\nabla_h(DC\nabla_h f^{n+1}) + SST, \qquad (7.20)$$

where $\tau = t_{n+1} - t_n$,

f – independent variable,

$\sigma = 0$ – corresponds to explicit scheme,

$\sigma = 1$ – corresponds to implicit scheme,

TC – time coefficient;

CC – convective coefficient;

DC – diffusion coefficient;

PC – pre-diffusion coefficient;

SST – source term;

κ – defines the type of function reconstruction (1^{st} or 2^{nd} precision order scheme);

s – defines the ″angularity ″ of the scheme.

Discretization of (7.19), (7.20) causes a linear algebraic equation system

$$Ax = b, \tag{7.21}$$

Where operator A is a self-adjoint operator for equation (7.19) and non-selfadjoint operator for equation (7.20).

To solve the system (7.21), the SOR method for operators (7.19) and (7.20) and Kholessky method for operator (7.20) are used.

Non-linearities iteration process is completed, if one of conditions is met:

$\left\| b - Ax^{(s)} \right\| < \varepsilon$,

$S \geq N_{max}$,

where ε is specified precision,

N_{max} – maximum number of iterations.

Calculation of lead target temperature maximum value with allowance made for independent parameters deviations from nominal values was carried out by limiting methods. For this purpose, independent parameters, at calculations by code FLOW VISION, were simultaneously deviated to worst values:

- lead target heat conductivity coefficient – 10%

- coolant temperature at target inlet – 5%

- coolant discharge through target pipes – 10%

- error expected due to roughness of difference grid inside pipes – 20%.

Coolant velocity in the gaps was assumed to be equal to minimum value 5.4 m/s in the cell-by-cell calculation of the core.

7.3.2 Calculation area and initial data

Lead target (Figure 7.11) consists of:

- central part, formed by «fusion» of 7 lead hexahedrons of 36 mm “wrench” size placed in unified housing made of steel 12X18H10T, 2 mm thick;

- outer part consisting of 12 lead elements, enclosed in housing made of steel 12X18H10T,

- tail-end elements and hold heads.

6 U-shaped pipes ∅6 mm × 0,5 mm pass through central target part, which form air cooling channels of the target. Central and outer target parts are cooled

with air flow passing through 1mm-slit gaps between outer target elements, and 1,5 mm-slit gaps – between central and outer parts of target. A-hole of diameter of 5.8cm and of height of 10cm is foreseen below internal target part is foreseen for proton beam input (Figure 7.12)

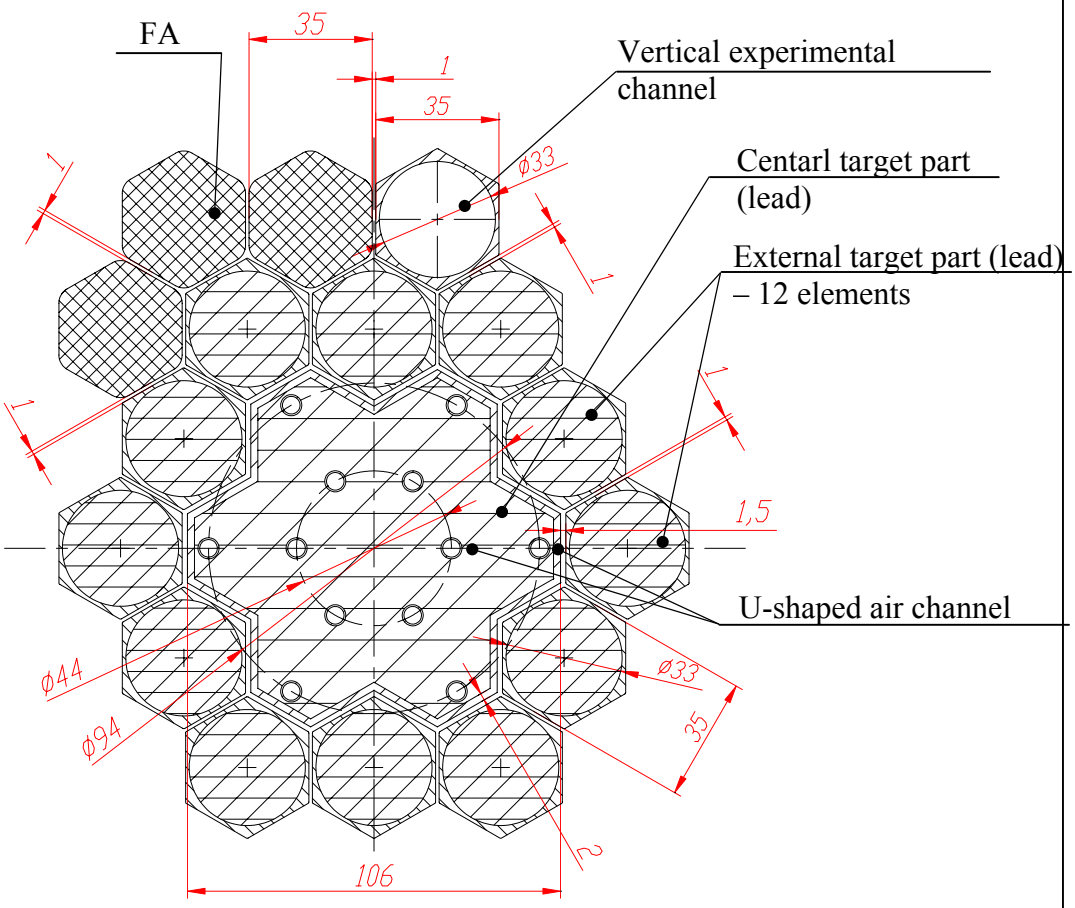

Figure 7.11 - Lead target cross-section

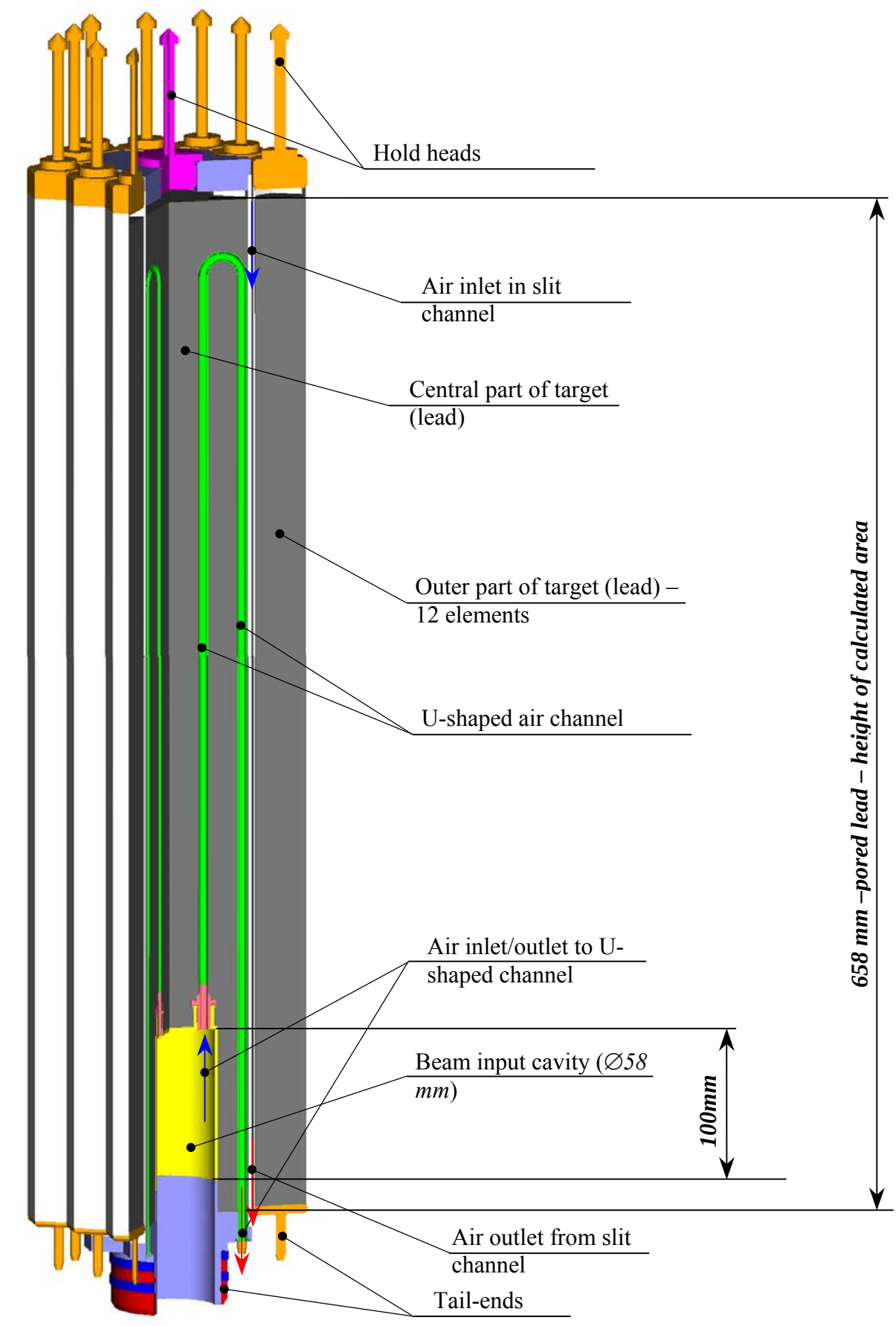

Figure 7.12 –Lead target

Lead target symmetry element (1/12) was used for calculation purposes. Height of model is 658 mm. Communicating heat exchange problem between 5 sub-areas was solved. U-shaped pipe, central target housing and outer target element housing were replaced for boundary condition «resistance» (with data δ - housing thickness and λ -its heat conductivity).

The following calculation areas were described in the model (Figures 7.13÷7.18):

- Central part of lead target;
- Outer part of lead target (2 elements);
- U-shaped air channel;
- three-beam air channel for external target streamline;

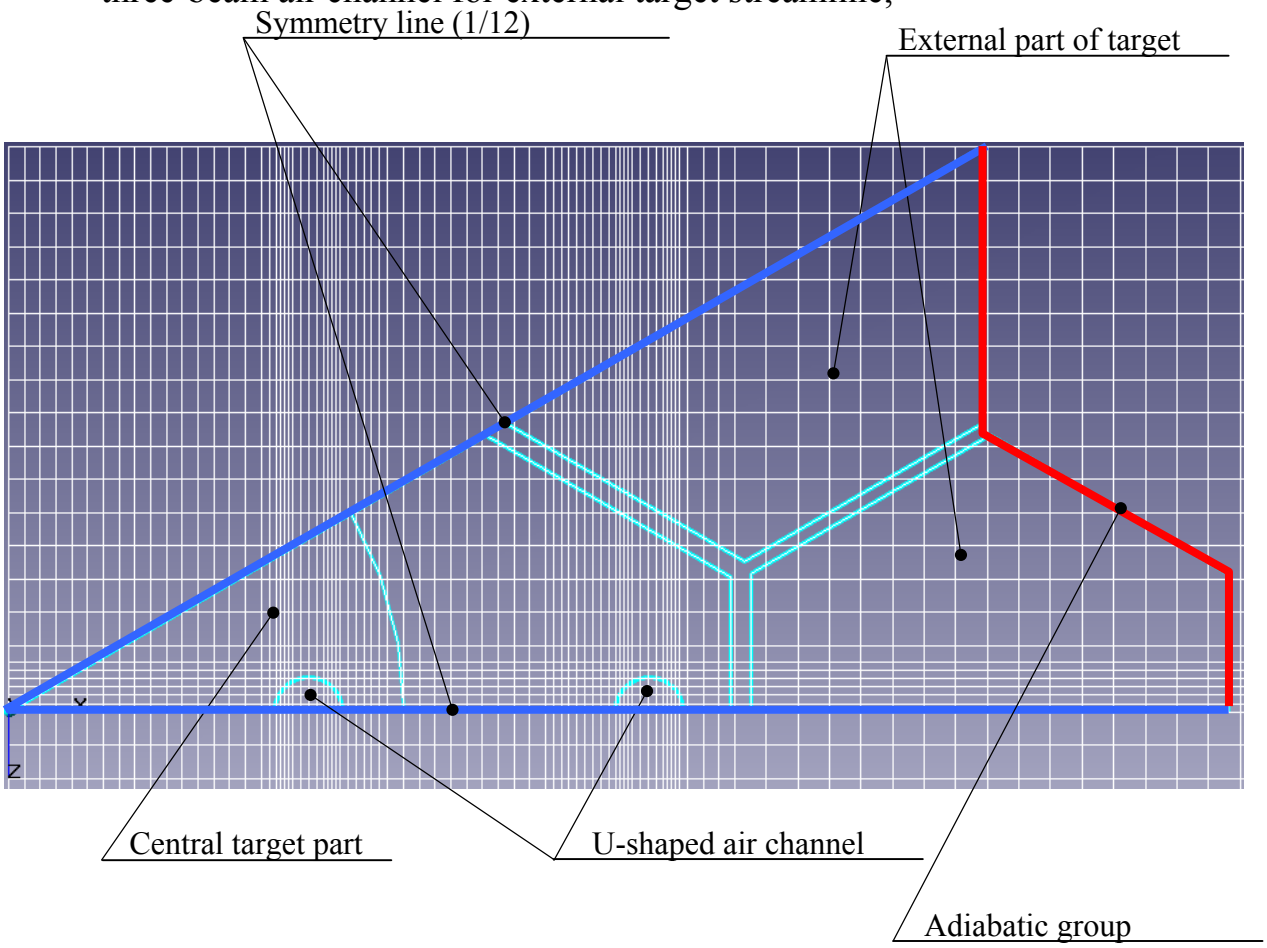

Figure 7.13 – Calculation area, lead target

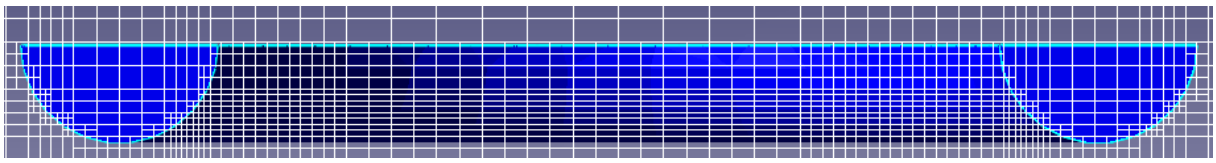

Figure 7.14 – Calculation area, U-shaped air pipe (∅6×0,5 mm), cross-section

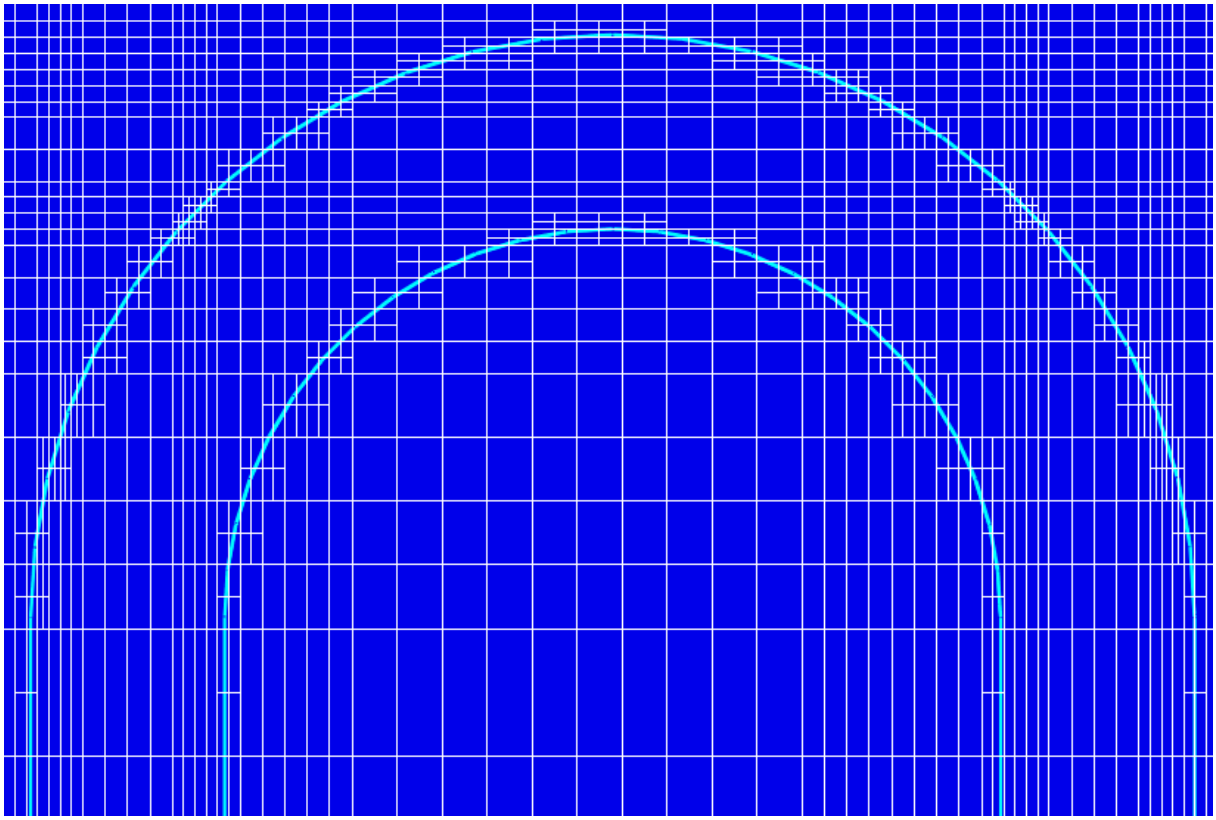

Figure 7.15 – Calculation area, U-shaped air pipe (∅6×0,5 mm), flow turn

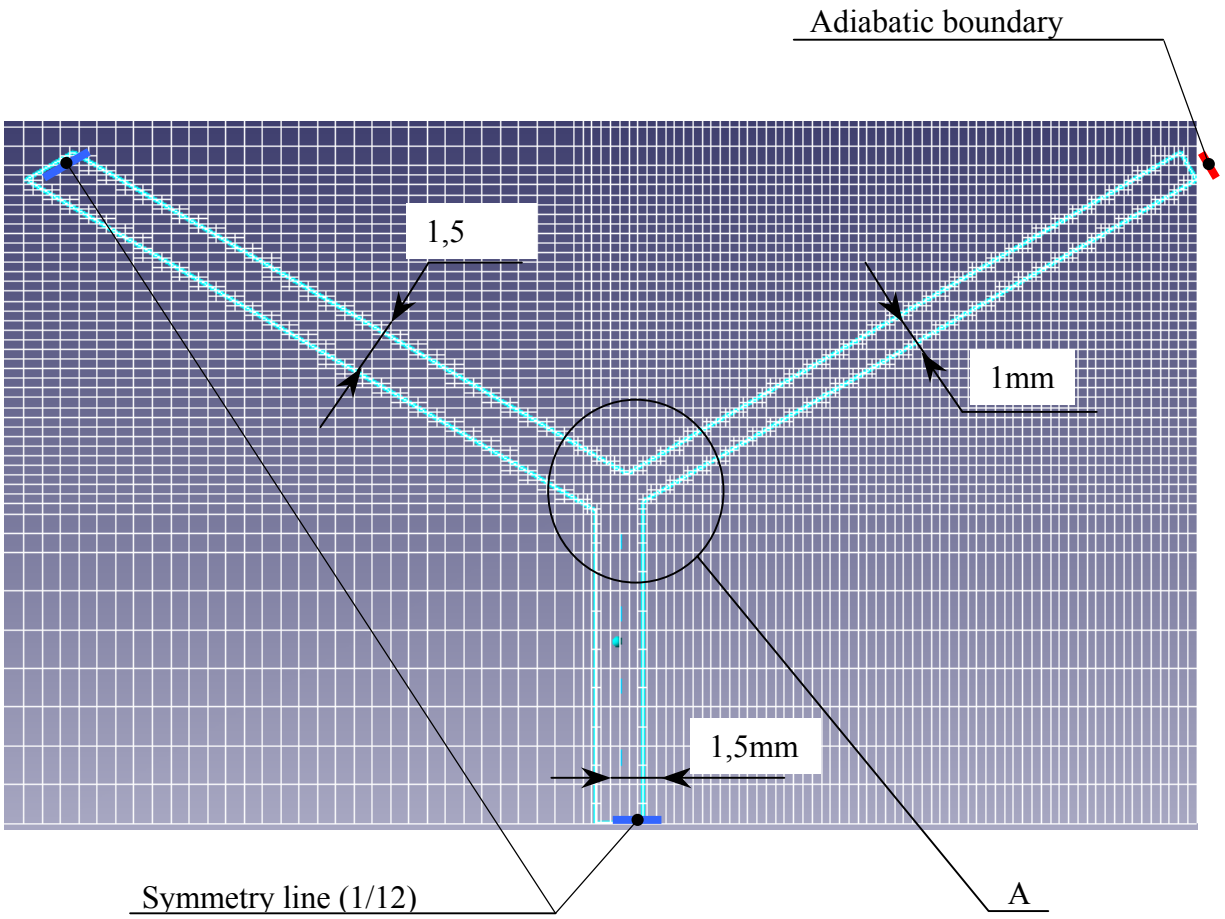

Figure 7.16 – Calculation area, three-beam channel of external target streamline

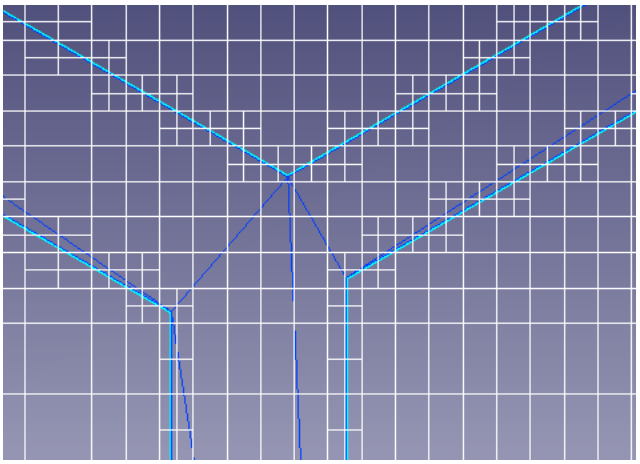

Figure 7.17 – Calculation area, three-beam channel of area A (Fig. 7.16)

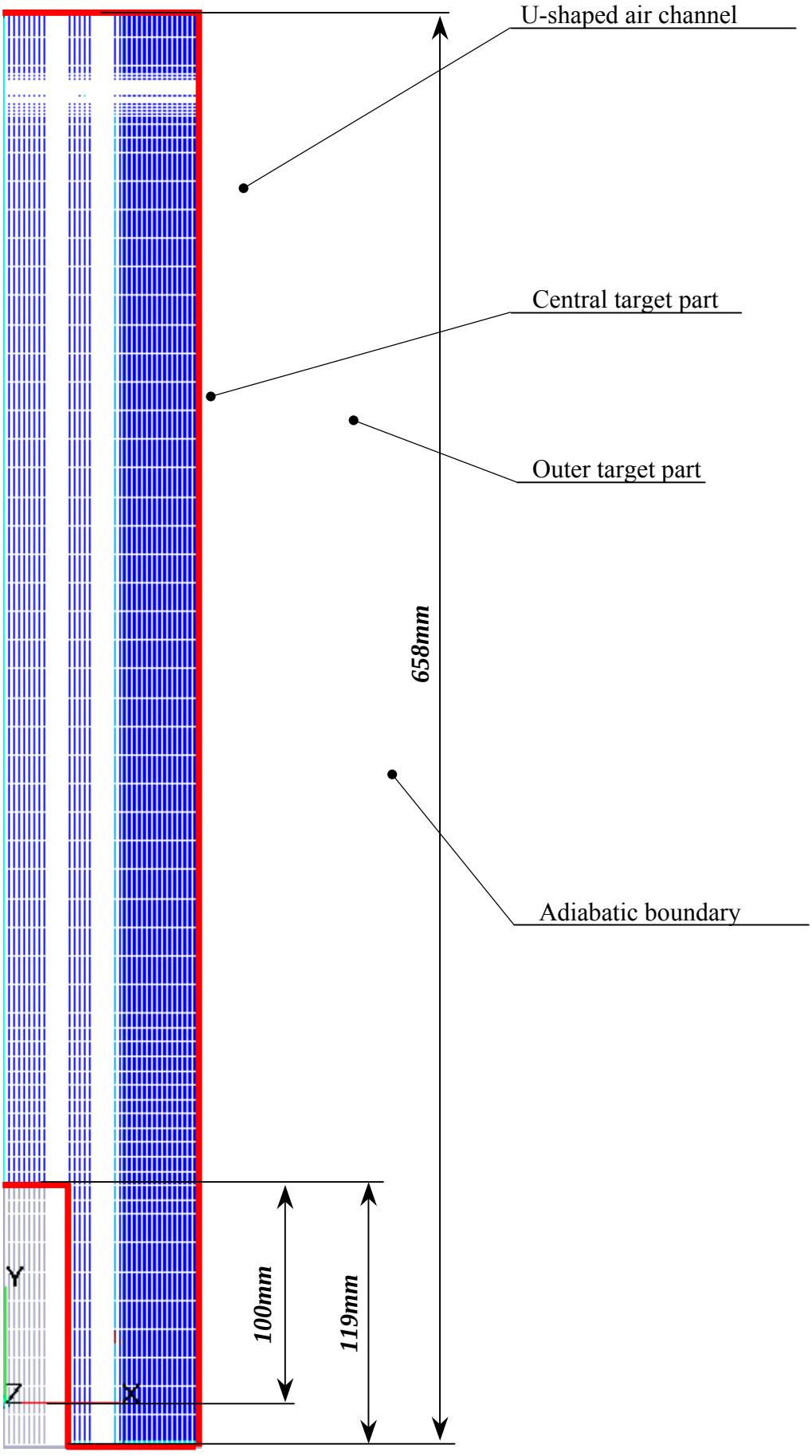

Figure 7.18 – Calculation area, lead target. Grid fragmentation by target height

Total number of calculated volumes – 308 thousand. To obtain information about precision of solution obtained by the code, the problem was calculated on grids of various degree of details in order to reach grid convergence. Calculations were executed on three types of grid for U-shaped air channel, slit channels and target. Divergence between control point temperature values of target and outlet temperature values for gas channels does not exceed 5 degrees (176°C – 181°C).

Initial data:

Coolant parameters

U-shaped channel

Pressure, MPa	0,135
Inlet temperature, °C	50
Discharge, kg/s (channel inlet velocity, m/s)	0,00662 (38,1)

Slit (three-beam) channel

Pressure, MPa	0,135
Inlet temperature, °C	50
Air velocity at inlet cross-section m/s	8,9

Energy release is represented in Figure 7.18a. Integral energy release is 840 W)

Energy release is represented in Figure 7.19. Integral energy release is 840 W).

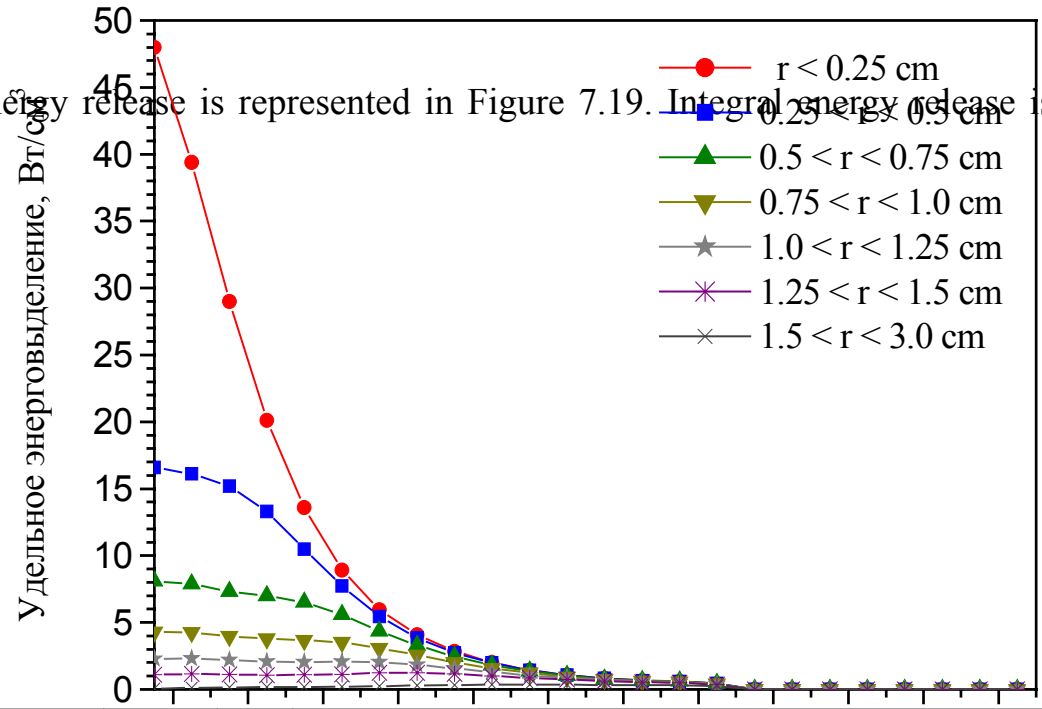

Thermo-physical properties of materials:

Thermo-physical properties of lead (lead S1 GOST 3778-98)
Density:

$$\rho = 11300\ kg/m^3.$$

Heat conductivity coefficient:

$$\lambda = 39.3227\text{-}0.013216 \times (t + 273),\ W/(m \times K).$$

Specific heat capacity:

$$c_p = 116 + 0.0435 \times (t + 273),\ J/(kg \times K).$$

Thermo-physical properties of air
Density:

$$\rho = \frac{p}{283{,}2 \cdot (t + 273)},\ kg/m^3.$$

Heat conductivity coefficient :

$$\lambda = 24{,}42 \cdot 10^{-3} \cdot \left(\frac{T + 273}{273}\right)^{0{,}82},\ W/(m \times K).$$

Dynamic viscosity coefficient:

$$\mu = 17{,}16 \cdot 10^{-6} \cdot \left(\frac{T + 273}{273}\right)^{0{,}68},\ Pa \times s.$$

Specific heat capacity :

$$c_p = 1034.04\text{-}0.22217 \times (t + 273) + 0.40952 \cdot 10^{-3} \cdot (t + 273)^2.$$

Thermo-physical properties of steel 12X18H10T:
Density:

$$\rho = 7850\ kg/m^3.$$

Heat conductivity coefficient :

$$\lambda = 10.26 + 0.01442 \times (t + 273),\ W/(m \times K).$$

Specific heat capacity :

$$c_p = 462 + 0.1174 \times (t + 273),\ J/(kg \times K).$$

7.3.3. Results of calculation

Integral calculation data are given below :

Coolant parameters:

U-shaped channel

Pressure loss in channel, Pa	9612
Outlet temperature, °C	109
Air discharge, kg/s	0,00662
Fraction of removed power	0,43

Slit (three-beam) channel

Pressure loss in channel, Pa	1390
Outlet temperature, °C	99
Velocity at inlet cross-section, m/s	8,9 м/с
Air discharge, kg/s	0,0105
Fraction of removed power	0,57

Maximum target temperature, °C	176

Temperature distribution across target axis is given in Table 7.5.

Table 7.5 – temperature distribution across target axis (nominal parameters)

coordinate Y (X = 0, Z = 0), mm	Temperature, °C (nominal parameters)
101	176
145	169
190	155
235	138
290	121
435	87
580	72

Target temperature distributions in longitudinal sections, drawn through cooling pipes and between them, correspondingly, are given in Figures 7.20-7.21. Target temperature distribution in cross-section (y =101mm) is given in Figure 7.22..

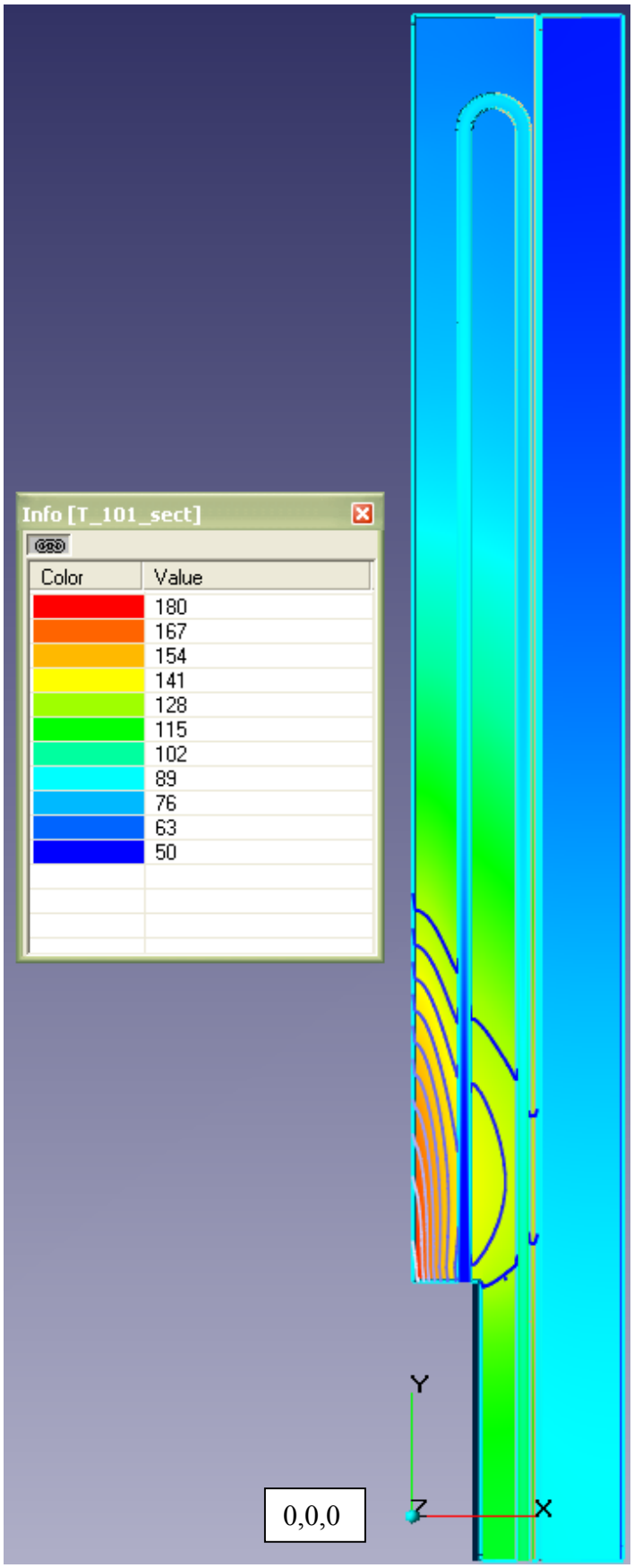

Figure 7.20 – Target temperature distribution in longitudinal section, drawn through cooling pipes

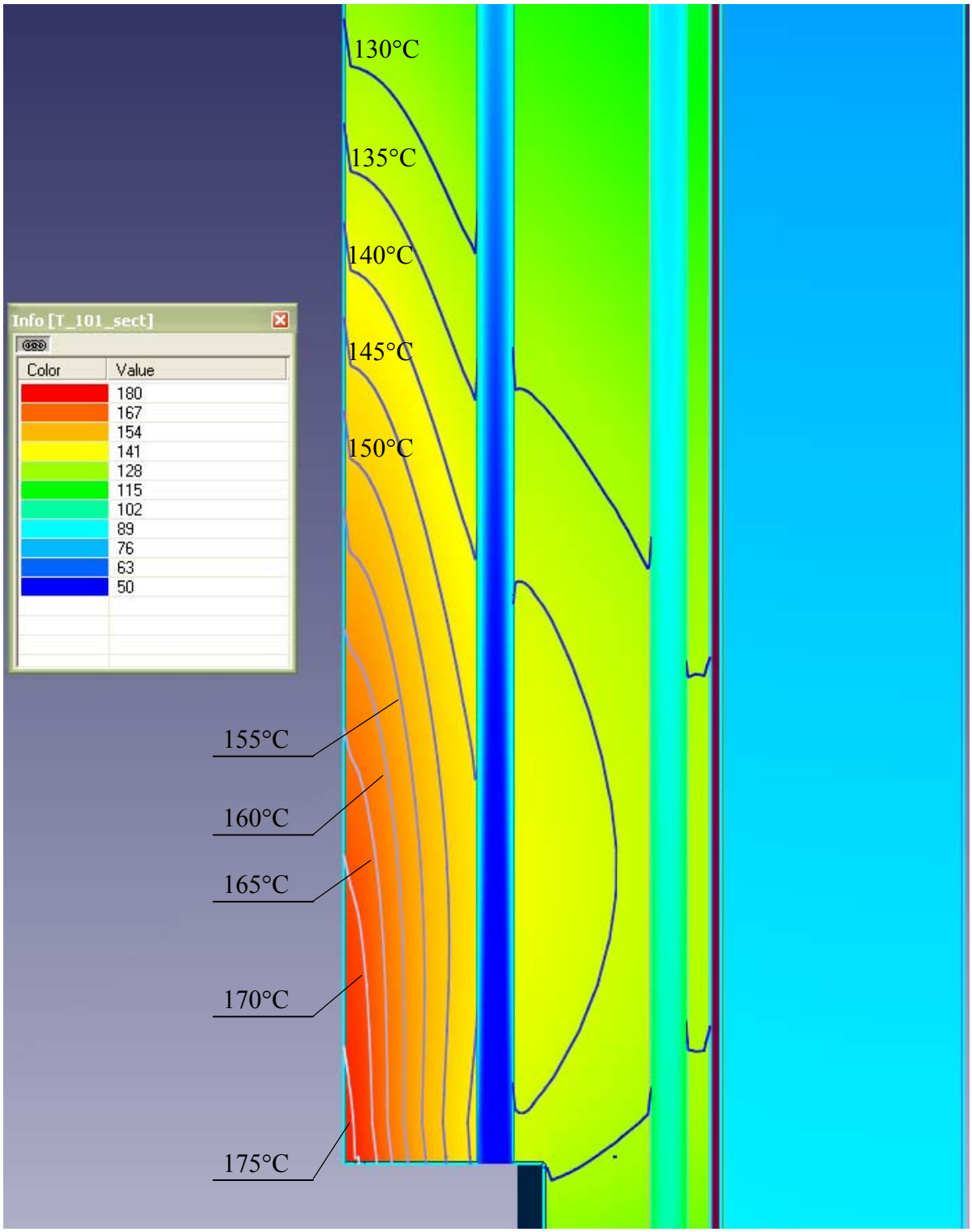

Figure 7.21 - Target temperature distribution in longitudinal section, drawn between cooling pipes

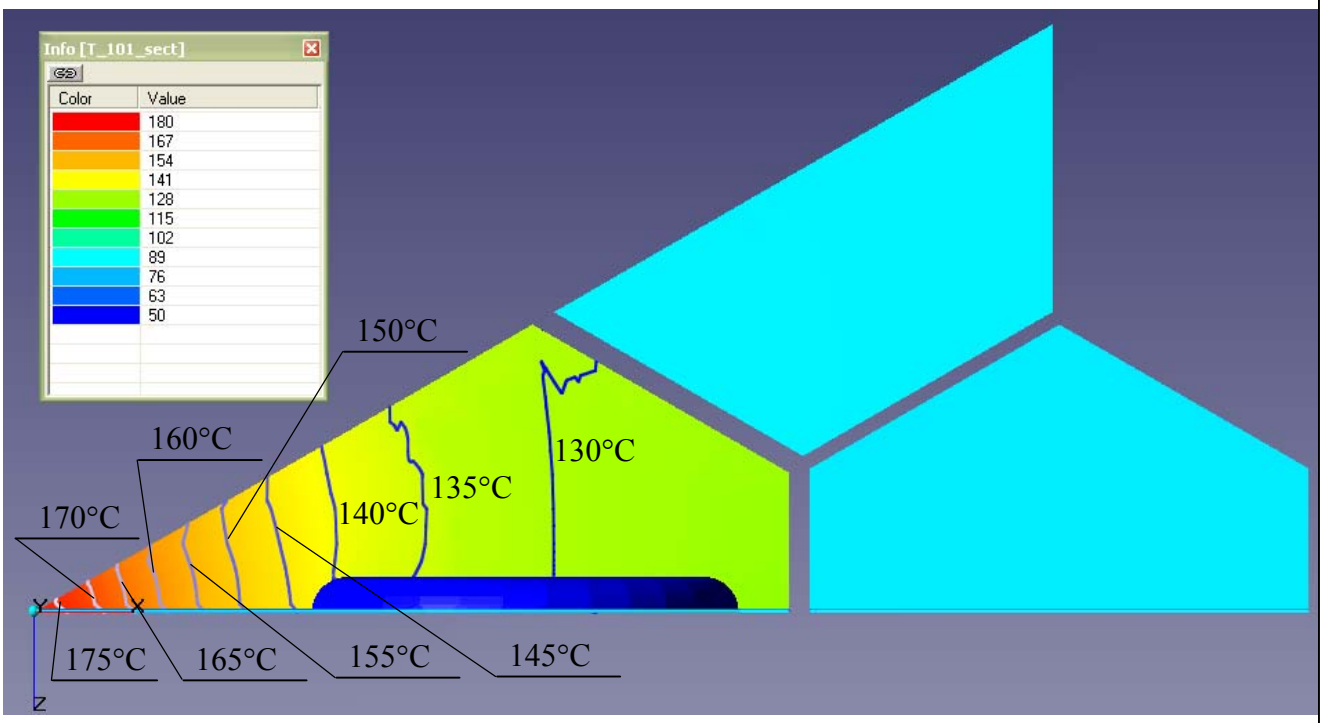

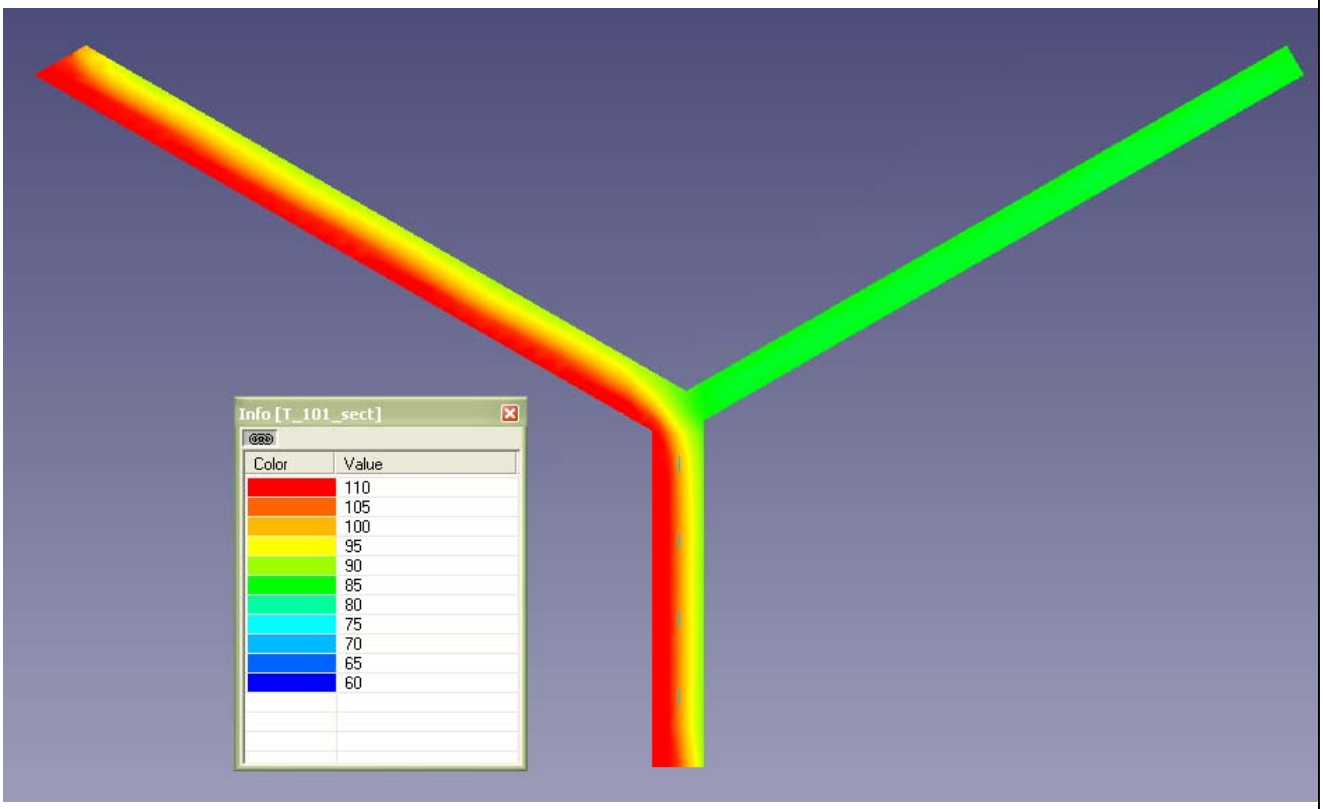

Figure 7.22 – Target temperature distribution in cross-section (Y= 101 mm)

Calculation results analysis showed that maximum target temperature value without allowance for deviations is 176°C.

Distributed pressure losses for friction were equal to 9612 Pa. With allowance for losses for target inlet and outlet they will be increased up to 13650 Pa.

Calculation of lead target temperature maximum value with allowance made for independent parameters deviations from nominal values was carried out by limiting methods. For this purpose, independent parameters were simultaneously deviated to worst values:

- lead target heat conductivity coefficient – 10%

- coolant temperature at target inlet – 5%

- coolant discharge through target pipes – 10%

- error expected due to roughness of difference grid inside pipes – 20%.

Coolant velocity in the gaps was assumed to be equal to minimum value 5.4 m/s in the cell-by-cell calculation of the core.

- Inlet temperature increase into slit channel and U-shaped pipe by 5°C;
- Discharge decrease in U-shaped pipes by 10%;
- Velocity decrease in slit channel up to 5,4 m/s;
- Decrease of lead heat conductivity coefficient by 10%;

Calculation results with deviations are given in Table 7.6.

Table 7.6 – Target temperature (deviation from nominal parameters)

Coordinate Y (X = 0, Z = 0), mm	Temperature, °C (nominal parameters)
101	209
145	201
190	184
235	165
290	145
435	106
580	87

Integral calculation data (for variant with parameter deviations)

Coolant parameters:

U-shaped channel

Pressure loss in channel, Pa	8495
Outlet temperature, °C	132
Air discharge, kg/s	0,00596
Fraction of removed power	0,49

Slit (three-beam) channel

Pressure loss in channel, Pa	829
Outlet temperature, °C	124
Velocity at inlet section, m/s	5,4 m/s
Air discharge, kg/s	0,00637
Fraction of removed power	0,51

Maximum target temperature, °C 209

With allowance made for error due to difference grid (5°C), the maximum temperature with allowance for deviations will be equal to 214°C, and that does not exceed the maximum permissible value 250°C.

7.4. Core with tungsten target

7.4.1. Calculation model

Thermohydraulic calculation of the core was carried out one-temperature model of porous body, realized in the code FLOW VISION. Heat conductivity equation was solved in the target. Solution of adjacent problem was used, on the one hand, to obtain temperature fields, and, on the other hand, to determine heat flows at side boundaries of the target in cell-by-cell calculation of the core at first stage. Equation (7.14) in the right-hand part was supplemented with components of volumetric forces of hydraulic resistance in the form of square and linear components from velocity vector V:

$$\frac{\partial(\rho V)}{\partial\tau}+\nabla(\rho V\times V)=\nabla P+\nabla(\mu\nabla V)+(1-\frac{\rho_{ref}}{\rho})g\rho-\frac{\rho}{2}E\left|V\right|V-\mu DV; \qquad (7.22)$$

In general case of anisotropic porous body, E and D are symmetric tensors.

Vector V is introduced for incident flow. Equations (7.17) and (7.18), describing turbulent data in porous body model, are missing.

The core is represented with porous body with constant porosity ε, equal to 0.35 . Isotropic flow approximation was assumed in the cross-section:

$D_{yy} = D_{xx}$; $E_{yy} = E_{xx}$.

Volumetric source of hydraulic resistance in longitudinal direction was recalculated with allowance made for porosity in incident flow.

$$D_{zz}=\frac{1}{2}\frac{V}{d_{\Gamma}}\frac{\lambda}{v\varepsilon^{2}},$$

$$E_{zz} = \frac{\lambda}{\varepsilon^2 d_Г} ,$$

where λ is hydraulic friction coefficient, calculated by "live" velocity (v/ε) and given above at description of cell-by-cell calculation method.

In accordance with recommendations [14], coefficients D and E in transversal direction are increased in comparison with longitudinal direction by ~10 times.

Coefficients E_{zz} for local resistance at inlet and outlet from the core was calculated by formula:

$$E_{zz} = \frac{\zeta}{l\,\varepsilon^2},$$

where l –is local resistance length;

ζ - local resistance coefficient, related to ″live″ velocity.

Within the framework of one-temperature model to take into account heat transfer through fuel elements, the air heat conductivity coefficient was artificially increased. For this purpose, the model heat conductivity problem in the fragment fuel element – environment (air) was solved. The solution of this problem showed that effective heat conductivity coefficient $\lambda_{эф}$ in transversal direction is equal to:

$\lambda_{эф} = 6.5 \cdot \lambda$.

where λ is air heat conductivity coefficient.

The same value wasassumed, from conservative considerations, in longitudinal direction. Additionally, allowance was made for thermal resistance of

gap (δ/λ), formed by target surface and adjacent fuel elements. In comparison to porous medium (core.), the gap does not possess the effect of increasing heat conductivity coefficient at the expense of heat transfer through fuel elements. The value δ/λ in the gap was calculated by the formula:

$$\frac{\delta}{\lambda} = \frac{d}{Nu \cdot \lambda},$$

where d is hydraulic gap diameter;

Nu – Nusselt number for laminar flow in the flat gap with one-side heating with allowance made for initial non-stabilized heat exchange section:

$$Nu = \frac{2.94}{z^{1/3}} - 2.78 \qquad \text{at } z \le 0.057\text{m}$$

$$Nu = 4.86 \qquad \text{at } z > 0.057\text{m}$$

where z – in meters.

Methods of cell-by-cell calculation of the core and closing dependences were described above.

Calculation of maximum temperature value of tungsten target with allowance made for deviations of independent parameters from nominal values was carried by limiting (maximum) methods. For this purpose, independent parameters in conjugate thermohydraulic model “core – target” were simultaneously deviated to worst value.:

- heat conductivity coefficient of tungsten target - 20%

- coolant temperature at core inlet – 5%

- coolant discharge through the core – 10%

- heat transfer coefficient from target to the core -20%

7.4.2. Calculation area and initial data

Calculations by porous body model were carried out in ½ symmetrical half of the core. One could restrict oneself to 1/12 part of the cross-section. However, making allowance for necessity of emergency modes consideration, connected with core blocking, ½ part of the core was chosen as calculation area. The calculation area shown in Figure 7.23, consists of 3 subareas – lead reflector, core and tungsten target. The core is represented as porous body and it is divided in 7 sub-zones with various values of porosity and energy release:

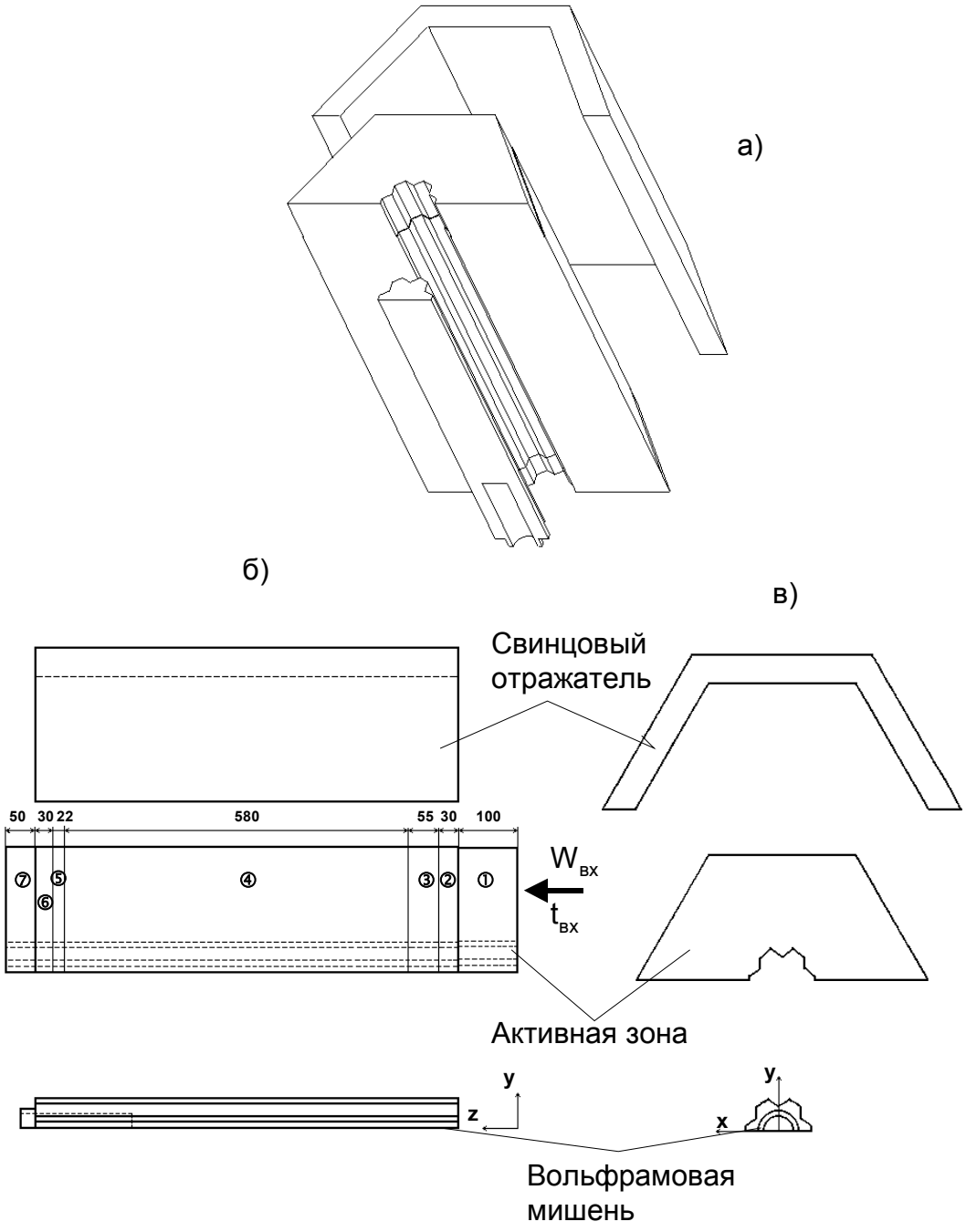

Figure 7.23 – Calculation area: a) three-dimensional image, b) side view, c) view from below

① - inlet collector (introduced for forming velocity profile at core inlet in emergency situations with blocking);

② - inlet spacer grid;

③, ④, ⑤ - fuel element part of the core with porosity ε =0,35 , which include

④ - heated part, ③ and ⑤ - not heated parts;

⑥ - bottom bearing plate;

⑦ - outlet section (introduced for more precise approximation of boundary condition at outlet).

Defference grid in longitudinal and transversal sections is shown in Figure 7.24. Total number of knots was 95898.

Below are given those initial data only, which differ from the variant with lead target:

- heat power of the core, kW – 23,8

- heat power of target, kW – 0,861

- coolant discharge through the core, kg/s – 0,649

Distribution of relative energy release by length and radius of the core is given in Figure 7.25.

Specific energy release distribution in tungsten target is shown in Figure 7.26.

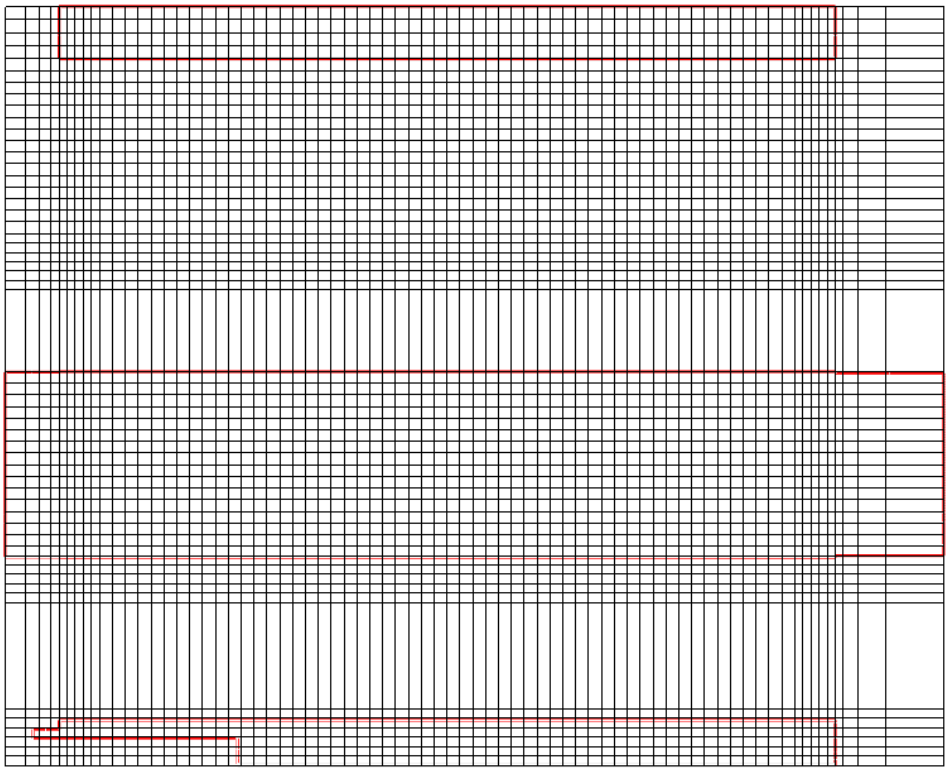

а)

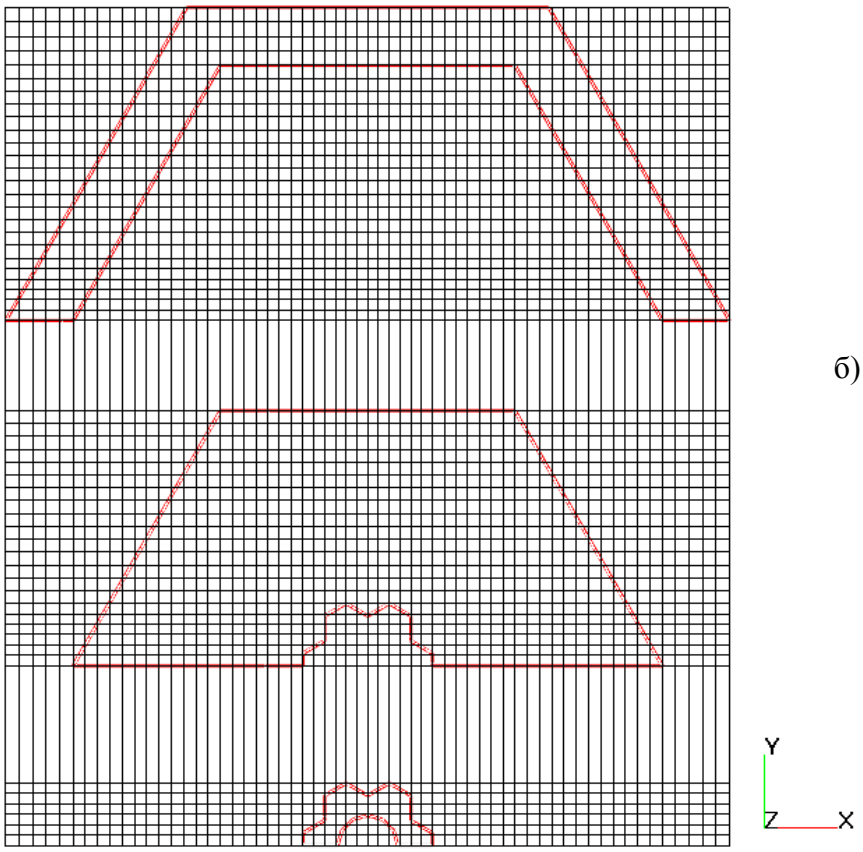

б)

Figure 7.24 – Calculation grid in longitudinal (a) and transversal (b) sections

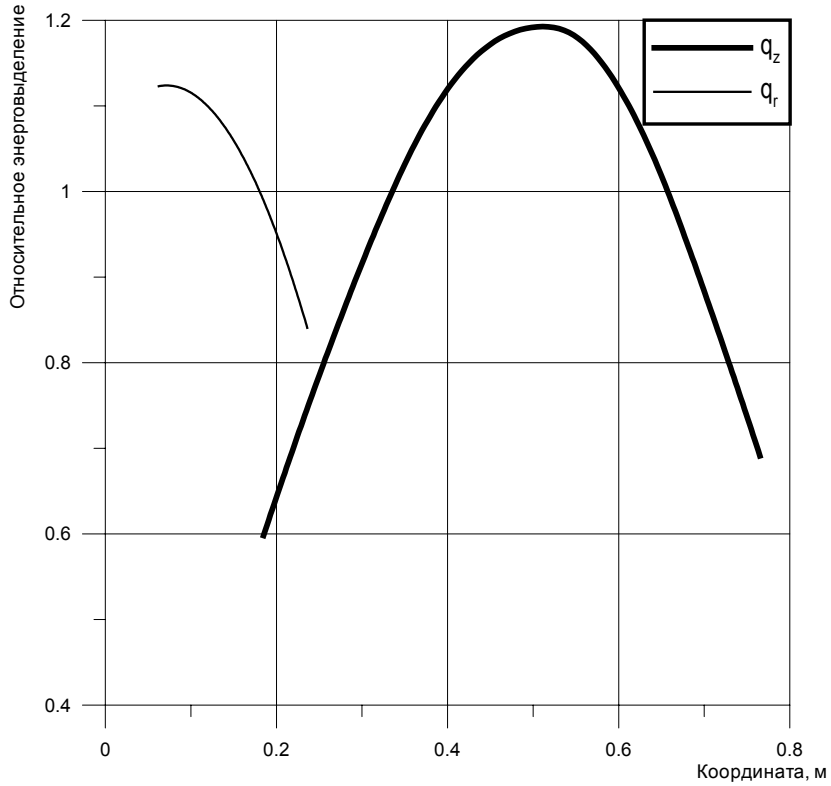

Figure 7.25 – Relative energy release distribution in the core by coordinate z (q_z) and radius (q_r)

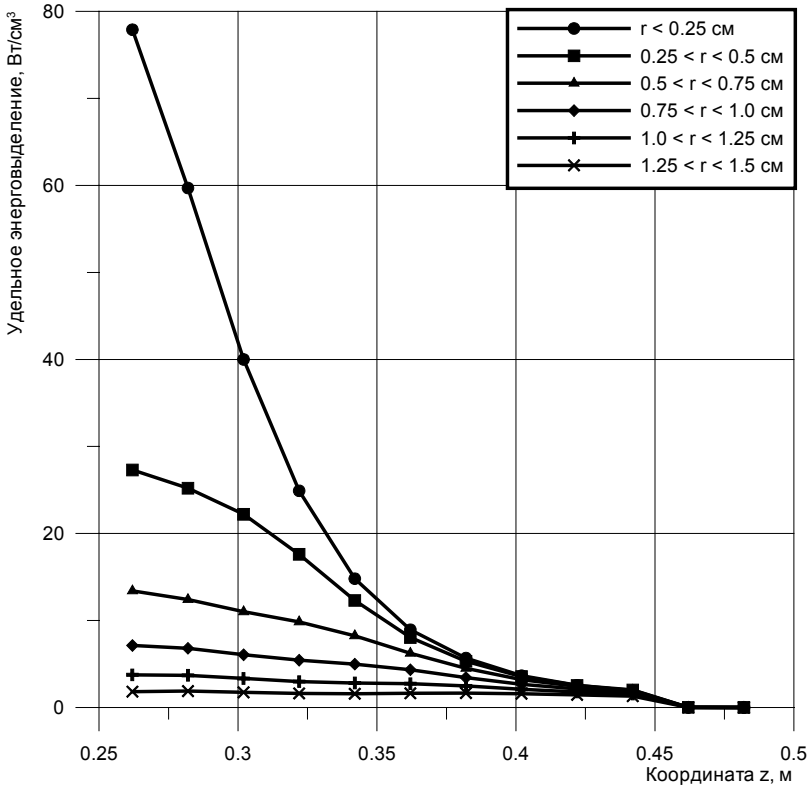

Figure 7.26 – Relative energy release distribution in tungsten target by coordinate z and radius

At the first stage, cell-by-cell thermohydraulic calculation of the core was carried out for 1/12 symmetrical part of transversal cross-section. However, in contrast to a variant with lead target, the calculation area, shown in Figure 7.27, included 15 cells and 29 links between selected cells. The Figure 7.27 gives also relative energy release values by FA. Table 7.7 gives geometrical parameters of 8 cell groups.

At the second stage, cell-by-cell thermohydraulic calculation of the core was carried out for 1/2 symmetrical part of the fuel assembly, where fuel element cladding temperature was maximal. Calculation area is shown in Figure 7.28. It includes 22 cells, 13 fuel elements and 28 links between selected cells. Geometrical cell parameters are given in Table 7.8.

In order to reduce the temperature of fuel elements, situated close to tungsten target and receiving additional heat from target, iteration calculations to choose transversal size of the target were carried out. Calculation results for transversal sizes of tungsten target finally chosen are given below.

Table 7.7 – Geometrical parameters of cell group – stage 1

Group number	Cell numbers, included in group	Area, mm^2	Perimeter, m	
			1	2
1	3, 6, 8, 9	396,99	0,39018	0,081367
2	4, 5, 7, 10, 11	198,49	0,19509	0,040684
3	13	396,99	0,39018	0,122946
4	15	396,99	0,39018	0,14372
5	14	198,49	0,19509	0,051076
6	1	225,49	0,19509	0,01923
7	2	211,99	0,19509	0,009610
8	12	396,99	0,39018	0,10216

Table 7.8 – geometrical parameters of cell groups- stage 2

Group number	Cell numbers, included in group	Area, mm^2	Perimeter, m			
			1	2	3	4
1	5, 6, 7, 9, 12, 14, 16, 17, 19	5,9631	3,6128e-3	3,6128e-3	3,6128e-3	1,6425e-3
2	1	5,3747	1,8064e-3	2,3921e-3	2,7380e-4	0
3	10, 15, 20, 21	17,7090	5,4193e-3	5,4193e-3	1,6425e-3	0
4	18	7,1556	3,6128e-3	5,4750e-4	0	0
5	2, 3	22,9773	5,4193e-3	5,4193e-3	7,600e-3	1,6425e-3
6	4	8,9525	3,6128e-3	2,3921e-3	5,4750e-4	0
7	8, 11, 13	5,9631	3,6128e-3	3,1610e-3	5,2553e-3	0
8	22	3,5778	1,8064e-3	2,7380e-4	0	0

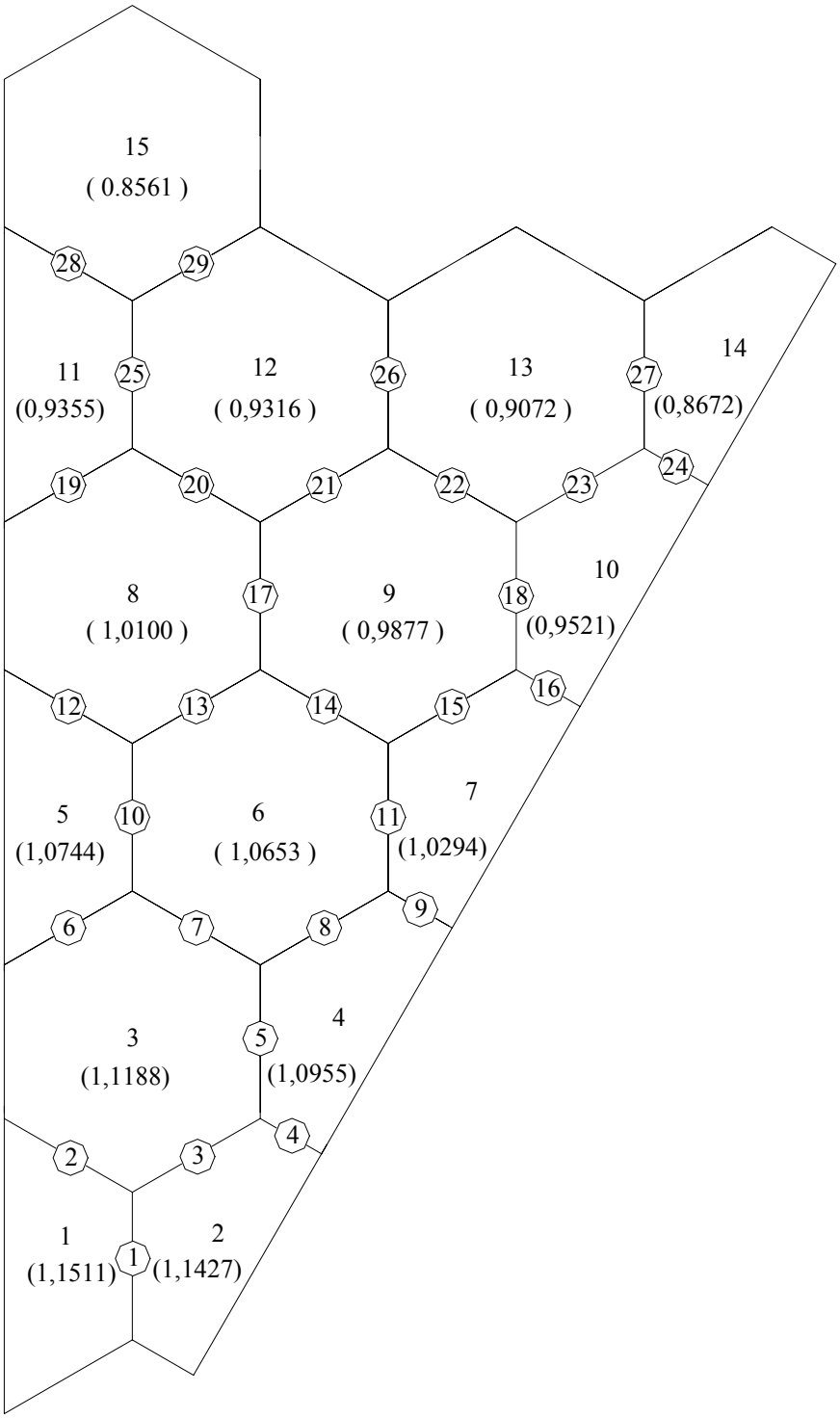

Figure 7.27 - Calculation area at stage 1

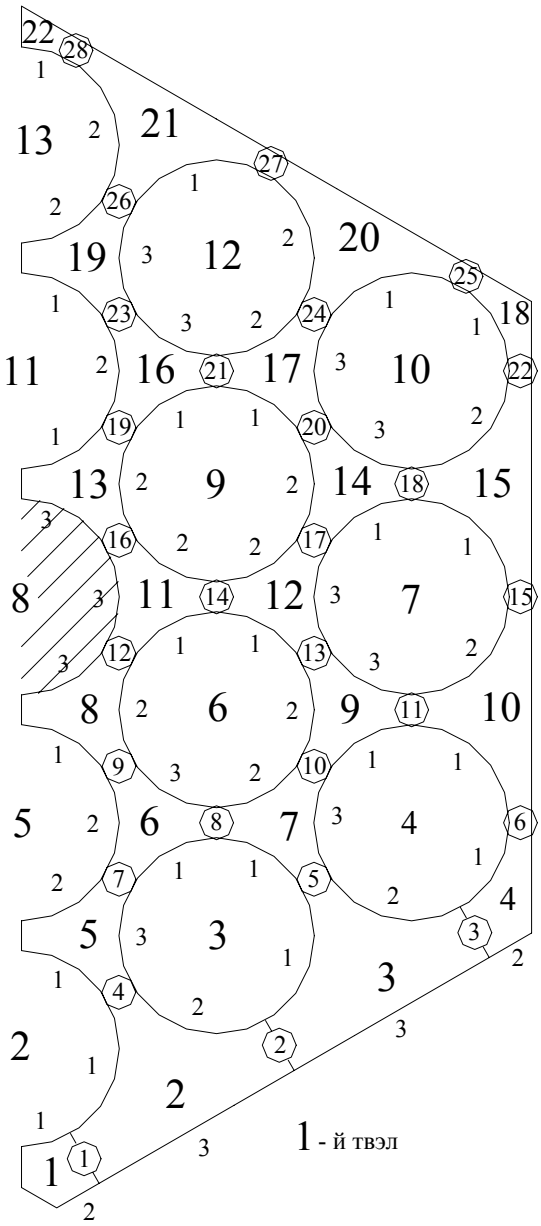

Figure 7.28 – Calculation area at stage 2

7.4.3. Calculation results

Let us first quote calculation results of conjugate problem core-target. The purpose of that calculation consists in obtaining data on temperature fields in tungsten target and heat flow distribution from target surface, necessary for the cell-by-cell calculation of the core.

Figure 7.29 shows, “with filling”, temperature fields in target section planes A(a), B(b), C(c) and their layout scheme (d). Maximum value of tungsten target temperature is 242°C and it is observed in maximum energy release area close to proton beam input channel end. Maximum temperature difference in target cross-section drawn through maximum energy release point is 13°C. The largest temperature difference in target was observed in axial direction and it is equal to 132°C.

Figure 7.30 shows heat flow density distribution q by target height (heat flow density is averaged along perimeter in cross-section). As one can see from Figure 7.30, the maximum heat flow is observed at the core inlet. As you are moving away from core inlet, the maximum is falling and runs up to its minimum value at core outlet. Such a character of heat flow distribution is caused by two factors: axial direction heat spread in target and coolant heating in the core.

With allowance made for parameter deviation, the maximum temperature value of the target was 286°C, and that is lower than maximal permissible value 300°C.

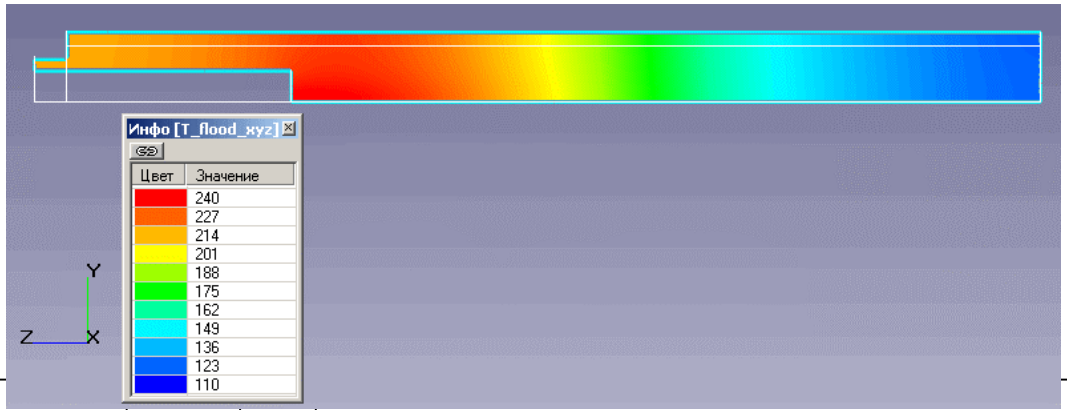

a)

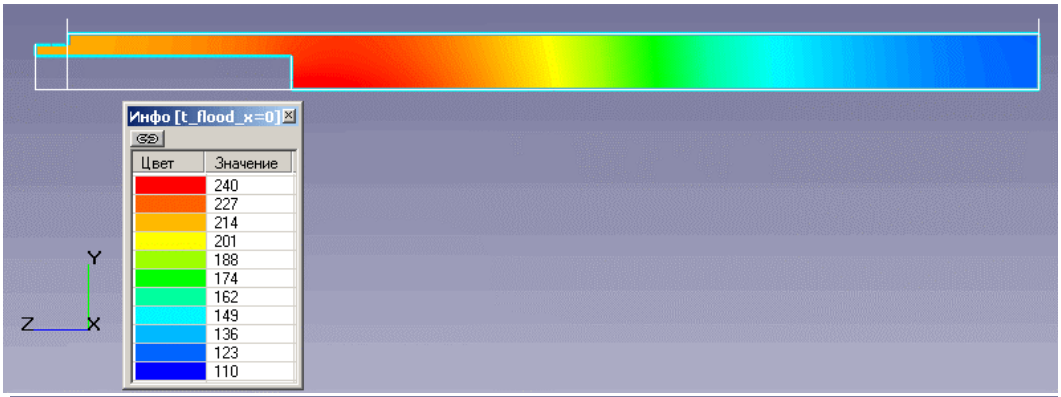

б)

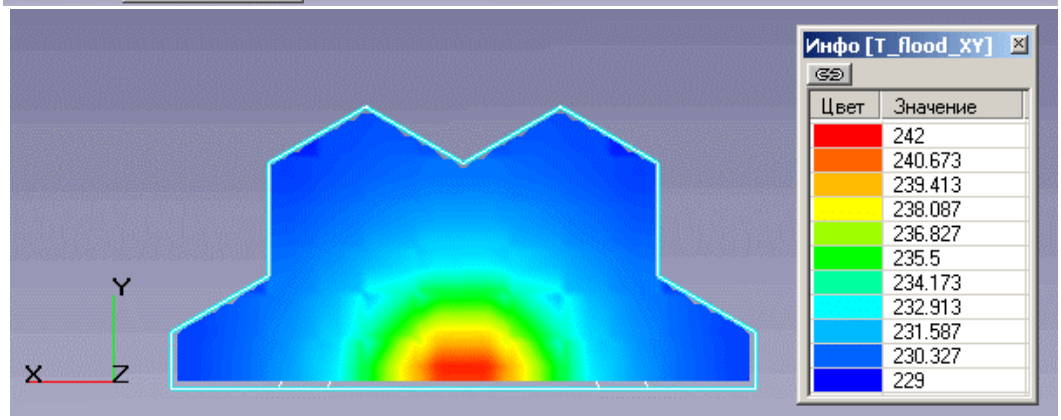

в)

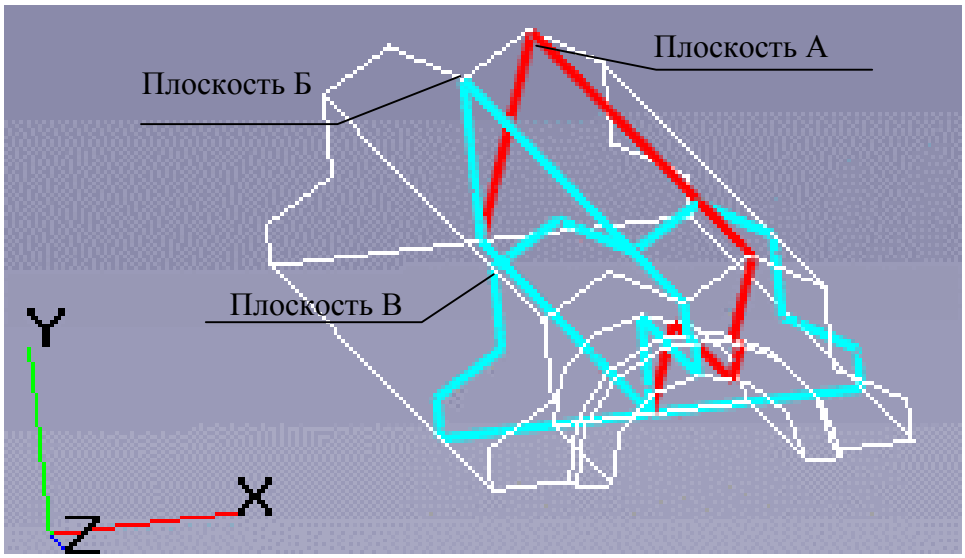

г)

Figure 7.29 – Temperature fields in section planes of target A (a), B (b), C(c) and their layout scheme (d). Nominal mode

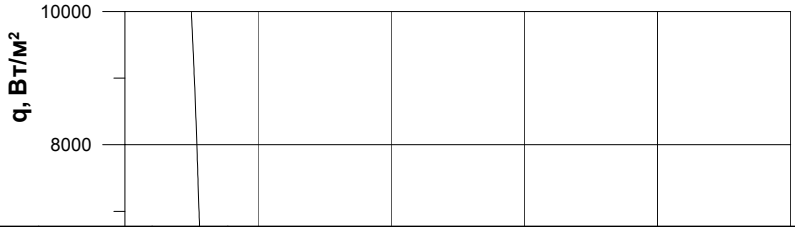

Figure 7.30 - Density change of heat flow q on target surface along axis

Let us proceed to analysis of cell-be-cell calculation results at first stage. Figure 7.31 shows coolant temperatures distribution by core height in ″cold″ cell (No.14), average temperature in cross-section, temperature in ″hot″ cell (No.1), as well as cladding temperature distribution in cell No. 1, where it runs up to maximum value. Average coolant heating in the core was 37.6°C. At core outlet, minimum coolant temperature value was 82.4°C, the maximum value - 106°C.

Maximum cladding temperature value is reached in the cross-section, which is approximately 572mm away from core inlet and is equal to 127°C. Coolant and cladding cell-by-cell temperature distribution cartogram at the same cross-section is given in Figure 7.32. The same distributions at core outlet are given in the same Figure 7.32. As one can see from Figure 7.32, coolant temperature distribution irregularity in core cross-section does not exceed 25°C. If compared with core

variant with lead target, the coolant temperature irregularity grew by 17°C, at the expense of somewhat greater energy release irregularity in cross-section and additional heat from tungsten target.

Figure 7.33 gives coolant velocity distributions in ″cold″ (No..14) and ″hot″ (No.1) cells. Figure 7.34 shows coolant velocity distribution cartogram at core outlet. The average FA coolant velocity is in the range 7.9÷10m/s.

Flow mode by local Reynolds number Re_i in FA was in transitional range to turbulent flow (1280÷2040). Hydraulic pressure losses at core sections were the following:

Core inlet., kPa – 0,86

Fuel element part of the core. kPa – 0,40

Core outlet, kPa – 11,4

Total losses, kPa – 12,66.

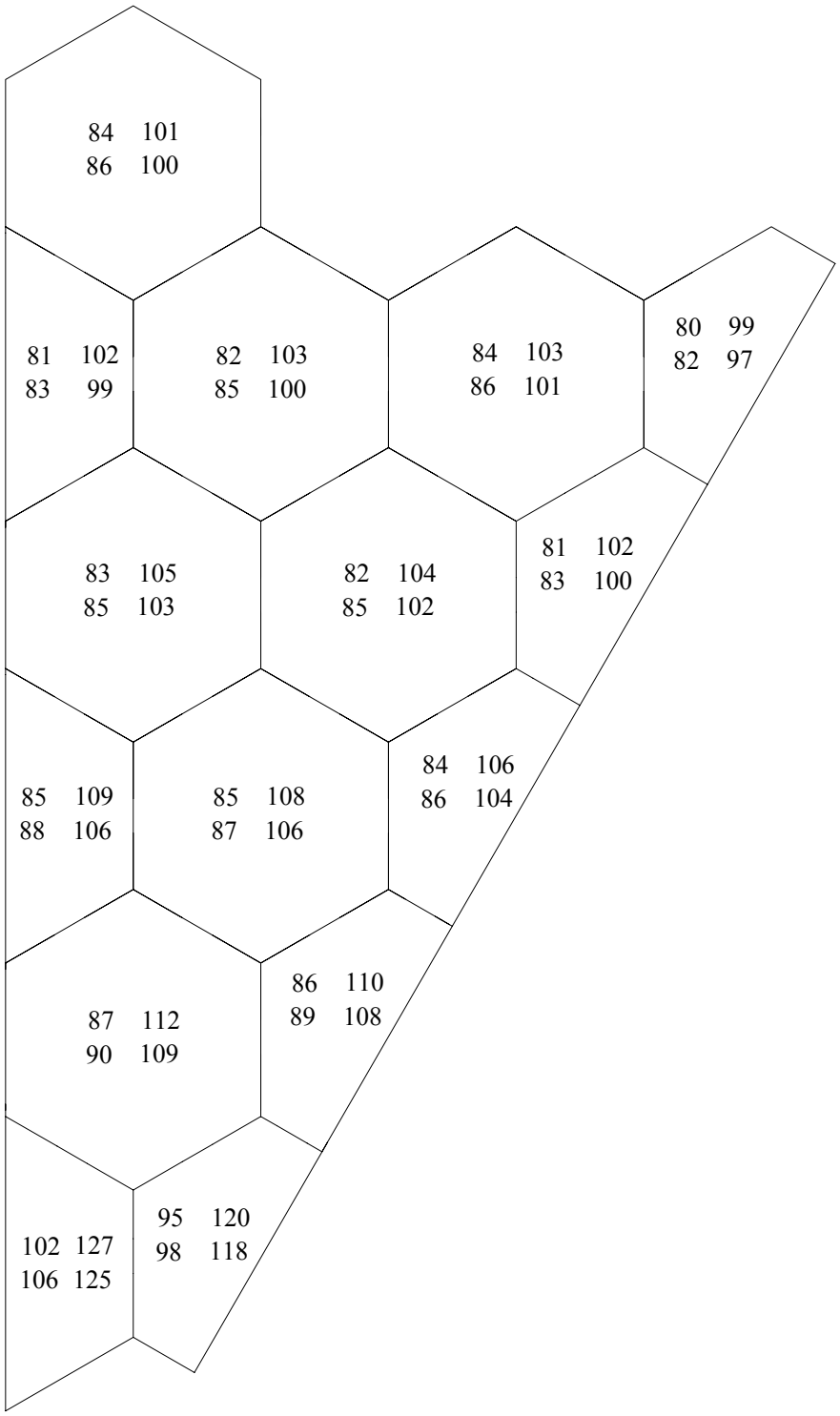

Figure 7.32 – Temperature distribution cartogram of coolant and cladding in cells in core cross-section, where the cladding temperature achieves maximum value (z = 572 mm), as well as at core output (variant with tungsten target)
Column 1 – coolant temperature, column 2 – cladding temperature;
Line 1 – section (z = 572 mm), line 2 – at core output.

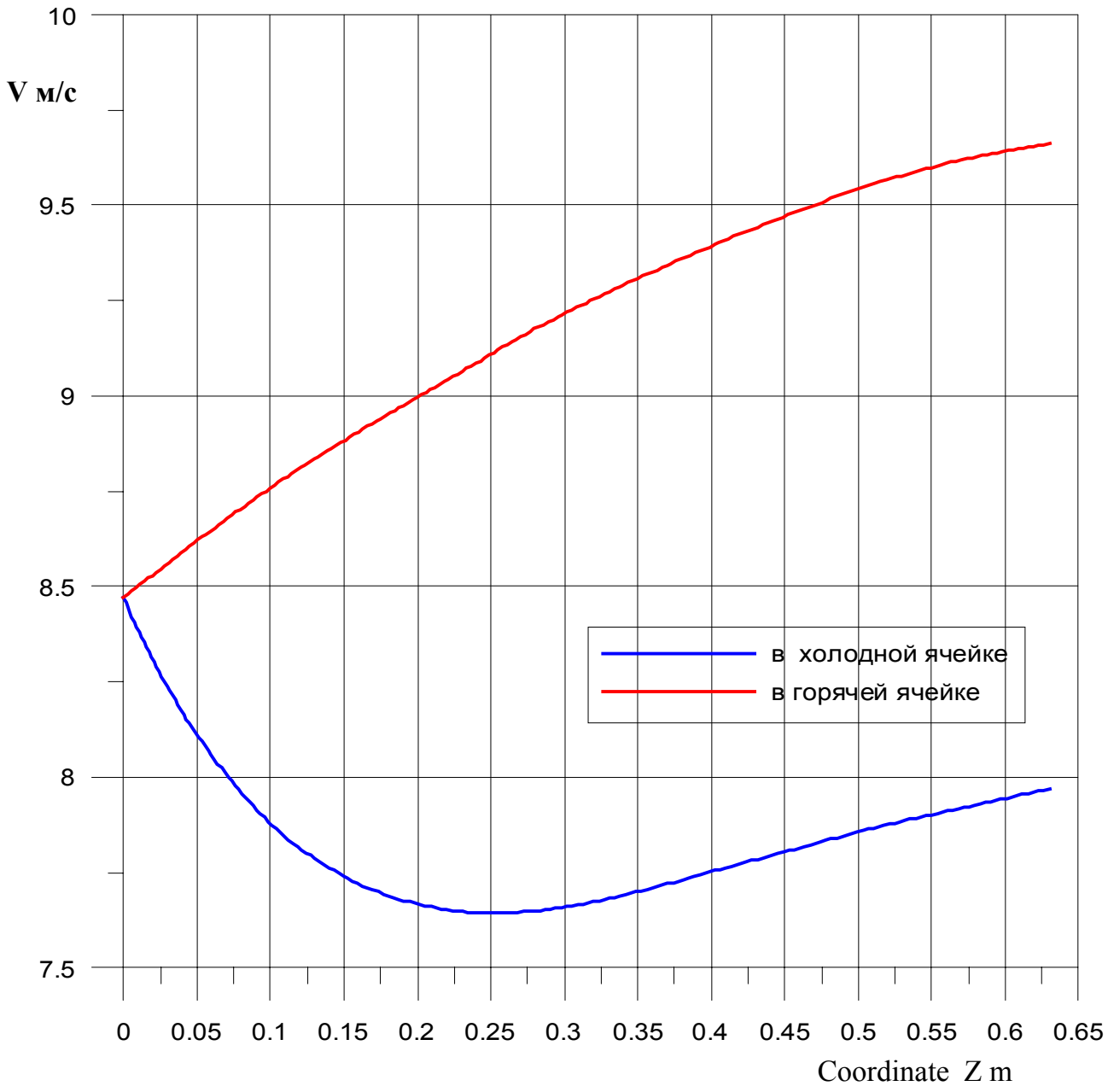

Figure 7.33 –Coolant velocity distribution (variant with tungsten target)

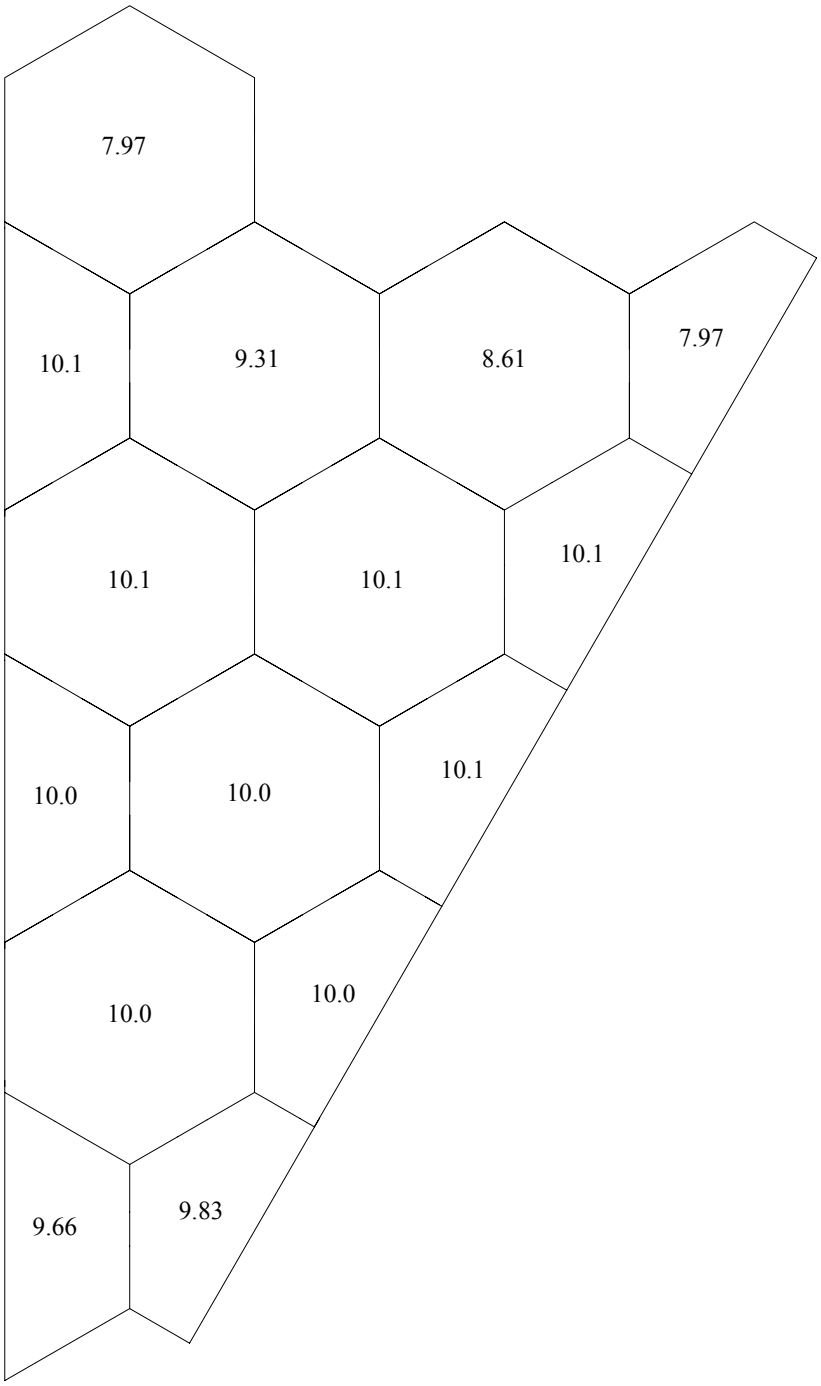

Figure 7.34 – Coolant velocity distribution cartogram in cells at core output (variant with tungsten target)

At the second stage, cell-by-cell calculations were carried out for “hot″ cell No.1, where cladding temperature had a maximum value. Figure 7.35 shows coolant temperature distributions by core height in ″cold″ cell (No.22), ″hot″ cell (No.1) and fuel element temperature (No.2). Irregularity of coolant temperature distribution in FA outlet section is 78°C, and that exceeds significantly the temperature distribution irregularity in maximally strained FA in the core with lead target (39°C). Maximum coolant temperature takes place in cell No. 1, at core outlet, and it is equal to 159°C.

Coolant and fuel element cladding temperature distribution cartogram is given in Figure 7.36. In contrast to first stage calculations, the temperature maximum in fuel element cladding was observed at core outlet in fuel element No.2 and was equal to 159°C, and that is 32°C higher than at first stage. Tha absence of autonomous cooling of tungsten target caused higher maximal temperature values of fuel elements of FA, located immediately next to target.

Calculation results showed that maximum fuel element temperature value with allowance made for parameter deviations (overheating factors) is 232°C, and that does not exceed maximum permissible value, equal to 250°C.

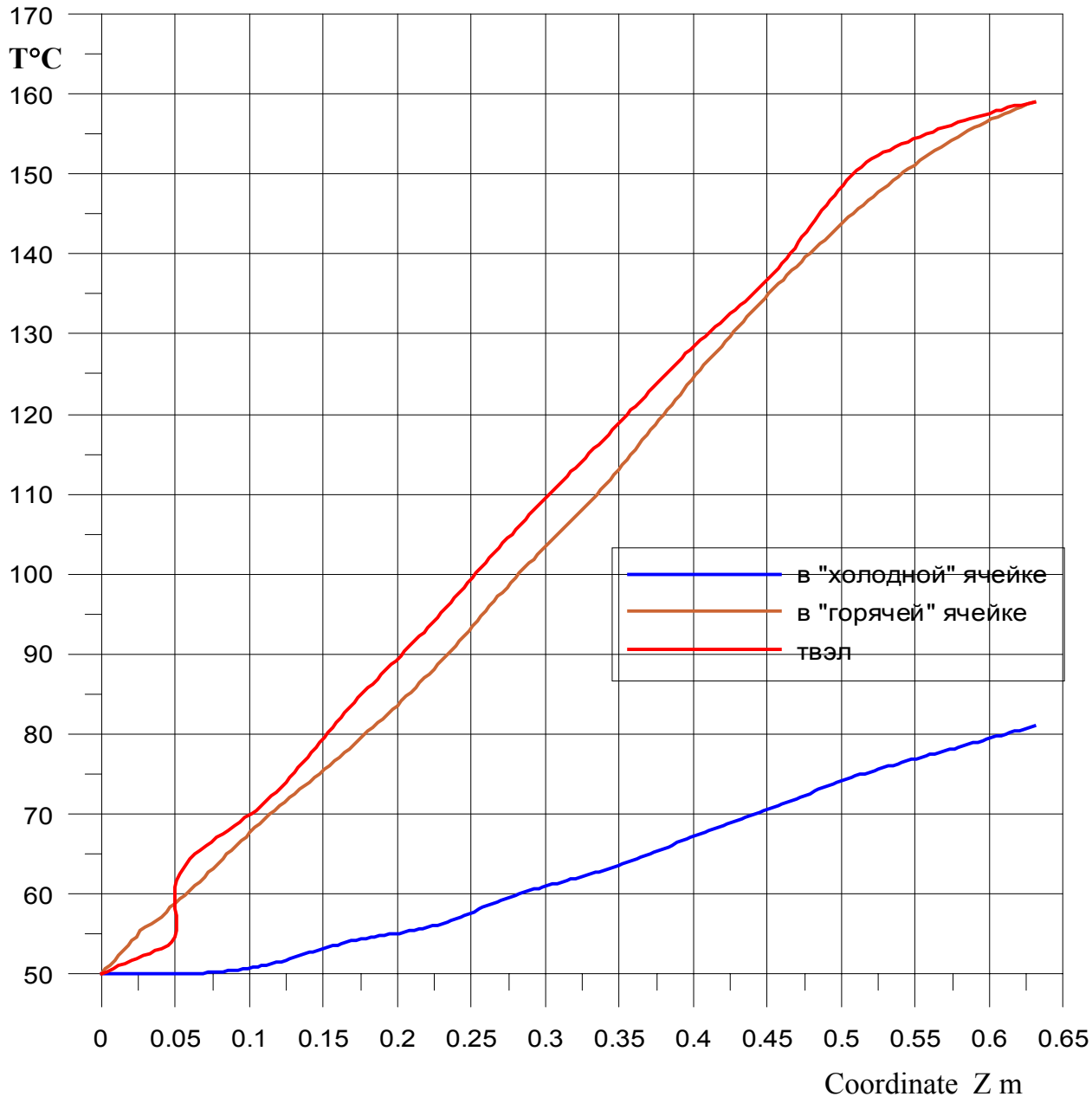

Figure 7.35 – Coolant temperature and fuel element temperature distributions by core height: (variant with tungsten target)

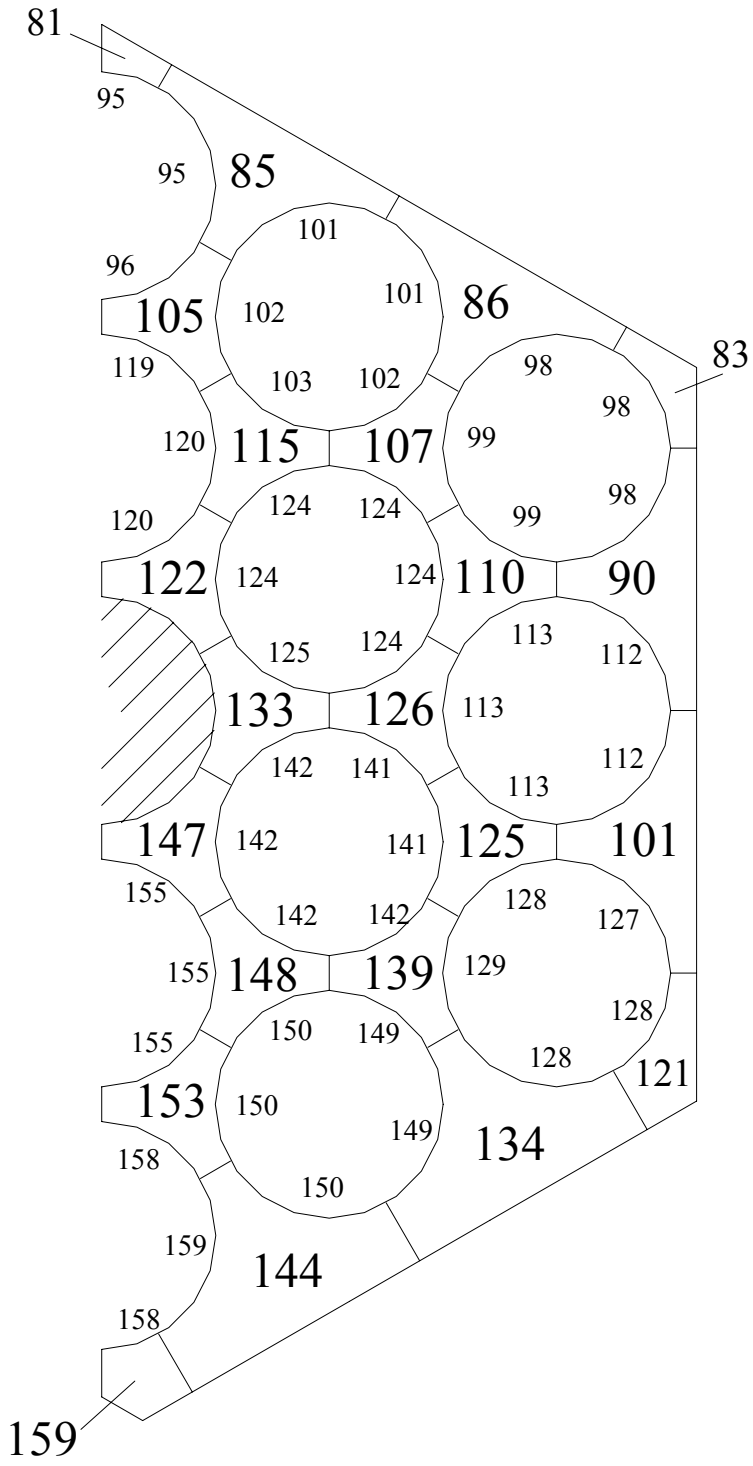

Figure 7.36 – Temperature distribution cartogram of coolant and fuel element cladding in output section (variant with tungsten target)

Подпись и дата | Инв. № дубл. | Взам. инв. № | Подпись и дата | Инв. № подл.

Лист

7.5 Summary data of calculation results

Calculation results of maximum temperature values of various elements of cooling loop without and with allowance for deviations are summarized in Table 7.9.

Table 7.9 – Maximum temperatures calculation results of elements core-target

Element name	Temperature, °C		
	Without allowance for deviations	With allowance for deviations	Maximal permissible values
Core fuel element with lead target	131	185	250
With tungsten target	159	232	250
Lead target	176	214	250
Tungsten target	242	286	300

As one can see from Table 7.9, maximum temperature values of all elements do not exceed assumed maximum permissible values..

Полученные Lower values of maximum element temperatures for the core variant with lead target are explained by autonomous way of target cooling if compared with a variant with tungsten target.

7.6 Conclusions

7.6.1 Thermohydraulic calculations for two core variants (with lead and tungsten targets) were carried out. Calculations were based on two-stage (variant with lead target) and three-stage (variant with tungsten target0 approaches with the use of Russian cell-by-cell code POOCHOK BM-SWEEP and three-dimensional code FLOW VISION.

7.6.2Thermohydraulic core and targets data are obtained:

- pressure at core inlet – 0.135MPa
- temperature at core inlet - 50°C
- total discharge
  - With lead target – 0.60662kg/s
  - With tungsten target – 0.65kg/s
- average air target at core outlet
  - For variants with lead target - 93°C
  - With tungsten target - 88°C
- pressure difference at core
  - For variants with lead target – 9.72 kPa
  - With tungsten target – 12.66 kPa
- discharge through lead target – 0.00662 kg/s
- pressure difference at lead target – 13,65 kPa